Spring 2022

Investigating the Impact of Maternal Antiviral Responses on Pregnancy and Fetal Development

Alice Lu-Culligan
Yale University Graduate School of Arts and Sciences, aliceluculligan@gmail.com

Abstract

Investigating the Impact of Maternal Antiviral Responses

on Pregnancy and Fetal Development

Alice Lu-Culligan

2022

The maternal-fetal interface during pregnancy is an underexplored environment rich in immunological factors that must propel developmental processes while simultaneously providing protection from invading pathogens such as viruses. Almost half of all cells in the maternal decidua in pregnancy are leukocytes, which are required for successful pregnancy, and the placenta has increasingly become recognized as an immunological organ. Viral infections during pregnancy are associated with significant mortality and morbidity, both for the pregnant female and the developing fetus. Notably, impacts on fetal development have typically been attributed to direct viral damage to cells and tissues during the course of infection, without a deep consideration of the potential collateral damage incurred upon the activation of antiviral immune responses. In this dissertation, I characterize the contribution of the immune system and antiviral responses to pathologies of pregnancy and fetal development, using both mouse models of maternal immune activation and human studies of viral infection and immunization during the coronavirus disease 2019 (COVID-19) pandemic.

First, I establish and characterize a novel model of maternal immune activation (MIA) in early pregnancy that leads to a high rate of neural tube defects (NTDs) and

craniofacial abnormalities in the affected offspring. Using systemic administration of the double-stranded RNA mimic poly(I:C) to pregnant mice, I demonstrate that the activation of antiviral immune responses alone is capable of driving fetal birth defects. These phenotypes mirror human NTDs, among the most common birth defects seen worldwide. I identify key immunological pathways and factors driving pathogenesis, which is TLR3- and STAT1-dependent. Strikingly, mice deficient in γδ T cells are protected from the development of MIA-induced NTDs. Together with collaborators, I use immunofluorescence imaging and a spatial gene expression approach to show that γδ T cells are associated with laminin loss at the ectoplacental cone of the primitive placenta. I demonstrate that these changes at the maternal-fetal interface are associated with decreased proliferation of neural progenitors in the developing fetus, resulting in the failure of neural tube closure. We thus uncover a previously unrecognized role for γδ T cells at the maternal-fetal interface and novel mechanism underlying NTD pathogenesis.

Next, I interrogate the impact of antiviral responses on outcomes in human pregnancy. The emergence of SARS-CoV-2 and the ongoing COVID-19 pandemic has highlighted the importance of studying the unique consequences of viral infections during pregnancy, as pregnant individuals are at much greater risk for severe COVID-19 disease than nonpregnant individuals. Working with a multidisciplinary team, I help to identify one of the first reports worldwide showing that SARS-CoV-2 is capable of infecting the placenta. I discover that SARS-CoV-2 is capable of infecting the placenta at the syncytiotrophoblast layer, the multinucleated layer of trophoblast derived from stem cell cytotrophoblasts, and that infection, while rare, is restricted to this region of the maternal-fetal interface. In pregnancies affected by asymptomatic SARS-CoV-2, the vast majority

of placentas are not infected due to a robust antiviral response at the maternal-fetal interface. However, I find that this powerful antiviral defense includes a distinct inflammatory profile at the placenta that is directly associated with preeclampsia and other inflammatory disorders of pregnancy, suggesting that antiviral immunity mounted to effectively shield the fetus from viral infection may come at the price of dysregulation of the maternal-fetal interface. This observation lends insight as to why pathogens typically are not able to invade the placenta during pregnancy and how even asymptomatic or mild infections limited to the respiratory tract can lead to severe maternal outcomes at a distant organ site.

Finally, I directly address some of the most prevalent vaccine misinformation encountered by the public today, including false theories that the COVID-19 mRNA vaccines cause infertility and harm developing fetuses *in utero* when administered in pregnancy. With a mouse model of vaccination during early pregnancy, I show that administration of the mRNA-1273 vaccine has no impact on fetal size at term and does not lead to birth defects. In contrast, poly(I:C) administration, which unlike the mRNA vaccines activates TLR3 pathways, significantly reduces crown-rump length and weight at term. I further demonstrate that mRNA-1273 vaccination even in the earliest stages of pregnancy, prior to formation of the definitive placenta, leads to high levels of protective antibodies in fetuses at term. In a large study of human volunteers, we challenge a common infertility myth by providing direct evidence that COVID-19 vaccination with either mRNA-1273 or BNT162b2 does not lead to an increase in circulating anti-syncytin-1 antibodies. Together, these contributions dispel a number of the most common vaccine rumors fueling vaccine hesitancy worldwide.

Investigating the Impact of Maternal Antiviral Responses on Pregnancy and Fetal Development

A Dissertation

Presented to the Faculty of the Graduate School

Of

Yale University

In Candidacy for the Degree of

Doctor of Philosophy

By

Alice Lu-Culligan

Dissertation Director: Akiko Iwasaki

May 2022

Table of Contents

List of Figures

Acknowledgements

This work would not have been possible without the inspiration and exceptional mentorship of my thesis advisor, Akiko Iwasaki. You have trained me to become more creative, more rigorous, and more courageous, not only in my science but in all that I do. Thank you for believing in me and for empowering me, as well as countless others. Your enthusiasm and generosity truly know no bounds, and I am so honored to be a part of the positive, thoughtful, incredibly special lab and research culture that you have established.

Thank you to my thesis committee: Carla Rothlin, Ruslan Medzhitov, and Peter Aronson. It has been a dream to work with such brilliant faculty toward this goal and I am so grateful to have had such a supportive team contributing key insights and a lot of joy at all of my committee meetings. Shelli Farhadian guided me through the pandemic and life beyond in so many ways. I am so appreciative of your energy and endless support. Thank you also to faculty including Vikki Abrahams, Paul Aronson, Jeanne Hendrickson, Harvey Kliman, Liza Konnikova, and Hugh Taylor, who have met with me for scientific or clinical advice and informal mentorship throughout the years.

To all my mentors at Yale School of Medicine, especially Marcella Nunez-Smith and Randi Hutter Epstein. Marcella, my trust in you is endless—thank you for keeping me going all these years in the way only you know how. Randi, the vision and mentorship that I have received from you has been transformative and I thank you for trusting in my voice.

I would like to acknowledge my incredible labmates in the Iwasaki lab and give a special thanks to my mentees, particularly Hannah Lee who continues to inspire me long

after graduating and has taught me so much more than I have been able to teach. Thank you to all of the collaborators with whom I have worked throughout my PhD, including Leah Connor, Lea Kiefer, and Jeremy Schofield (Simon lab), Edward Courchaine (Neugebauer lab), and Arun Chavan, Emily Condiff, and Scott Pope (Medzhitov lab). Nothing brings me more excitement in the lab than to share in our scientific adventures together and I am grateful to call you dear friends in addition to colleagues.

To my former research mentors: Volker Vogt, Stephen J. Turner, and Peter C. Doherty, thank you for giving me the foundation for a lifelong love of science and for nurturing my curiosity into focus. Thank you to my former labmates in the Vogt lab, Turner lab, and Doherty lab for all the long days, late nights, wisdom, and so many laughs that propelled me into graduate school.

To the many communities in New Haven that have created a home for me as I pursued this PhD, thank you for the moments of peace and perspective. To my original YSM 2012 family, HAVEN Free Clinic, Yale IBIO and IWGDI, I could not imagine moving through this journey without you. To my teachers at Breathing Room Community Center who have made me a better student, teacher, and human. Thank you for showing me to fly in acroyoga, flow in power, and rest in nidra.

To my family, especially my parents Fulong and Joann, who have made everything possible for me. Mom and Dad, I have witnessed the deepest expressions of patience and tenacity from your example and I am so proud to be your daughter. Thank you for your support, sacrifice, and wisdom throughout all these years. To my brother, Ethan, thank you for making me feel so supported all these years of training no matter what.

To my husband William, thank you for your endless love and support. You have been my constant in this journey, and I can only be excited for what is next together. You inspire me to do better every day and I could not imagine this adventure without you. And finally, to our silly animals—thank you to Fitzgeraldine and Xena for making sure we never take ourselves too seriously, with or without a PhD.

Chapter 1: Introduction

This chapter contains excerpts from:

Lu-Culligan A, Iwasaki A. 2020. The Role of Immune Factors in Shaping Fetal Neurodevelopment. *Annu Rev Cell Dev Biol*. 36:441–68

1.1 Overview of the immune system in pregnancy and fetal development

The maternal immune system has been increasingly recognized as a critical participant in the processes that propel embryonic and fetal development[2]. Long mischaracterized as a host-versus-graft response, the rich immunological landscape of the maternal–fetal interface facilitates the establishment and support of the conceptus throughout all stages of pregnancy, from the priming of the uterus for blastocyst implantation to the promotion of immune tolerance to the initiation of parturition[3].

In parallel to immune pathways in the mother, the fetus itself is now recognized to express a diverse array of immunological factors from the earliest stages of development[4,5]. The expression of Toll-like receptors (TLRs), cytokines, and other molecules with important functions in immunity can be detected in both embryonic and extraembryonic tissues with distinct spatial and temporal patterns of expression[4,5]. These observations suggest a role for various immune pathways in normal development; however, a functional understanding of these contributions and their relative importance is still emerging.

The complexity of studying these maternal and fetal microenvironments is compounded not only by their adjacency and interactions but also by the rapid developmental changes taking place on each side. Nevertheless, epidemiological and experimental studies have together demonstrated that infections and inflammation during pregnancy can lead to poor maternal and fetal outcomes[6-8], with many pathologies being traced to cross talk at or across the interface.

Early interest in the relationship between maternal immunity and fetal neurodevelopment can be traced to the ever-growing body of epidemiological studies linking infections during pregnancy to neurological and psychiatric diseases in offspring. The 1964 rubella epidemic in the United States produced multiple studies that found an extremely high rate of autism in children with known in utero exposure[9]. Interestingly, these pioneering studies document a range of coinciding neurological abnormalities in rubella-affected neonates including seizures, cerebral palsy (CP), and microcephaly[10].

Fittingly, the first categorical descriptions of TORCH [*Toxoplasma gondii*, others (including *Treponema pallidum*, *Listeria monocytogenes*, varicella-zoster virus, and parvovirus B19), rubella virus, cytomegalovirus, and herpes simplex virus] pathogens and their shared clinical sequelae were also released during this time[11], with central nervous system (CNS) abnormalities notably documented as the most frequent presentation of in utero TORCH infections. The introduction of the term TORCH into the lexicon formally canonized the common observation that a diverse collection of pathogens can elicit similar fetal pathologies.

Numerous additional studies have since linked public health outbreaks of other infectious diseases (e.g., influenza and measles) to subsequent increases in the incidence

of neuropsychiatric disorders. Concurrently, the number of pathogens within the TORCH classification known to cause congenital neurological anomalies continues to rise. The most obvious example from the recent decade is the Zika virus (ZIKV) epidemic that swept the Americas from 2015 to 2016 and captured a high degree of public attention due to its dramatic association with microcephaly. While some features of infection are specific to the virus, ZIKV shares remarkable similarities with other TORCH pathogens in terms of its biology and the spectrum of congenital defects displayed following *in utero* exposure[12].

Indeed, the dizzying collection of diverse pathogens capable of producing neurodevelopmental disease, whether autism spectrum disorder (ASD) or microcephaly, is puzzling when each pathogen is considered individually. Advances in our understanding of both sides of the maternal–fetal interface have coalesced into new breakthroughs that instead shift focus onto a conserved component of these wide-ranging insults: the maternal immune system.

Maternal immune activation has now been implicated in a broad range of distinct disorders in offspring, and an outsized proportion of these are, strikingly, brain pathologies long suspected to have developmental origins[6,13]. The capacity of pathogens to induce MIA during pregnancy suggests a pathway to developmental disease distinct from that of direct infection and damage.

At the same time, perturbations in maternal immunity are continually being linked to disorders of pregnancy such as preeclampsia and preterm labor. Although the causes of these pathological conditions are complex and heterogenous, numerous studies have identified key immune-related alterations and shared immunomodulatory signatures associated with poor maternal outcomes[14].

The emerging principles underlying immune dysregulation at the maternal-fetal interface can thus inform our understanding of both maternal and fetal disorders of pregnancy. For example, knowledge of the relative contribution of maternal immunity to TORCH infections can be applied not only to ZIKV but can also more widely inform an assessment of the risks posed by the current novel coronavirus (COVID-19) pandemic or future pathogens. While the potential for vertical transmission remains an important question for any novel pathogen, including severe acute respiratory syndrome coronavirus 2 (SARS-CoV-2), studies of MIA suggest that systemic perturbations of maternal immunity can be detrimental to both mother and fetus even without transfer of the infection across the maternal–fetal interface. In this introduction, I provide a brief overview of the maternal-fetal interface, MIA, and the consequences of activating immune responses on maternal and fetal health.

1.2 Structure and composition of the maternal-fetal interface

The maternal-fetal interface is centrally composed of the decidua of the maternal uterus and the extraembryonic tissues of the developing fetus[15,16]. Formation of the interface is initiated with blastocyst invasion of the uterine mucosa, during which the endometrial lining of the maternal uterus undergoes a dramatic remodeling process called decidualization that is marked by a significant influx of immune cells into the environment[16]. Other maternal cell types such as decidual stromal and endothelial cells are also being established and expanded at during this time[15].

The immunological renovation establishing the maternal-fetal interface is not confined to the maternal tissues, however; fetal trophoblasts invading the maternal tissue

are potent immune signalers as well. Later in pregnancy, these trophoblasts form the placenta, where early fetus-derived immune populations from the yolk sac also reside. Together, the interactions of these maternal and extraembryonic tissues dictate immunological communication across the interface.

1.2.1 Maternal leukocytes at the maternal-fetal interface

From the first stages of pregnancy, the maternal decidua is characterized by a remarkable proportion of leukocytes. Following decidualization, leukocytes ultimately comprise 30-40% of all cells in the decidua in the first trimester[17,18]. NK cells predominate in early pregnancy, comprising approximately 70% of leukocytes in the decidua basalis[15]. Macrophages make up roughly 20% of the population, with T cell numbers varying from around 3-10%; as in other tissues, dendritic cells are relatively infrequent comprising 1-2%[19,20]. After the first trimester, these proportions shift dramatically, with NK cell and macrophage numbers decreasing and T cells becoming the predominant immune cell subset by the end of the third trimester[17,21].

Importantly, cytokines play a critical role in the infiltration and development of these maternal immune populations at the maternal-fetal interface. Non-leukocytes such as stromal and endothelial cells in the decidua also directly contribute to this regulation through the release of cytokines and chemokines[15].

1.2.1 Fetal leukocytes and trophoblasts at the maternal-fetal interface

The fetus is typically regarded as highly vulnerable to infections in utero due to the absence or immaturity of the prenatal immune system. However, a deeper examination of

the fetal immune system during pregnancy paints a more complex picture than mere deficiency. Although commonly overlooked, leukocytes derived from both fetal and extraembryonic structures are present and display a surprising degree of maturity and functionality prior to birth[18,22-24].

Indeed, a significant body of recent work has emphasized the critical importance of fetal leukocytes such as microglia and Hofbauer cells in both developmental processes and immune regulation. Microglia are the resident macrophages of the CNS and arise from primitive macrophages in the yolk sac early in development. It is well-established that microglia play a central role in the pruning of synapses in the brain postnatally, but microglia have been implicated in a number of prenatal neurodevelopmental processes as well[25-27]. While microglia shape neurodevelopment both during and after pregnancy, Hofbauer cells, or placental macrophages, play a significant role in immune regulation, particularly during infections and inflammatory pathologies. Hofbauer cells are a heterogeneous population of fetal macrophages that reside in the placenta throughout pregnancy from their initial appearance at roughly 4 weeks post-conception in humans. While they are known to be fetus-derived, their precise developmental origins remain unknown though they are predicted to arise from primitive hematopoiesis[28].

A central source of immune signaling also stems from nonhematopoietic cell types. Trophoblasts serve as both immune sensors and signal propagators long before the formation of the definitive placenta, which is itself now considered an immune organ. Virtually all known TLRs and cytokines are expressed in placental tissues throughout gestation[4,29]. Trophoblasts secrete numerous factors, including cytokines, complement factors, and exosomes, that establish distinct spatial and temporal patterns of immunity at

the maternal–fetal interface[30-33]. They confer protection against pathogens even to non-trophoblast cells in the local environment[31,34-36] and modulate the migration and function of maternal leukocytes[15]. In addition to these baseline functions in pregnancy, trophoblasts also exhibit differential responses to immune stimulation in a pathogen-associated molecular pattern (PAMP)-specific manner[37-39].

By facilitating maternal–fetal cross talk, the placenta is a key crossroads capable of directly impacting fetal neurodevelopmental outcomes. However, while the hormonal and physiological functions of the placenta are well known to impact fetal development, fewer studies have explored the importance of converging immune signals at the placenta.

1.3 Role of immune factors in fetal neurodevelopment

A striking but underappreciated aspect of prenatal brain development is the regulated expression of numerous components of the immune system in distinct spatiotemporal patterns. The piecemeal expression of these immunity-associated genes can be detected from the blastocyst stage onward and is highly conserved even in oviparous model organisms such as zebrafish and *Xenopus*[5]. Why are these classic immune factors expressed so early in development? Although the expression of some factors may confer intrinsic immune protection, others are clearly not involved in pathogen defense; their potentially pleiotropic roles in fetal development remain an open question. Here I review fetal expression of immune pathways relevant to *in utero* neurodevelopment, and present their proposed physiological functions.

1.3.1 Physiological roles of Toll-like receptors in normal brain development

The *Toll* gene was originally discovered in Drosophila to dictate dorsal-ventral patterning during development, and later demonstrated to be involved in antimicrobial defense[40]. The mammalian homologs of Toll, the Toll-like receptors (TLRs), play a critical role in host recognition of microbial signatures, or pathogen-associated molecular patterns (PAMPs), and their importance in innate immunity has been well-characterized[41].

Far less explored, however, is the involvement and function of TLRs in early development, despite the knowledge that TLRs and their adaptor proteins MyD88 and TRIF are highly expressed within the nascent embryonic brain in distinct patterns over the prenatal timeline[4,44]. Furthermore, seemingly separate from their central role in mediating the host response to infectious insult, TLRs have been implicated in a spectrum of non-infectious CNS diseases impacting neurogenesis and cognitive development[42]. Although TLR deficiencies are known to impact adult neurogenesis and postnatal behaviors[43,44], in many studies it is impossible to discern the impact or relative contributions of prenatal vs. postnatal TLR deficiency, or the impact of compensatory mechanisms engaged in the absence of TLRs to respond to microbial infections. However, shared features in the behavioral abnormalities of TLR knockout mice and models of MIA during pregnancy suggest that prenatal TLR signaling play a major role in shaping adult phenotypes. In this section, I focus on studies examining prenatal TLR3, TLR7, and TLR8 deficiency due to their relevance to innate antiviral responses with an emphasis on *in vivo* evidence.

TLR3 signaling in the embryonic period provides proliferative control, as TLR3-deficient neural progenitor cells (NPCs) show increased proliferation[45] and *Tlr3*$^{-/-}$ mice exhibit increased hippocampal neurogenesis including increased dentate gyrus volumes[46].

Tlr3$^{-/-}$ mice also exhibit reductions in cued fear conditioning and anxiety-associated behaviors[46].

Studies utilizing a combination of *in vitro* culture and *in utero* electroporation in mouse models have shown that TLR7 and TLR8 deficiency results in abnormalities in the differentiation and maturation of embryonic-stage neurons, even in the absence of infection or immune stimulation. *Tlr7*$^{-/-}$ neurons display increased dendritic and axonal outgrowth in vitro, which can be attenuated by exogenous TLR7 expression[47]. These observations are dependent on IL-6 and MyD88 signaling and associated with decreased exploratory behaviors in *Tlr7*$^{-/-}$ mice[47]. TLR7 and TLR8 knockdown using miRNA delivered by *in utero* electroporation were also shown to impact dendritic arborization in neurons analyzed postnatally, albeit at distinct timescales for each[48].

In addition, various behavioral alterations have been reported in *Tlr7*$^{-/-}$ mice, including impairments in contextual memory[49]. A potential caveat in interpreting the link between TLR and neurodevelopment is that TLR deficient mice often have outgrowth or dysbiosis of the virome and microbiome[50], as evidenced by the emergence of endogenous retroviruses in *Tlr7*$^{-/-}$ mice[51,52]. Whether changes in the virome is responsible for the various neurologic phenotypes observed in these TLR-deficient mice needs to be explored in the future.

1.3.2 Physiological roles of cytokines in normal brain development

Cytokines are expressed during normal neurodevelopment in prenatal life and play multifaceted roles in the process of brain formation, among them 1) the modulation of proliferation, apoptosis, and survival programs, 2) the induction, differentiation, and

maturation of neural precursors, and 3) the direction of neuronal migration paths[53]. The final outcome of these pleiotropic functions is informed by developmental stage and other environmental cues. Comprehensive reviews detailing the function of cytokines across all stages of neurodevelopment and a significant body *in vitro* studies can be found elsewhere[53-57]. I instead highlight a selection of *in vivo* work implicating cytokines and chemokines in functions of normal brain development during the *in utero* period.

Cytokines exhibit specificity in temporal and spatial expression within the developing brain during pregnancy[53,58-60]. While numerous *in vivo* data demonstrate fundamental roles for specific cytokines in shaping CNS development, many key mouse knockouts in cytokines such as IFN-γ and IL-1β do not exhibit overt neurological deficits. However, this may be due at least in part to significant redundancy and synergism in these cytokine networks[60]. For example, TGF-β signaling is required for progenitor maturation into dopaminergic neurons in the murine E14.5 midbrain; this reduction was significantly higher in TGF-$\beta2^{-/-}$TGF-$\beta3^{-/-}$ double knockout mice compared to mice carrying a single competent allele in either gene[61]. TGF-β2 appears to be more broadly important for CNS development, however, as TGF-$\beta2^{-/-}$ mice are unviable perinatally due to synaptic dysfunction at the brainstem[62]. Downstream of TGF-β, both BMPs and the SMAD family of transcription factors have been extensively studied for their wide-ranging functions in embryonic CNS development and severe knockout phenotypes, including many that are lethal *in utero*[63,64]. Among their many functions, various Smad proteins as well as interacting partners such as Sip1, have been implicated in neural crest specification, primary neurogenesis, neural tube closure, oligodendrocyte differentiation, astrogliogenesis, interneuron specification, and axon growth[63]. Specifically, Smad2- and

Smad4-deficient mice each exhibit abnormalities in anterior development, including craniofacial and forebrain defects[64], while BMP knockout mice display a range of aberrant cerebellar phenotypes. Cytokines in other signaling pathways show distinctive effects; TNFα$^{-/-}$ mice for example exhibit reduced motor and sensory neuron death[65,66].

The gp130 family of cytokines, also known as the IL-6 family, represents a group of structurally and functionally related proteins that includes IL-6, IL-11, LIF, CNTF, and CT-1. These cytokines are known to have pleiotropic and redundant functions, and the receptor complexes for all family members include gp130 as a common signal transducer, typically activating STAT3. gp130-mediated signaling pathways are important for the maintenance of radial glial cell (RGC) progenitor populations during embryonic brain development. Knockdown of STAT3 at E13.5-14.5 leads to increased neuronal differentiation with increased expression of βIII-tubulin and decreased expression of RGC markers[67,68]. In addition, mice deficient in either gp130 or LIFRβ expression exhibit forebrain hypoplasia and a reduction in the number of mitotic RGCs at E15 and E12.5, respectively[69,70]. Human studies have supported these findings established in mice; a recent single-cell sequencing study of the human neocortex found that outer radial glia selectively express the LIFR components and signaling through this pathway is necessary for cell cycle progression and support of the neural stem cell niche in the outer subventricular zone (OSVZ)[71].

Astrogliogenesis is also impacted by the loss of endogenous gp130 signaling pathways. Mice deficient in either gp130 or LIFRβ expression exhibit decreased astrogliogenesis in late gestation[72-74]. Similarly, neonatal mice lacking CT-1 exhibit

reduced astrocyte numbers, suggesting this cytokine may contribute to the activation of downstream gp130 pathways *in utero*[74].

CSF1R expression is required for the development of all macrophage lineages, but unlike bone marrow-derived macrophages, microglia are not dependent on CSF-1 and instead require IL-34 for their establishment[75]. Nonetheless, CSF-1 null mice exhibit cortical processing deficits and neonates show blunted responses to external visual or auditory stimuli[79,80]. *Csf1r*$^{-/-}$ mice on the other hand exhibit loss of microglia and major perturbations in brain architecture as well as olfaction[76].

Other cytokines have also been implicated in promoting microglial functions during neurodevelopment. IL-33 deficient mice exhibit behavioral abnormalities, including decreased anxiety-associated behaviors and impaired social novelty recognition[77]. Although there are conflicting reports regarding whether microglia express IL-33[78,79], the production of IL-33 by developing astrocytes directly impacts microglial functions, such as synapse engulfment[80].

Chemokines also influence the development of brain progenitors by modulating migration, survival and proliferation activities. CXCL12, also known as SDF-1, binds to the CXCR4 receptor; this is the only known interaction for each[81]. CXCR4 is expressed by neurons, astrocytes, and microglia of the CNS, where levels peak during embryonic brain development[81] and SDF-1 serves as chemoattractant for these CXCR4-expressing progenitors[82,83]. CXCR4-deficient mice exhibit abnormalities in dentate gyrus development due to reduced proliferation and the inhibition of normal migratory pathways of dentate granule cells[84,85]. Both CXCR4 and SDF-1 KO embryos exhibit aberrant

migration of gonadotropin-releasing hormone neurons and precerebellar neurons as well[86,87].

CXCR4 deficiency also reduces the number of oligodendrocyte progenitors in the spinal cord at E14[88]. In the peripheral nervous system, CXCR4 deficient mice also have profound loss of spinal cord motoneurons and dorsal root ganglion neurons leading to reduced innervation of the developing mouse forelimbs and hindlimbs at E20 but not at E14[89]. Finally, CXCR4 plays role in axon pathfinding during both retinal and motor neuron growth[90,91].

1.3.3 Physiological roles of Toll-like receptors in normal brain development

Separate from its well-known roles in host defense, the complement system has more recently been recognized to have distinct expression patterns and functions in development[5,92,93]. While much of the work describing complement in neurodevelopment has focused on its role in peri- or postnatal synaptic pruning, complement factors serve distinct functions in the prenatal period as well. Complement factors are expressed at high concentrations in neural progenitor cells in addition to their demonstrated presence on all mature neuronal and glial cells of the brain. The importance of complement pathways across brain development has been well-reviewed elsewhere[5,92,93], but I summarize some of the most salient work implicating complement in embryonic neurodevelopmental processes during pregnancy.

Developmental expression of complement pathway components appears highly regulated from the earliest stages of brain formation and maturation. During murine neurulation (E7.5-E10.5), a wide range of complement factors are expressed in the neural

tube with distinct temporal and spatial distributions. Notably, each of the complement pathways are represented in a piecemeal manner and the absence of key initiating factors precludes complement activation[94]. Supporting the existence of novel, immune-independent roles in promoting normal development at this stage, the deficiency or pharmacological antagonism of the complement C5a-C5aR axis has been demonstrated to increase the risk of neurulation defects in mouse models. *C5ar1*$^{-/-}$ mice do not exhibit impaired fertility or congenital abnormalities; however, in combination with dietary folate deficiency, loss of C5a-mediated signaling using either genetic C5aR1 knockout mice or treatment with the C5aR antagonist PMX53 at E4.5 leads to a high rate of neural tube defects in the resulting litter[95].

Concordant with these findings, pharmacologic C5aR1 blockade results in reduced neural progenitor proliferation, while endogenous or exogenous C5a exposure leads to increased proliferation of neural progenitors both *in vitro* and *in vivo*[96]. These models also reveal impacts on progenitor cell polarity; the C5a-C5aR pathway promotes the organization and maintenance of NPCs into neural rosettes in culture, while injection of a C5aR antagonist into the ventricles of embryos *in utero* alters progenitor division planes[96]. C5aR1 is localized to the apical surface of the ventricular zone of the developing brain at E14.5 and C5a levels in embryonic CSF are significantly higher than in normal adult CSF at this time, further suggesting a developmental function[96]. Perturbations of C5a-C5aR signaling during embryonic life are associated with postnatal motor and behavioral abnormalities and *C5ar1*$^{-/-}$ mice also display impairments in short-term memory[97].

Interestingly, different complement signaling pathways appear to have differential effects on NPCs. At E14.5, C3aR exhibits a similar pattern of distribution to C5aR at the

apical pole of progenitors in the ventricular zone, but exerts opposite effects on progenitor proliferation[98]. Injection of C3aR antagonist into the embryonic ventricle leads to increased proliferation, while C3aR agonist injection leads to reduced proliferation[98], potentially by driving progenitor differentiation[92,99]. *C3ar*$^{-/-}$ mice also do not display overt abnormalities in viability or development, but exhibit cognitive deficits in spatial memory in adulthood[98]. The C3-mediated pathway has also been demonstrated to dictate the migration patterns of neurons and neural crest cells, along with other complement factors. In mice, knockdown of C3, Masp1, and Masp2 using shRNAs delivered by *in utero* electroporation at E14.5 results in impaired neuronal migration in the neocortex, a defect that could be rescued by mimics of C3 cleavage products or pharmacological activation of downstream C5aR or C3aR[100]. Studies in zebrafish models, which also exhibit high levels of complement expression strikingly restricted to neural structures, have allowed for a more detailed elucidation of the mechanism by which complement-mediated interactions coordinate complex migratory paths. In zebrafish, the C3-C3aR1 axis was shown to drive the coattractive forces necessary for collective cell migration of neural crest cells. Loss of these factors leads to significant disruptions in the self-organizing properties and coordinated movement of these cells[101].

1.4 Maternal immune activation and models

Human epidemiological studies have identified a multitude of associations between maternal inflammatory signatures and poor fetal outcomes, but these links are challenging to pinpoint and explore in-depth because the manifestations of MIA can be experienced as mild or subclinical in pregnant women, and the outcomes in offspring are highly variable

in regard to timing, onset, and phenotype. Studies of maternal infections are further complicated when considering the contributions of two confounding potential sources of damage: the pathogen and the maternal immune response.

Rodent models of MIA have thus provided a breakthrough in our ability to isolate the effects of maternal immunity and attain a more mechanistic understanding of the processes underlying neurodevelopmental pathologies stemming from pregnancy (Figure 1.1). The most common models of MIA invoke the use of PAMPs, including polyinosinic:polycytidylic acid [poly(I:C)], a TLR3 agonist that stimulates antiviral responses, and lipopolysaccharide (LPS), which induces antibacterial responses through TLR4. Although some models of MIA use direct infection of pregnant dams with live pathogens such as influenza virus and *Escherichia coli*, the relative contributions of immune activation versus pathogen-inflicted damage cannot easily be ascertained with infectious models. In this section I will focus exclusively on the most established models of MIA induced by exposure to the TLR3 ligand poly(I:C) in mid-gestation, leading to behavioral changes associated with autism spectrum disorder (ASD) and schizophrenia. I have previously summarized work on MIA models of cerebral palsy (CP), epilepsy, and adult-onset neurological diseases such as Alzheimer's disease (AD) and Parkinson disease (PD) elsewhere (see Figure 1.1)[1].

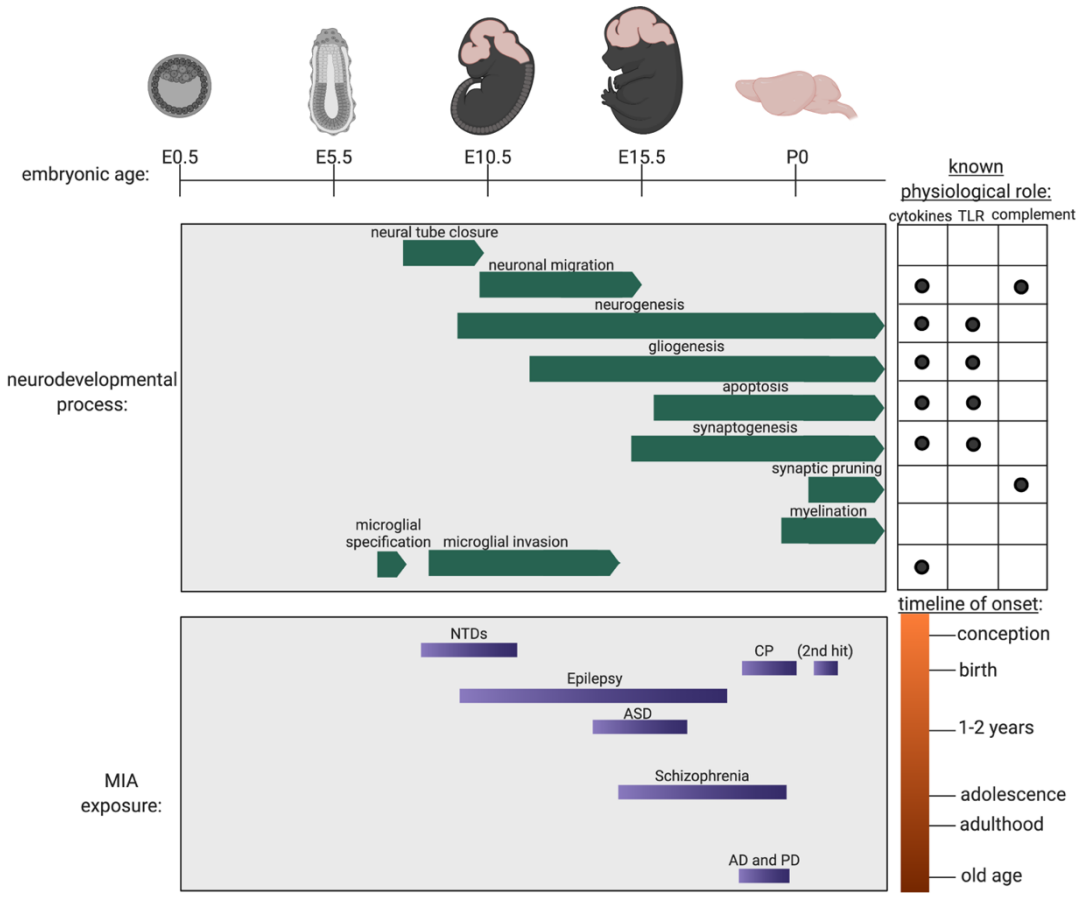

Figure 1.1: Fetal neurodevelopment and maternal immune activation throughout the timeline of pregnancy. Immune pathways are known to participate in normal physiological processes of brain formation and development. The timing, character, and intensity of maternal immune activation relative to the timing of development dictates fetal vulnerability to a spectrum of neurological diseases. NTDs, neural tube defects; CP, cerebral palsy; ASD, autism spectrum disorder; AD, Alzheimer's disease; PD, Parkinson disease. Created with Biorender.com.

1.4.1 Autism spectrum disorder (ASD)

The most established body of work on MIA has focused on the induction of behavioral abnormalities linked to ASD and schizophrenia. Epidemiological and clinical data have long suggested that maternal infection and inflammatory conditions increase the risk for ASD and schizophrenia in offspring[102-107]. These disorders share striking commonalities in their genetic and environmental origins: A recent meta-analysis of genome-wide single-nucleotide polymorphism (SNP) data across eight neuropsychiatric

conditions including ASD and schizophrenia revealed significant overlaps in genetic risk, with approximately three-quarters of significant SNPs associated with more than one disorder. These pleiotropic genes were also enriched in associations with neurodevelopmental function[108].

In support of these observations, recent work using MIA models has critically allowed the identification of specific cytokines driving these aberrant phenotypes during pregnancy and in utero fetal development. There are numerous models of MIA-induced ASD, and the heterogeneity of these approaches may contribute to variability in reproducibility and conclusions[109-111].

Intraperitoneal injection of poly(I:C) to pregnant dams mid-gestation (e.g., E12.5) leads to transient increases in maternal IL-6 levels and offspring defects in prepulse inhibition, latent inhibition, and social and exploratory behaviors commonly associated with both ASD and schizophrenia. *Il6*$^{-/-}$ mice and wild-type mice treated with neutralizing antibodies to IL-6, however, are protected from this phenotype[112]. These findings align with reports in humans that correlate increased maternal IL-6 levels during pregnancy with changes in amygdala volume and connectivity and lower impulse control in offspring at 2 years of age[113]. Further changes in neural network structure have been described in mouse models of MIA-induced ASD-like behavioral abnormalities, in particular changes to the dysgranular zone of the primary somatosensory cortex (S1DZ)[114].

Although human and rodent studies suggest that IL-6 can cross the placenta[115,116], fetal trophoblasts are central to the development of MIA-driven behavioral abnormalities. Maternal IL-6 induces distinct immune and endocrine changes in the placenta[117], and IL-6

responsiveness in placental trophoblasts is required for the development of MIA-associated behaviors[118].

Subsequent studies have identified the importance of IL-17a as a downstream mediator of ASD-associated phenotypes. IL-17a deficiency or the administration of blocking antibodies protects the offspring of poly(I:C)-treated dams from the development of behavioral deficits[119]. Direct intraventricular injection of IL-17a into fetal brains at E14.5 is sufficient to induce ASD-like behaviors in offspring[119]. The source of IL-17a in susceptible pregnancies was traced to the activity of maternal T helper 17 (Th17) cells, a RORγt-expressing subset of $CD4^+$ T cells[119]. Interestingly, the microbiome composition was key in modulating susceptibility to MIA because IL-17a is secreted by a memory Th17 population induced in the mother's gut only in the presence of segmented filamentous bacteria[120,121].

1.4.2 Schizophrenia

Despite the considerable etiological overlap with ASD, schizophrenia also exhibits distinct differences in risk factors and disease pathogenesis. Genetic risk factors for schizophrenia reveal links to both neurodevelopmental and immune genes. The most striking genetic association of schizophrenia is with the major histocompatibility complex (MHC) locus, which spans several megabases on chromosome 6[122]. This association is explained at least in part by copy number variation and isotype structure at the complement factor *C4* genes, *C4A* and *C4B*. Increased *C4A* copy number and expression is linked to increased schizophrenia risk. Interestingly, this association was especially pronounced for structural variants containing a human endogenous retrovirus (HERV) embedded in an

intron of the *C4* isotypes (*C4-HERV*); an increased copy number of *C4-HERV* was associated with a highly significant increase in risk[123]. Further studies are warranted to explore why dysfunction at the *C4* locus is associated with schizophrenia risk; most of the prevailing hypotheses have centered on the potential effects on postnatal synaptic pruning, but the existing links between *C4* and increased risk for infection and autoimmunity may also provide potential clues from an immunological framework of development[124].

Epidemiological studies further support the link between levels of various maternal immune factors and subsequent schizophrenia risk in offspring[125,126]. For example, elevated maternal levels of the complement factors (e.g., CRP, C1q)[124,127,128] and cytokines (e.g., IL-8/CXCL8, TNF-α)[129,130] during pregnancy have each been associated with significantly increased risk for psychosis in offspring. Analysis by MRI of a cohort of human patients exposed during their fetal life in the second or third trimester to maternal IL-8 also showed a dose-dependent association with structural brain changes commonly associated with schizophrenia[131].

In MIA models, other cytokines, including IL-1β and IL-10, have additionally been linked to vulnerability of offspring to schizophrenia[132,133]. Constitutive overexpression of IL-10 by macrophages prevents the development of long-term behavioral abnormalities in a poly(I:C)-induced mouse model of schizophrenia[134]. However, intriguingly, normal pregnancies are negatively impacted by IL-10 overexpression; in the absence of MIA, macrophage-driven IL-10 overproduction alone results in aberrant behaviors, suggesting the critical importance of cytokine balance in neurodevelopment[134]. As in ASD, there is evidence for persistent structural changes in the brains of offspring following transient exposure to MIA during early in utero development.

1.4.3 Summary of MIA models

MIA models have provided an important paradigm for the consideration of immunity during pregnancy. While major inroads have been made in characterizing the immune landscape of the maternal decidua, a comprehensive atlas of leukocyte composition and the expression of immune molecules at the maternal-fetal interface across time is absent. A better understanding of the pathways regulating leukocyte access and immune activation in the pregnant uterus would help pinpoint the relative contributions of systemic vs. local immunity to specific fetal outcomes. Similarly, the ability of maternal cytokines and other circulating immune factors to cross the maternal-fetal interface is poorly characterized, but has important implications for fetal pathogenesis. In many MIA models, it is unknown whether PAMPs or systemic maternal cytokines cross the maternal-fetal interface to directly impact fetal pathways of immunity, or if these factors trigger secondary pathways of signal transduction mediated by fetal tissues such as the placenta. Heterozygous crosses can be used in future studies to determine the relative contributions of maternal and fetal immune pathways to neurodevelopmental pathogenesis.

The expression of TLRs in the developing fetus and tissues of the brain in particular suggests that neural precursors may be PAMP-responsive. A major unanswered question remains as to the identity and source of the endogenous TLR ligands that guide neural development, as well as what factors control access to these ligands. A comprehensive molecular characterization of which precursors are expressing or co-expressing TLRs at each stage of development is also missing. There is evidence suggesting these TLR pathways intersect and interact with one another during neurogenesis, further complicating

an in-depth study of their functions in development[43,48]. Similarly, the function of complement factors expressed in the developing brain and their potential role in precursor migration or other programs remains to be elucidated. However, new technologies and even existing studies in the field of developmental neurobiology offer an opportunity to uncover new details regarding immune expression in early brain formation, for example in established single-cell sequencing datasets[135-137].

A deeper consideration of developmental timing is also critical to unraveling the mysteries behind the diverse manifestations of neurodevelopmental abnormalities. The rapid pace of changes on both sides of the maternal-fetal interface generates enormous variability and represents a major barrier in the execution, interpretation, and sharing of studies; details of embryonic dating and timing remains poorly standardized and reported in studies of prenatal development and MIA, even in mouse models. The character and intensity of exposures also contribute to differential outcomes in neurodevelopmental risk of disease and heterogeneity in MIA studies[109,138]. Finally, the complexity of modulating maternal factors such as the microbiome can profoundly impact pathogenesis; the contributions of maternal immune status must be better understood and standardized in future studies[109]. Understanding the relationships between maternal exposures, developmental timing, and subsequent phenotypes throughout life will be key to preventing MIA and treating its consequences (Figure 1.2).

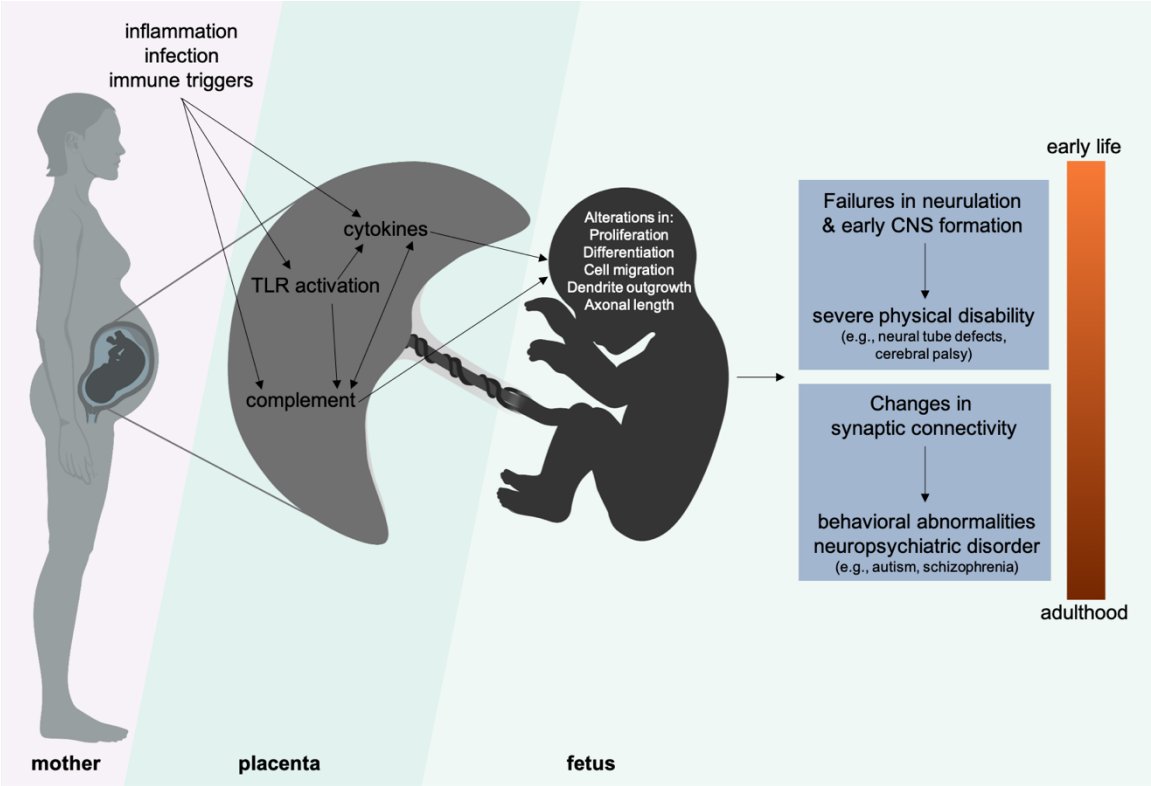

Figure 1.2: Maternal immune activation alters immune programs at the maternal-fetal interface to directly impact fetal neurodevelopment. Various maternal conditions (e.g., infection, inflammation, autoimmune disease) can lead to perturbations in immune factor expression at the maternal-fetal interface, leading to disruptions in neurodevelopment. Created with Biorender.com.

Regardless of these obstacles, the lifelong consequences of perturbed immunity in prenatal life provides a compelling drive for the continued expansion of this highly intersectional field. Indeed, an investigation of immunity has the potential to synergize with other fields to explain enduring mysteries, such as sex biases observed in various neuropsychiatric diseases[139]. Emerging evidence suggests that these skews may be driven by sex-based differences in prenatal responses to MIA, rather than by purely hormonal or endocrine pathways as widely presumed [140]. These processes also clearly represent a major avenue of investigation directly relevant to the prevention, intervention, and treatment of a vast array of neurological anomalies and disorders. Such work has the potential to not only

inform practices of prenatal screening and care, but also postnatal practices when considering the care of high-risk, MIA-exposed neonates.

1.5 Maternal inflammation and disorders of pregnancy

Many disorders of pregnancy are associated with maternal inflammatory states, either with or without an identifiable infectious cause. While bacterial and viral infections are known triggers of poor outcomes, in most cases of the following complications the etiology is unknown. In this section, I briefly summarize some of what is known about the contribution of the immune system to two mysterious and heterogenous disorders of pregnancy: preterm labor and preeclampsia.

1.5.1 Preterm labor

Labor is an inflammatory event driven by an influx innate immune cells into the pregnant uterus. By term, neutrophils, macrophages, and mast cells are among the key players primed at the reproductive tissues to initiate labor[141]. The activation of labor processes includes increased expression of inflammatory cytokines (e.g., IL-1β and TNF-α), chemokines, and matrix metalloproteases (e.g., MMP-8 and MMP-9) that serve to breakdown components of the extracellular matrix[142].

Preterm labor shares a common pathway of proinflammatory processes with normal labor; however, the switch to this proinflammatory state is pathologic and can be attributed to multifaceted processes. The leading cause of preterm labor is intrauterine infection leading to inflammation[143]. Both maternal and fetal immune pathways have been implicated in propelling preterm labor via the activation of TLRs and subsequent cytokine

and chemokine cascades[144,145]. Maternal and fetal T cells also contribute to the breakdown of maternal-fetal tolerance in preterm labor[142,146].

Mouse models of preterm labor have further elucidated the role of immune activation in the initiation of preterm labor. Intrauterine injection of LPS at midgestation (E14.5-16.5) leads to the initiation of parturition, with cytokine induction including TNF-α and IL-1β, a known driver of parturition[141,143]. In this model, fetal demise occurs in the majority of pups exposed to maternal LPS treatment, demonstrating a shared role for inflammatory effectors in driving both preterm labor and pregnancy loss.

1.5.2 Preeclampsia

Preeclampsia is a serious disorder of pregnancy characterized by the new onset of hypertension and typically presenting with proteinuria. It can present with or without severe features, such as central nervous system dysfunction, liver or renal function abnormalities, and thrombocytopenia. The complex etiology of preeclampsia remains unknown but it is now understood as a multisystemic syndrome with a significant inflammatory component rather than a simple hypertensive disorder[147]. Indeed, key inflammatory signals from the placenta are thought to play a distinct role in linking trophoblast oxidative stress to the signs of vascular dysfunction characteristic of preeclampsia[147,148], and circulating levels of proinflammatory cytokines such as IL-6 and TNF-α are increased in cases of preeclampsia compared to healthy controls[14]. Reduced Treg cell numbers and Treg/Th17 imbalance are also associated with the development of preeclampsia, suggesting a role for decreased maternofetal tolerance[14,148]. NK cells in preeclampsia similarly exhibit immune dysregulation with a disrupted ratio of IL-10 and

proinflammatory cytokines[149] and are proposed to play an important role in pathogenesis due to their role in early placentation. Their role in guiding trophoblast invasion and spiral artery remodeling involves critical interactions mediated by killer immunoglobulin-like receptors (KIRs) expressed by NK cells and HLA-C expressed by extravillous trophoblasts of the fetus, and certain combinations are more frequently observed in preeclamptic pregnancies[150]. NK cell dysfunction has also been proposed to contribute to the increased risk of preeclampsia seen in certain autoimmune diseases (i.e., systemic lupus erythematous and type 1 diabetes)[151].

1.6 Summary

Understanding the complex interplay between the immune system and fetal development is critical to advancing human health both during pregnancy and across the lifespan. Pregnancy is uniquely dependent on pathways and drivers of the immune system, which must continue to defend against pathogens while serving these physiological functions. Thus, the immune system must balance the broad responsibilities required of both defense and development, which evolved as complementary processes in favorable conditions but can conflict under conditions of stress or dysregulation. Infection and inflammation are capable of significantly disrupting the fine-tuned orchestration of immune pathways during gestation, which can have long-lasting consequences for maternal and fetal health. The rewiring of normal developmental programs can lead to altered homeostasis or prime individuals toward disease or pathogenesis manifesting much later in life.

In this dissertation, I describe three projects that expand our knowledge of the dynamic relationship between these dual functions of the immune system during pregnancy and fetal development: pathogen defense and physiological support. First, I describe a novel model of antiviral maternal immune activation leading to the development of fetal neural tube defects. I elucidate the immune pathways involved in translating systemic maternal responses to associated changes at the maternal-fetal interface and show that γδ T cells play a unique role in driving these poor fetal outcomes in response to maternal immune activation. Next, I describe a set of human studies investigating the impacts of SARS-CoV-2 infection on pregnancy. I demonstrate that while placental infection by SARS-CoV-2 is possible, the more frequent danger of maternal SARS-CoV-2 infection during pregnancy is inflammation and immune dysregulation that may increase the risk of pregnancy complications such as preeclampsia. Finally, I describe a direct investigation of the claims behind two popular COVID-19 misinformation theories surrounding fertility and pregnancy outcomes. These results add to the growing body of evidence supporting the safety of COVID-19 mRNA vaccines. Together, this body of work seeks to contribute to a collective understanding of the dynamic complexity of maternal-fetal interactions and how the immune system shapes both maternal and fetal health during pregnancy.

Chapter 2: Establishment and characterization of a novel model of maternal immune activation leading to fetal neural tube defects

2.1 Author Contributions

I conceived, designed, and oversaw all experiments with Akiko Iwasaki. I performed all experiments with assistance from Hannah J. Lee. Laura J. Yockey contributed experiments and data to the model of maternal immune activation. Emily Condiff performed immunofluorescence imaging of tissue sections. Arun Chavan and Scott D. Pope processed and analyzed bulk sequencing and spatial gene expression datasets from experiments that I performed. Orr-El Weizman contributed to flow cytometry experiments. Jeanne Hendrickson generously supplied *Cr1*$^{-/-}$*Cr2*$^{-/-}$ and *C3*$^{-/-}$ mice.

2.2 Summary

Antiviral immunity during pregnancy serves key defensive functions, but maternal immune activation (MIA) at the maternal-fetal interface can have significant consequences for the developing fetus. Using the TLR3 agonist and double-stranded RNA mimic

polyinosinic-polycytidylic acid, or poly(I:C), to induce antiviral responses in early pregnancy, I establish and characterize a novel mouse model of MIA that leads to a high incidence of neural tube defects (NTDs) and craniofacial defects in exposed litters. I demonstrate that NTD pathogenesis is dependent on maternal TLR3/TRIF signaling and interferon pathways, as well as the presence of γδ T cells. Poly(I:C)-induced MIA is associated with increased γδ T cell numbers and the loss of laminins at the ectoplacental cone in pregnant mice. *Tcrd*$^{-/-}$ mice deficient in γδ T cells, however, are protected from both laminin loss and the development of NTDs following poly(I:C) injection. Using spatial gene expression data, we pinpoint the localization of γδ T cell and laminin shifts at the maternal-fetal interface, as well as identify unique gene expression signatures and associations. This work is the first to describe the teratogenic potential of antiviral MIA in early pregnancy independent of viral infection. I demonstrate a novel role for γδ T cells at the maternal-fetal interface and propose a quality control function for γδ T cells that can lead to detrimental fetal outcomes in the context of activated antiviral immunity. Together, an expanded understanding of antiviral responses and maternal-fetal biology in early gestation may help to inform future approaches in the prevention of MIA in pregnancy and the management of MIA-associated complications such as NTD birth defects.

2.3 Introduction

During the most sensitive periods of pregnancy and *in utero* development, the activation of maternal immunity can have an outsized impact on fetal outcomes. The immune system propels the complex coordination of both pathogen defense and development, and the intertwined biology of these processes means that perturbations to

one can have the further consequence of disrupting the other. Maternal immune activation (MIA) has thus become increasingly recognized as a potential contributor to early development with the ability to shape fetal susceptibility to pathology and disease, not only during gestation but across the lifespan. The complex course of brain development appears particularly vulnerable to the effects of rerouted maternal immunity, with multiple studies demonstrating the links between midgestational MIA and the later development of brain pathologies such as behavioral abnormalities associated with autism spectrum disorder (ASD) and schizophrenia. Epidemiological studies have also suggested large-scale associations between MIA and the prevalence of neuropsychiatric disorders.

While the connections between MIA and disease have been most established in neuropsychiatric diseases that manifest in offspring long after the perinatal period, the recent Zika virus (ZKV) outbreak and its specific association with microcephaly has generated increased interest in other neurodevelopmental outcomes of infection and perturbed maternal immunity[12,138]. Studies of congenital abnormalities such as those induced by ZIKV in early pregnancy have largely focused on genetic susceptibility, known teratogens, and TORCH infections capable of directly invading fetal neurons and neuronal precursors. The resulting birth defects include neural tube defects (NTDs) such as exencephaly and anencephaly, which arise during poorly characterized timepoints in early gestation, often before individuals are even aware of a pregnancy. Despite being one of the most common birth defects worldwide, the myriad causes of structural brain abnormalities such as NTDs remain mysterious[152,153].

Interestingly, a common theme underlying many investigations of these etiologies is the intricate involvement of the immune system in directing or modulating outcomes.

For example, mouse models have implicated the complement pathway of the innate immune system in driving NTD formation in combination with environmental factors. A combination of dietary folate deficiency and E4.5 administration of an antagonist targeting C5aR during pregnancy induces a high rate of NTDs in offspring in the absence of an infectious or immunogenic stimulus[95]. While nutritional folate status has become the primary public health focus in NTD prevention today, a potential complement-mediated role in NTD pathogenesis accords with the observation that folate status in the mother appears to be a modulating factor, not a primary causative agent, in the development of NTDs and that a significant number of NTDs are refractory to folate supplementation[153].

Even the impact of known teratogens can be modulated by immunogenic agents. The medication valproic acid is known to cause a high incidence of NTDs in offspring exposed *in utero*, but the emergence of exencephaly phenotypes is effectively blocked by pretreatment with immunogenic agents such as pyran copolymer, bacillus Calmette Guérin (BCG), or Freund's complete adjuvant (FCA)[154]. Thus, the term MIA represents a broad and diverse array of immunomodulatory processes that together shape the immune landscape of the maternal-fetal interface in heterogeneous ways. These studies underscore the complexity inherent in the investigation of MIA influences on fetal development, and serve to emphasize that the specific balance of signals through various immune pathways is more important than a simplistic binary of activation or quiescence alone.

Finally, while there are no previously known studies of antiviral MIA leading to NTD formation, a number of rodent studies activating other antimicrobial responses in early pregnancy further demonstrate the potential of immune dysregulation to lead to teratogenesis. Administration of CpG oligodeoxynucleotide (ODN) at E6.5 in mice leads

to the development of NTDs in addition to craniofacial and distal limb defects[155,156]. CNS malformations in response to LPS exposure have also been characterized in E8.5 treatment of the golden hamster[157,158] and in a model of multiple injections across E7 to E16 in the rat[159]. In mouse models, either a single subcutaneous injection of LPS on E7.5, or a series of intraperitoneal LPS injections from E8.5 to E12.5 leads to increased incidence of severe neural tube defects such as exencephaly. LPS administration results in an increase in cytokines like TNF-α and direct administration of TNF-α during early pregnancy has been shown to recapitulate neural tube defects seen following LPS administration in mice[160].

Although these previous studies establish broad links between certain birth defects and antibacterial defense pathways, the mechanisms translating systemic maternal immunity into developmental shifts at the maternal-fetal interface remain elusive. Furthermore, viruses are among the most common pathogens encountered during pregnancy and in maternal infections. The potential contribution of antiviral immunity to the pathogenesis of structural birth defects, such as those seen in ZIKV or other viral TORCH infections, is unknown and has not yet been explored using a model system of MIA.

In this chapter, I present the first model of antiviral MIA in early pregnancy leading to fetal NTDs. I investigate the impact of antiviral MIA in early pregnancy on systemic maternal immunity, the immune landscape at the maternal-fetal interface, and ultimately the developing fetus *in utero*.

2.4 Results

2.4.1 Establishment of a novel model of maternal immune activation

In order to determine the impact of MIA on fetal outcomes in early pregnancy, I performed timed matings of C57BL/6J mice and administered 100 µg of poly(I:C) by intraperitoneal (i.p.) injection to pregnant dams on gestational day E7.5 (Figure 2.1, A). This period in early pregnancy is equivalent to the first trimester prior to the formation of the definitive placenta and the establishment of fetal circulation. Following poly(I:C)-induced MIA exposure in these syngeneic wild-type crosses, litters exhibited a high incidence of neural tube defects (NTDs), craniofacial abnormalities (CFAs), and eye defects (i.e., anophthalmia and microphthalmia) that were clearly evident at E12.5 and E17.5 (Figure 2.1, B-C). PBS-injected control pregnancies did not exhibit any incidence of NTDs, CFDs, or eye defects (Figure 2.1, C).

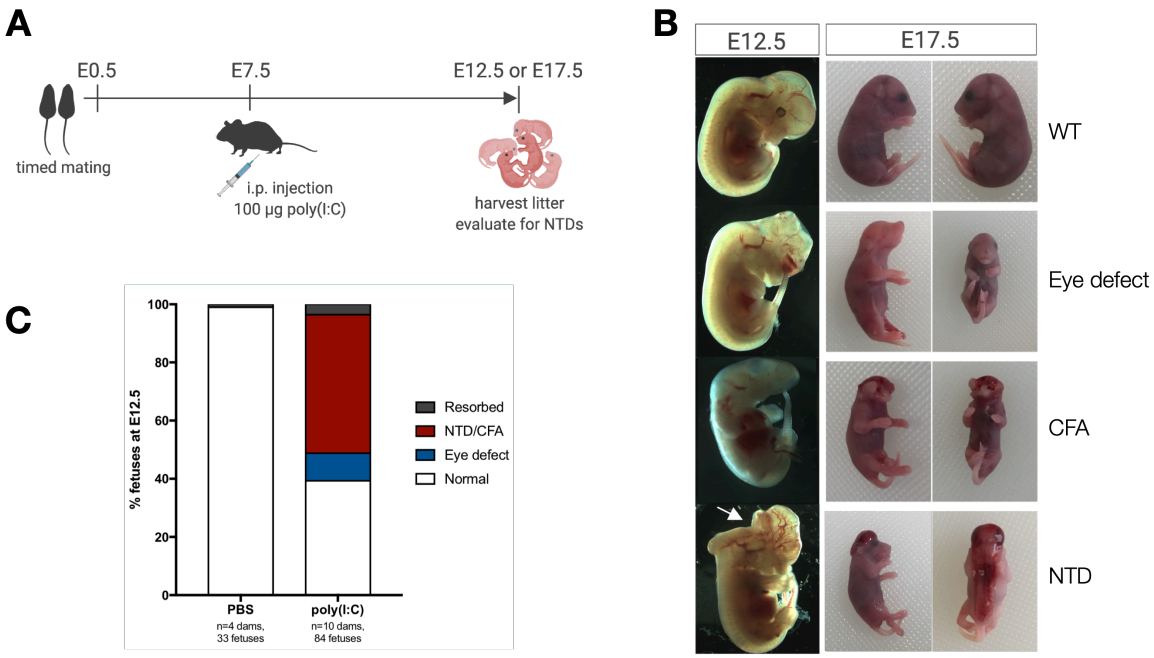

Figure 2.1: A novel model of maternal immune activation leading to neural tube defects. (A) Schematic of MIA model in early gestation. Timed matings were performed and presence of seminal plug was designated E0.5. Pregnant dams were injected i.p. with 100 µg of poly(I:C) at E7.5. Fetuses were collected at E12.5 and E17.5 for phenotypic analysis. (B) Examples of normal and abnormal fetal phenotypes following MIA. Wild-type (WT) phenotype is shown in comparison to eye defects, craniofacial abnormalities (CFAs), and neural tube defects (NTDs) at E12.5 and E17.5. (C) Quantitation of phenotypes observed in control PBS-treated pregnancies vs. poly(I:C)-treated MIA pregnancies.

The NTD phenotype was most frequently seen and commonly presented in tandem with CFAs and eye defects. In extremely rare cases, craniorachischisis was observed (Figure 2.1, B). Fetuses with NTDs, CFAs, and eye defects all survived to term. For the purposes of classification, NTD and CFA phenotypes were combined and considered together as one group in all analyses. In the sections to follow, I will characterize this model of poly(I:C)-induced MIA at E7.5 leading to these diverse presentations, with a particular focus on the NTD phenotype.

2.4.2 Characterization of the maternal-fetal interface by flow cytometry

To investigate whether MIA leads to changes in the composition of the maternal-fetal interface, I used flow cytometry to quantitate immune cell populations in the pregnant uterus. Pregnant C57BL/6J dams were subjected to i.p. injection of 100 ul of either PBS or 100 µg poly(I:C) at E7.5. 48 hours later at E9.5, tissues at the maternal-fetal interface were collected for analysis. The pregnant uterus was dissected to separate the outer maternal myometrium from the interior of each conceptus, containing largely fetus-derived tissues (e.g., fetus and extraembryonic tissues including trophoblasts, yolk sac) and associated maternal decidua (Figure 2.2).

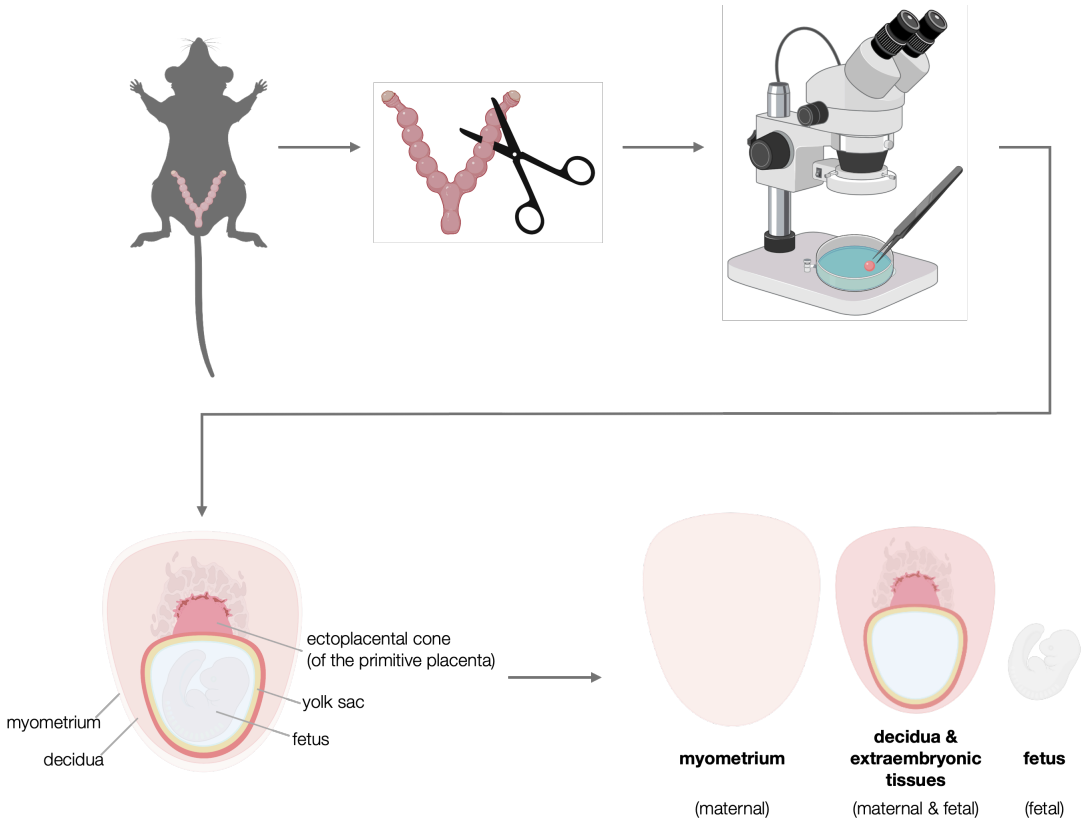

Figure 2.2: Approach to the dissection of the maternal-fetal interface. The pregnant uterus was isolated and individual concepti were dissected. Bottom depicts a cross-section view of the maternal-fetal interface and the separation of tissue components used for experiments.

I found a number of striking changes in the myeloid compartment of the maternal fetal interface including a major loss of dendritic cells (DCs) globally from the maternal-fetal interface. Monocytes increased in maternal myometrium but not in mixed-origin trophoblast and decidual tissue, but there were no changes in macrophages. Neutrophils were slightly increased in fetal and primitive placental tissue along with decidua, but not in the myometrium (Figure 2.3).

Lymphoid populations were similar in control and MIA-exposed pregnancies. Poly(I:C) treatment was associated with a slight increase in NK cells in both the

myometrium and decidua/trophoblast, as well as increased expression of proliferation marker Ki67 (Figure 2.4).

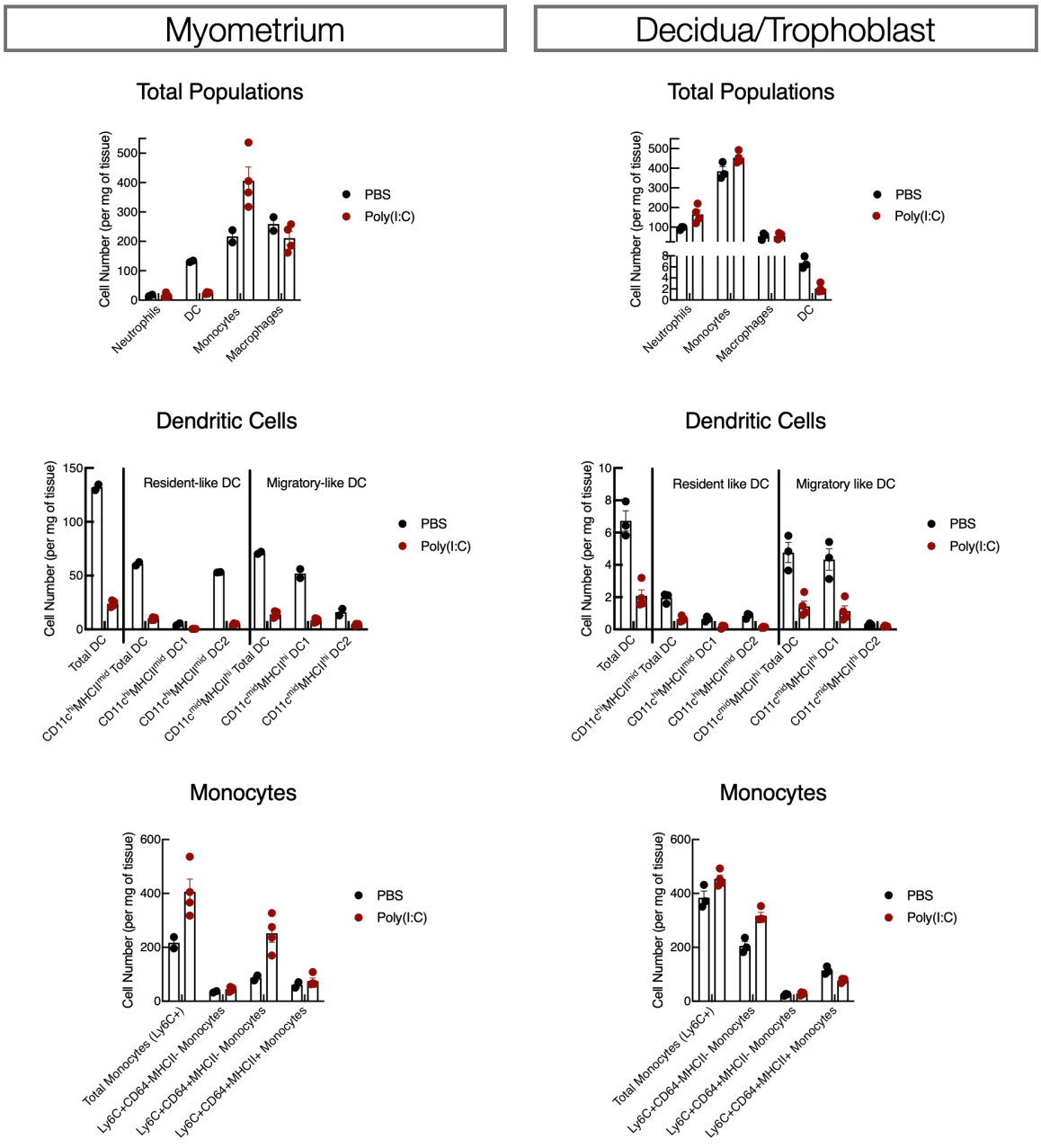

Figure 2.3: Shifts in myeloid populations following MIA. Pregnant C57BL/6J dams were i.p. injected with either PBS or 100 µg poly(I:C) at E7.5 and tissues were collected 48 hours later on E9.5. Flow cytometry of E9.5 myometrium (left) and pooled decidua and extraembryonic tissues (right) showing total myeloid populations, dendritic cells (DCs), and monocytes.

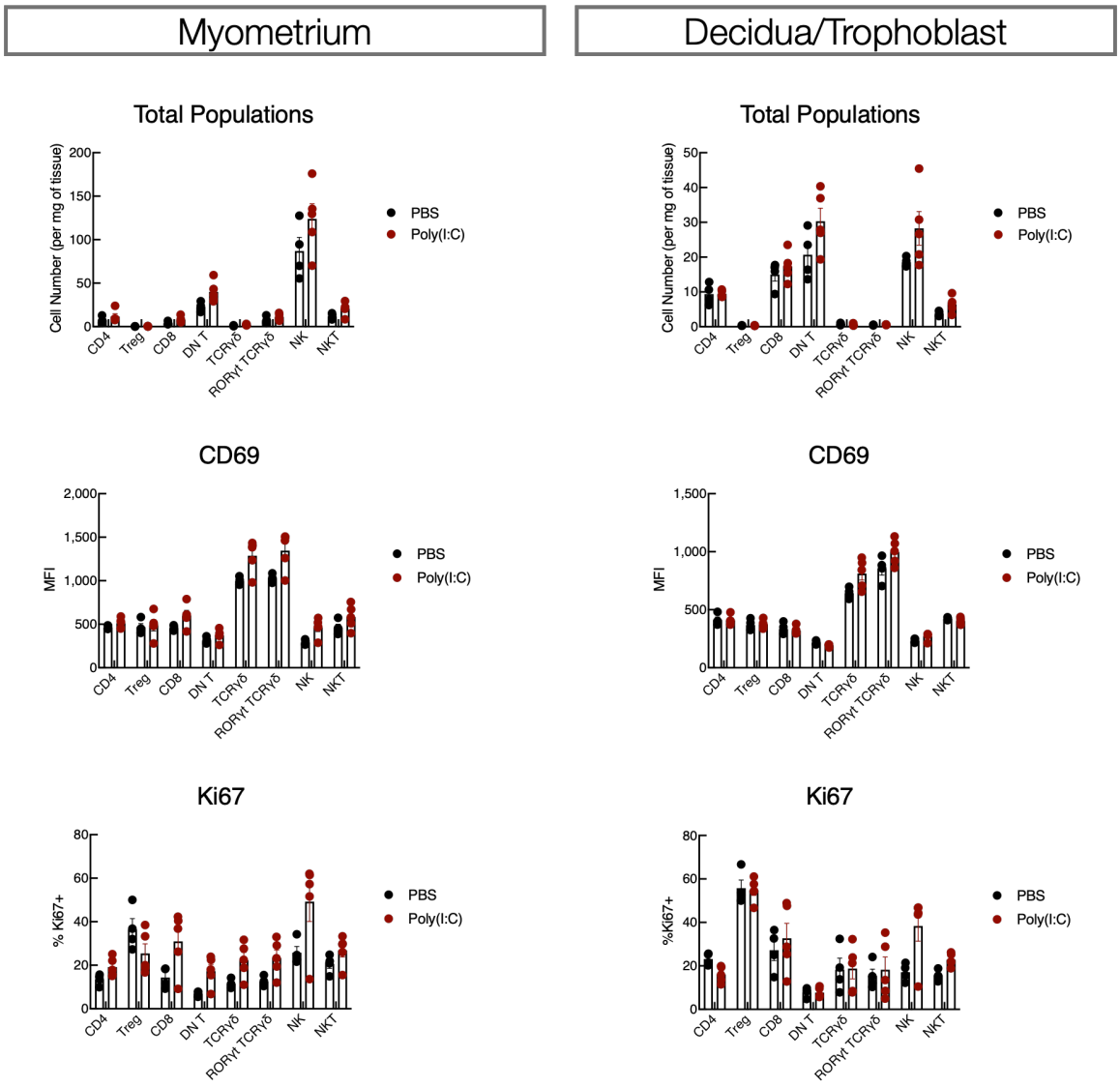

Figure 2.4: Shifts in lymphoid populations following MIA. Pregnant C57BL/6J dams were i.p. injected with either PBS or 100 µg poly(I:C) at E7.5 and tissues were collected 48 hours later on E9.5. Flow cytometry of E9.5 myometrium (left) and pooled decidua and extraembryonic tissues (right) showing total lymphoid populations, mean fluorescence intensity (MFI) of CD69 activation marker, and Ki67 proliferation marker.

2.4.3 Identification of immune populations and pathways driving MIA-induced NTD phenotype

Using genetic knockout mice, I explored the immunological requirements leading to the development of NTDs following poly(I:C)-induced MIA in early pregnancy.

Poly(I:C) is a double-stranded RNA mimic, which can be sensed by either TLR3 or RIG-I-like receptors (RIG-I and MDA5)[161,162]. To determine the relevant pattern recognition receptors involved in this model of MIA, we crossed mice deficient in either TRIF, the adaptor protein required for downstream TLR3 signaling, or MAVS, a key signaling protein in RIG-I-like signaling pathways. Litters from both crosses of *Trif*$^{-/-}$ mice and crosses of *Trif*$^{-/-}$ females to wild-type C57BL/6J males were all protected from the development of NTDs, while crosses of *Mavs*$^{-/-}$ mice were not (Figure 2.5, A).

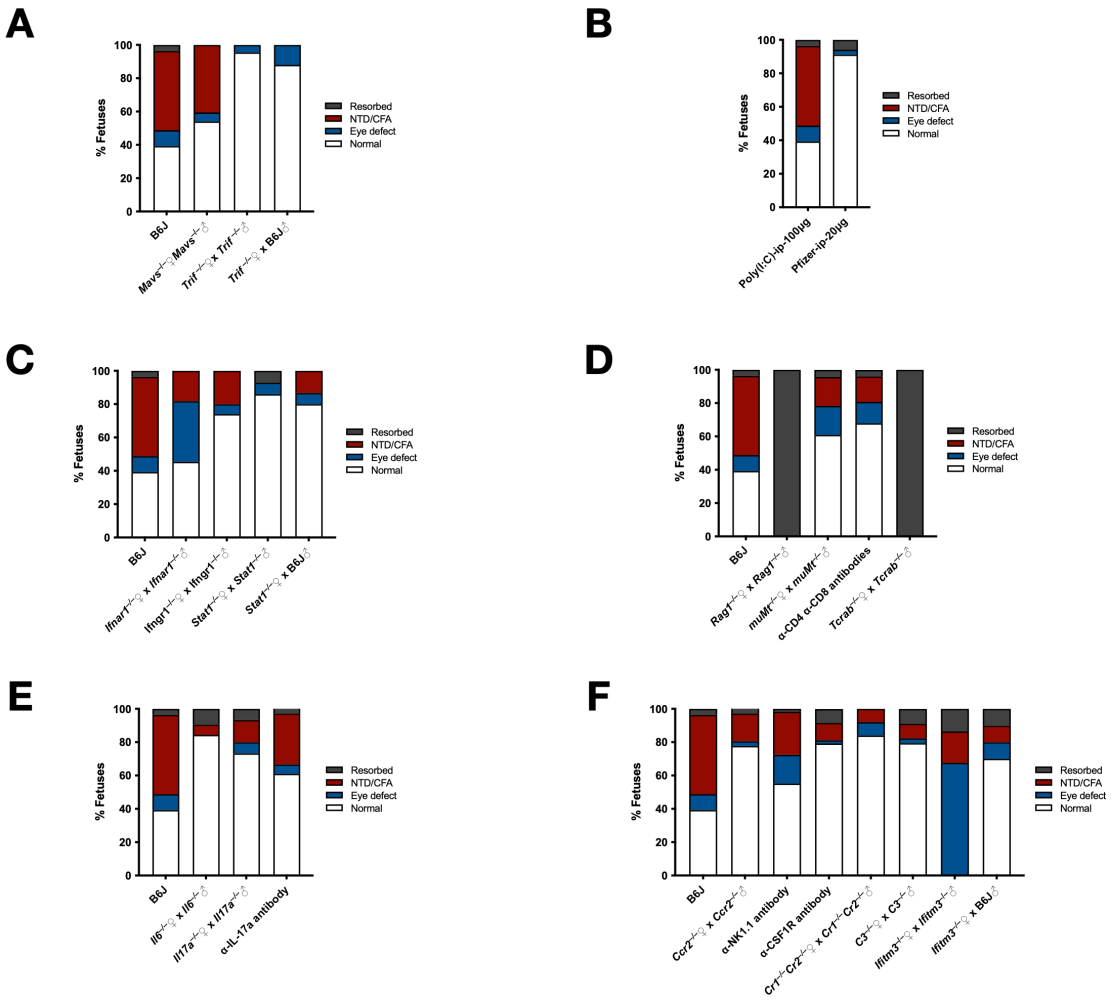

Figure 2.5: Immune pathways involved in NTD formation following MIA. All crosses shown were subjected to i.p. injection of poly(I:C) at E7.5. Litters were harvested at E12.5 for phenotyping. Genotypic background of crosses or antibody depletion status are indicated. Shown are phenotypic data from experiments investigating the contribution of: (A) pattern recognition receptors, (B) interferon pathways, (C) SARS-CoV-2 mRNA vaccine, (D) adaptive immunity, (E) IL-6 and IL-17a pathways, and (F) other immune components surveyed.

Given the requirement of TLR3/TRIF signaling for NTD pathogenesis following MIA and its relevance to vaccine safety during pregnancy, I investigated whether the SARS-CoV-2 mRNA vaccines such as Pfizer-BioNTech BNT162b2 could induce poor fetal outcomes comparable to the effects of poly(I:C) when administered at E7.5. 20 μg of BNT162b2 was i.p. injected into C57BL/6J pregnant dams at E7.5 and no NTDs or abnormal phenotypes were observed (Figure 2.5, B).

Type I interferons are known to play a role in fetal demise during Zika virus infection in early pregnancy[163]. However, applying our model to *Ifnar1*$^{-/-}$ crosses, I found that type I interferon signaling is not required for manifestation of MIA-induced NTDs (Figure 2.5, B). Type II interferon signaling is also not required for MIA-induced NTDs as demonstrated using *Ifngr1*$^{-/-}$ mice (Figure 2.5, C). To test for redundancy between type I and type II interferons in our system, we used *Stat1*$^{-/-}$ females crossed to *Stat1*$^{-/-}$ males, and found that fetuses were protected from NTDs (Figure 2.5, C). When we crossed *Stat1*$^{-/-}$ females to C57BL/6J males, fetuses were also largely protected from NTDs, but there was a very low incidence of NTDs in this group (Figure 2.5, C), indicating that in rare cases intact fetal STAT1 signaling can be sufficient to drive this phenotype even in the absence of maternal STAT1 signaling.

After interrogating the components of innate immunity contributing to poly(I:C)-induced NTDs, we wanted to explore the relative contributions of the adaptive immune system to this MIA phenotype. Crosses of *muMt*$^{-/-}$ mice demonstrated that B cells are not required for MIA-associated NTD development and antibody-mediated depletion of CD4 and CD8 T cells also were not protective (Figure 2.5, D). Notably, the administration of

100 μg poly(I:C) at E7.5 to crosses of *Rag1*$^{-/-}$ mice devoid of T and B cells led to 100% fetal loss in all treated litters (Figure 2.5, D).

Given the importance of IL-6 and IL-17a signaling in previously established MIA models of ASD-like behavioral abnormalities (see Section 1.4), I investigated whether IL-6 and IL-17a signaling are required for NTD development in our model of MIA in early gestation. Neither cytokines were required as demonstrated in knockout crosses of *Il6*$^{-/-}$ mice and *Il17a*$^{-/-}$ mice treated with poly(I:C) (Figure 2.5, E), although the rate of NTD formation was reduced particularly in *Il17a*$^{-/-}$ crosses. In IL-17a depletion experiments using i.p. injection of anti-IL-17a antibodies, fetuses similarly were not protected from NTD formation (Figure 2.5, E).

I tested a number of other knockout crosses in order to determine whether other previously implicated immune cell types and pathways were critical for MIA-induced NTD development. A wide array of players tested including monocytes, complement factors, and other cytokines/chemokines were not critical to driving the NTD phenotypes following poly(I:C) exposure (Figure 2.5, F). Interestingly, all fetuses from homozygous *Ifitm3*$^{-/-}$ crosses exhibited a complete absence of eyes following poly(I:C)-induced MIA (Figure 2.5, F).

The most striking finding in exploring these immune pathways was that γδ T cell-deficient pregnancies using crosses of *Tcrd*$^{-/-}$ mice are protected from NTD formation in our model of poly(I:C)-induced MIA (Figure 2.6, A). Additionally, *Tcrd*$^{-/-}$ females crossed to wild-type C57BL/6J males were largely protected, but an extremely low incidence of NTDs following poly(I:C) administration was observed (Figure 2.6, A). Given the importance of circulating maternal IL-6 and IL-17a in driving other MIA-associated

phenotypes, I investigated whether levels of these key cytokines in MIA-exposed wild-type and *Tcrd*$^{-/-}$ pregnancies. IL-6 and IL-17a levels did not differ between C57BL/6J and *Tcrd*$^{-/-}$ crosses (Figure 2.6, B).

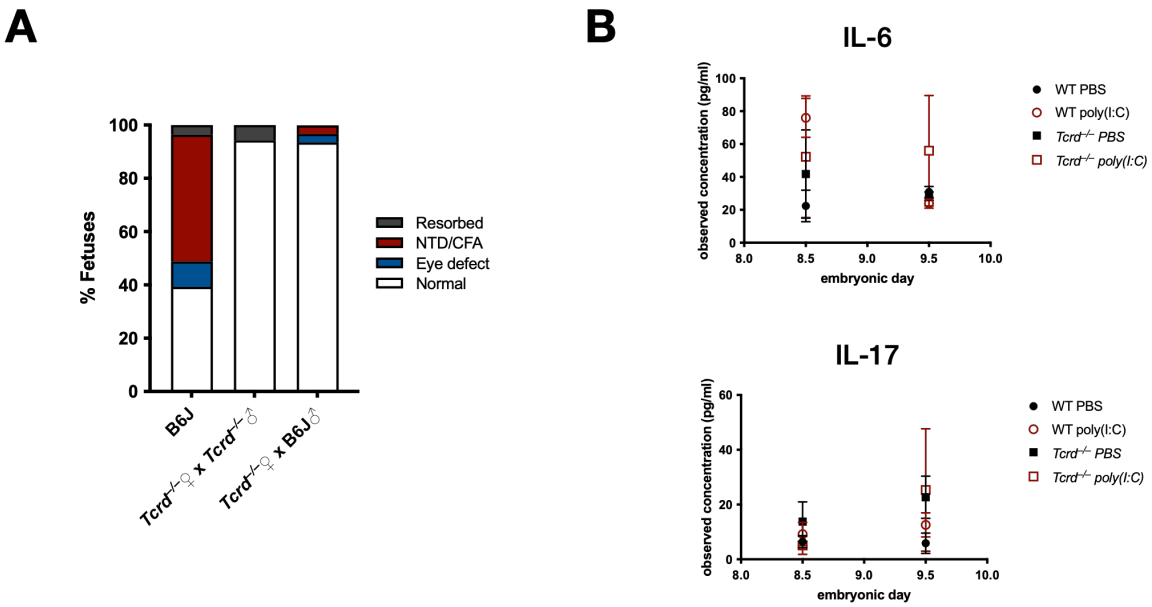

Figure 2.6: *Tcrd*$^{-/-}$ mice are protected from NTD development following MIA. Maternal gamma delta T cell deficiency is associated with . (A) *Tcrd*$^{-/-}$ females were crossed to *Tcrd*$^{-/-}$ or B6J males and i.p. injected with poly(I:C) on E7.5. Fetal phenotypes were assessed at E12.5 and quantified as shown. (B) Maternal serum from MIA-exposed pregnant dams was collected at E8.5 and E9.5, 24 and 48 hours following either PBS or poly(I:C) injection at E7.5. All data were generated from homozygous crosses of either C57BL/6J (WT) or *Tcrd*$^{-/-}$ mice (n=3 per condition). Horizontal bars represent mean values and standard deviation is shown.

2.4.4 γδ T cells at the maternal-fetal interface

Considering the low number of γδ T cells at the maternal-fetal interface described earlier by flow cytometry (Figure 2.4), I further explored the characteristics of this population. Although the γδ T cell population represents a minor proportion of the immune cells at the maternal-fetal interface, the majority of γδ T cells in the maternal myometrium and a substantial number in the decidua/trophoblast region are RORγt^{+} with roughly a third in all tissues exhibiting IL-17 production following stimulation (Figure 2.7).

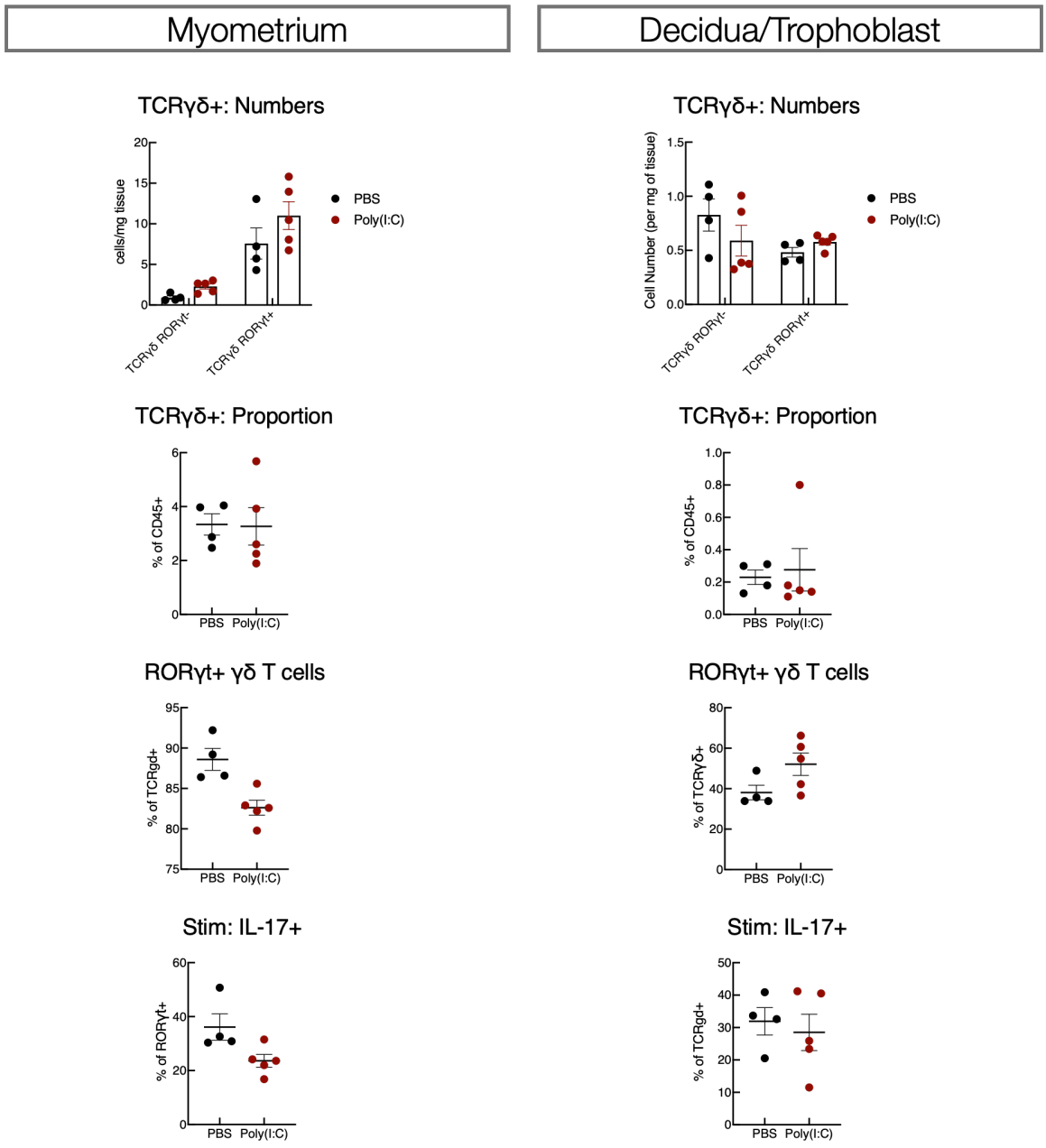

Figure 2.7: TCRγδ⁺ populations following MIA. Pregnant C57BL/6J dams were i.p. injected with either PBS or 100 µg poly(I:C) at E7.5 and tissues were collected 48 hours later on E9.5. Flow cytometry of E9.5 myometrium (left) and pooled decidua and extraembryonic tissues (right) showing γδ T cell numbers and proportions, RORγt T cells, and IL-17 expression following 4-hour stimulation.

To further investigate the contribution of γδ T cells to the maternal-fetal interface in the MIA model, I collected, fixed, and visualized the pregnant uterus in cross section (Figure 2.8, A) to determine the distribution of γδ T cells in the pregnant uterus at E9.5, 48

hours after maternal poly(I:C) administration. Consistent with my findings by flow cytometry, γδ T cells were detected at the E9.5 maternal-fetal interface at low frequency in control PBS-treated pregnant dams. γδ T cells were most commonly found at the ectoplacental cone region (EPC) and the yolk sac, as well as in surrounding tissues (Figure 2.8, B and C). Comparing control PBS-treated tissues to poly(I:C)-treated tissues exposed to MIA, γδ T cells were found in increased number in the ectoplacental cone region of the maternal-fetal interface (Figure 2.8, C).

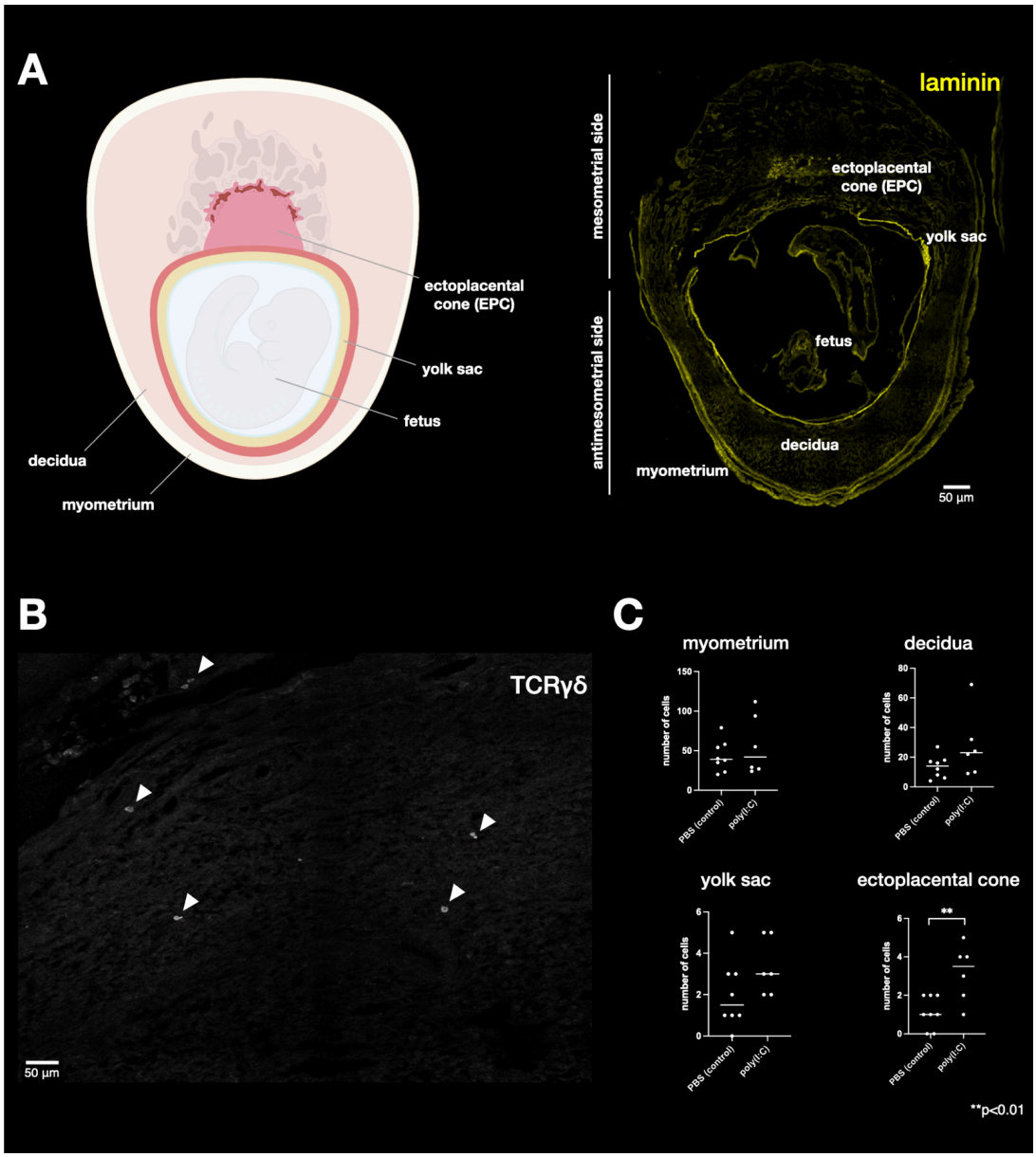

Figure 2.8: TCRγδ$^+$ populations at the E9.5 maternal-fetal interface following MIA. (A) Schematic of the maternal-fetal interface and corresponding tissue view with pan-laminin staining. (B) Identification of γδ T cells at the maternal-fetal interface. (C) Quantification of γδ T cells counted at various regions of the E9.5 maternal-fetal interface, 48 hours following either PBS or poly(I:C) injection at E7.5. Horizontal bars represent mean values. **p<0.01.

Next, I used RNA sequencing to identify key differences between MIA-exposed interfaces from C57BL/6J crosses vs. *Tcrd*$^{-/-}$ crosses. In both wild-type and *Tcrd*$^{-/-}$ pregnancies, poly(I:C) administration was associated with robust induction of antiviral responses and immune gene expression. To pinpoint the specific differences between NTD-forming conditions (i.e., poly(I:C)-treated wild-type crosses) and non-NTD-forming conditions (i.e., all other groups: PBS-treated C57BL/6J, PBS-treated *Tcrd*$^{-/-}$, and poly(I:C)-treated *Tcrd*$^{-/-}$), I performed a direct analysis of differential gene expression between these groups. I detected decreased expression of the *Lamc2* gene in the E9.5 mixed-origin fetal and maternal decidual tissues of the NTD-forming group compared to all groups without NTD development (Figure 2.9, A). Decreased *Lamc2* expression was also observed in the E8.5 myometrium (Figure 2.9, B). This finding suggests that changes in laminin expression at the maternal-fetal interface is associated with MIA leading to increased NTD risk. Other differentially expressed genes of note in this analysis include a number of trophoblast markers including *Tpbpb, Tpbpa,* and *Prl2c2* shown (Figure 2.9, A-B).

Finally, gene ontology (GO) was used to analyze differential gene expression between poly(I:C)-treated *Tcrd*$^{-/-}$ crosses and poly(I:C)-treated C57BL/6J crosses. At E9.5, the majority of GO terms enriched in *Tcrd*$^{-/-}$ downregulated transcripts were related to immune responses and pathogen defense in the myometrium, whereas GO terms related

to developmental and metabolic pathways dominated in the decidua/trophoblast compartment (Figure 2.9, C).

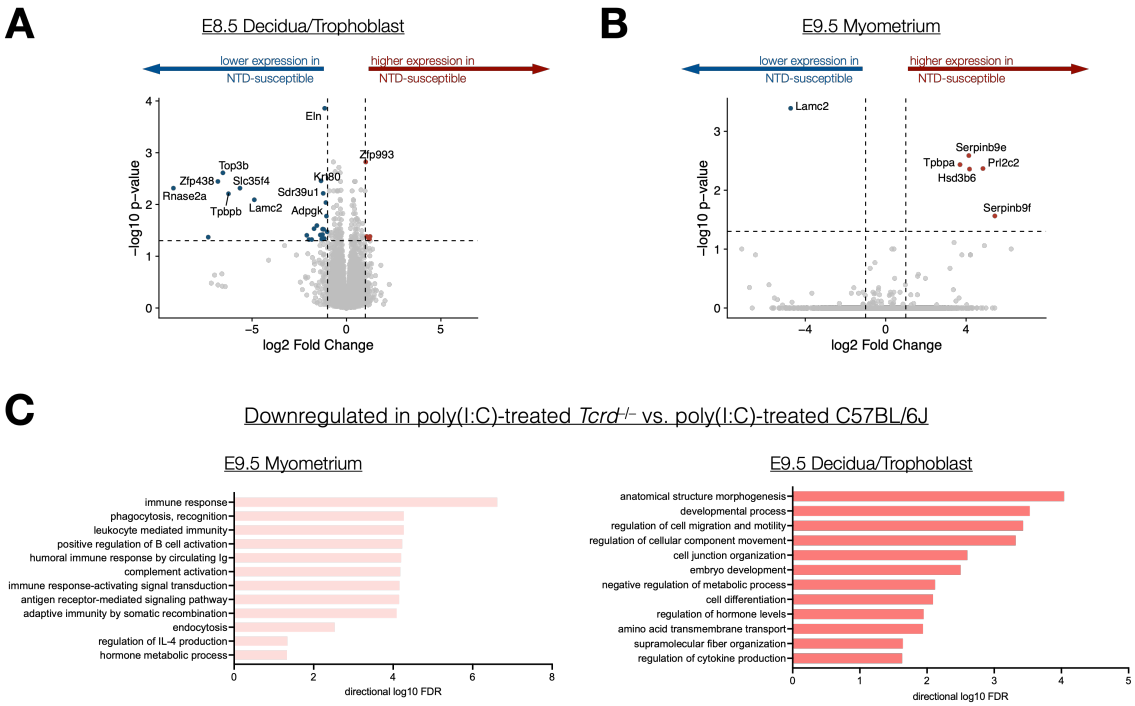

Figure 2.9: Bulk sequencing of the maternal-fetal interface shows sequential loss of *Lamc2* and changes in trophoblast marker expression in the E8.5 decidua/trophoblast and E9.5 myometrium. Bulk sequencing was performed on dissected myometrial and decidual/trophoblast tissues from the maternal-fetal interface of homozygous C57BL/6J crosses or *Tcrd*$^{-/-}$ crosses at E8.5 and E9.5, following treatment with either PBS or poly(I:C). (A and B) Volcano plots indicating differentially expressed genes between NTD-susceptible group (i.e. poly(I:C)-treated C57BL/6J only) and NTD-resistant group (PBS-treated C57BL/6J, PBS-treated *Tcrd*$^{-/-}$, poly(I:C)-treated *Tcrd*$^{-/-}$) from bulk RNA-seq of E8.5 decidua/trophoblast tissue (A) and E9.5 myometrium (B). Significant hits with an absolute log2 fold change>2 and p <0.00001 are color-labeled. Blue points indicate transcripts that are decreased in poly(I:C)-treated C57BL/6J (NTD-susceptible) compared to all other groups (NTD-resistant). Red points label transcripts that are increased in poly(I:C)-treated C57BL/6J (NTD-susceptible) compared to all other groups (NTD-resistant). (C) Gene ontology of differentially expressed genes (p<0.05) between poly(I:C)-treated *Tcrd*$^{-/-}$ pregnancies and poly(I:C)-treated C57BL/6J pregnancies was performed. Downregulated transcripts in poly(I:C)-treated *Tcrd*$^{-/-}$ pregnancies are shown from E9.5 myometrium (left) and E9.5 decidua/trophoblast (right).

2.4.5 Loss of laminin at the maternal-fetal interface

Using immunofluorescence confocal microscopy, we visualized laminins at the maternal-fetal interface of wild-type pregnancies exposed to either PBS or poly(I:C) at

E7.5. Imaging reveals that laminins are most concentrated at the ectoplacental cone of the maternal-fetal interface (Figure 2.10, A). Poly(I:C)-induced MIA in wild-type C57BL/6J mice led to loss of laminin at the ectoplacental cone in maternal-fetal interfaces examined as compared to control mice treated with PBS (Figure 2.10, A).

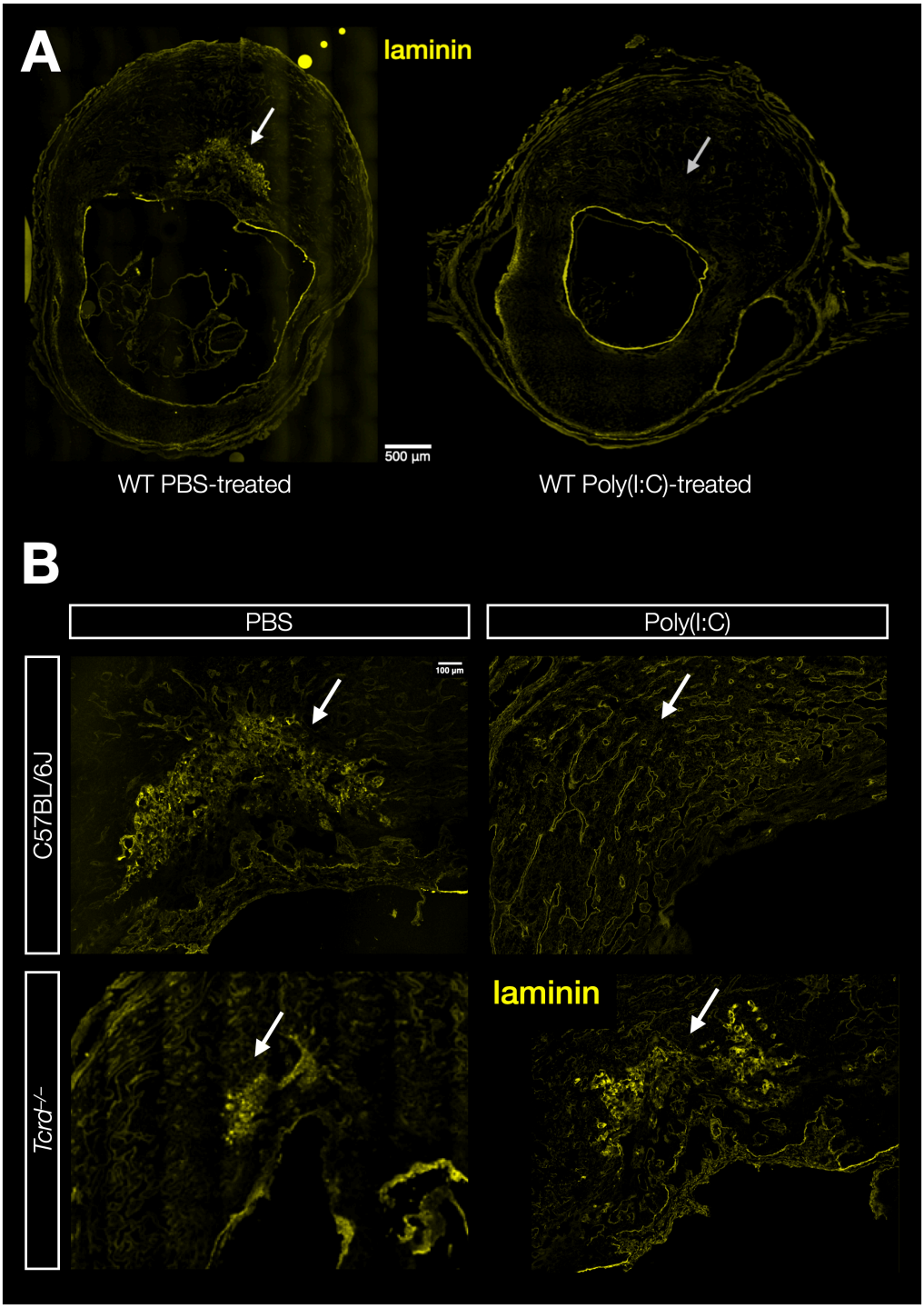

Figure 2.10: *Tcrd*$^{-/-}$ pregnancies are protected from MIA-associated laminin loss at the E9.5 maternal-fetal interface. (A) Pan-laminin staining of the C57BL/6J wildtype (WT) E9.5 maternal-fetal interface, 48 hours following either PBS or poly(I:C) injection at E7.5. Laminins are concentrated at the EPC region in control PBS-treated pregnancies and absent in poly(I:C)-treated pregnancies (white arrows). (B) *Tcrd*$^{-/-}$ pregnancies do not exhibit MIA-associated laminin loss at the EPC region of the E9.5 maternal-fetal interface following poly(I:C)-induced MIA at E7.5. Pan-laminin staining of EPC region of wildtype C57BL/6J and *Tcrd*$^{-/-}$ crosses. Pregnant dams were i.p. injected with either PBS or poly(I:C) at E7.5 and tissue was collected for analysis at E9.5. EPC laminins are absent in poly(I:C)-treated C57BL/6J pregnancies, but are present in poly(I:C)-treated *Tcrd*$^{-/-}$ interfaces, similar to control PBS-injected C57BL/6J and *Tcrd*$^{-/-}$ tissues (white arrows).

Next, we analyzed laminin expression in γδ T cell-deficient interfaces using homozygous *Tcrd*$^{-/-}$ crosses. In tissues collected from PBS-treated *Tcrd*$^{-/-}$ pregnancies, laminins were concentrated in the ectoplacental cone region similar to PBS-treated C57BL/6J pregnancies (Figure 2.10, B). Strikingly, however, *Tcrd*$^{-/-}$ interfaces exposed to poly(I:C)-induced MIA in our model also exhibited significant laminin expression at the ectoplacental cone and did not display a loss of laminins in this region as observed in poly(I:C)-treated C57BL/6J interfaces (Figure 2.10, B).

2.4.6 Investigating changes at the fetal neural tube in MIA model of NTD pathogenesis

Given the myriad of changes taking place at the maternal-fetal interface, I directly explored the nature of these effects on fetal neural progenitors by using the proliferation marker phospho-histone H3 (p-hH3) to quantify mitotic cells at the fetal neural tube. E9.5 fetuses were harvested and fixed, 48 hours following either PBS or poly(I:C) treatment at E7.5. Axial sections of the fetal neural tube were obtained and subjected to immunofluorescence staining with an anti-p-hH3 antibody (Figure 2.11, A). By restricting this analysis to a defined section of the fetal neural tube only and counting proliferative

cells over area, I found that proliferation rates at the fetal neural tube are decreased in poly(I:C)-treated fetuses compared to PBS-treated controls (Figure 2.11, B-C).

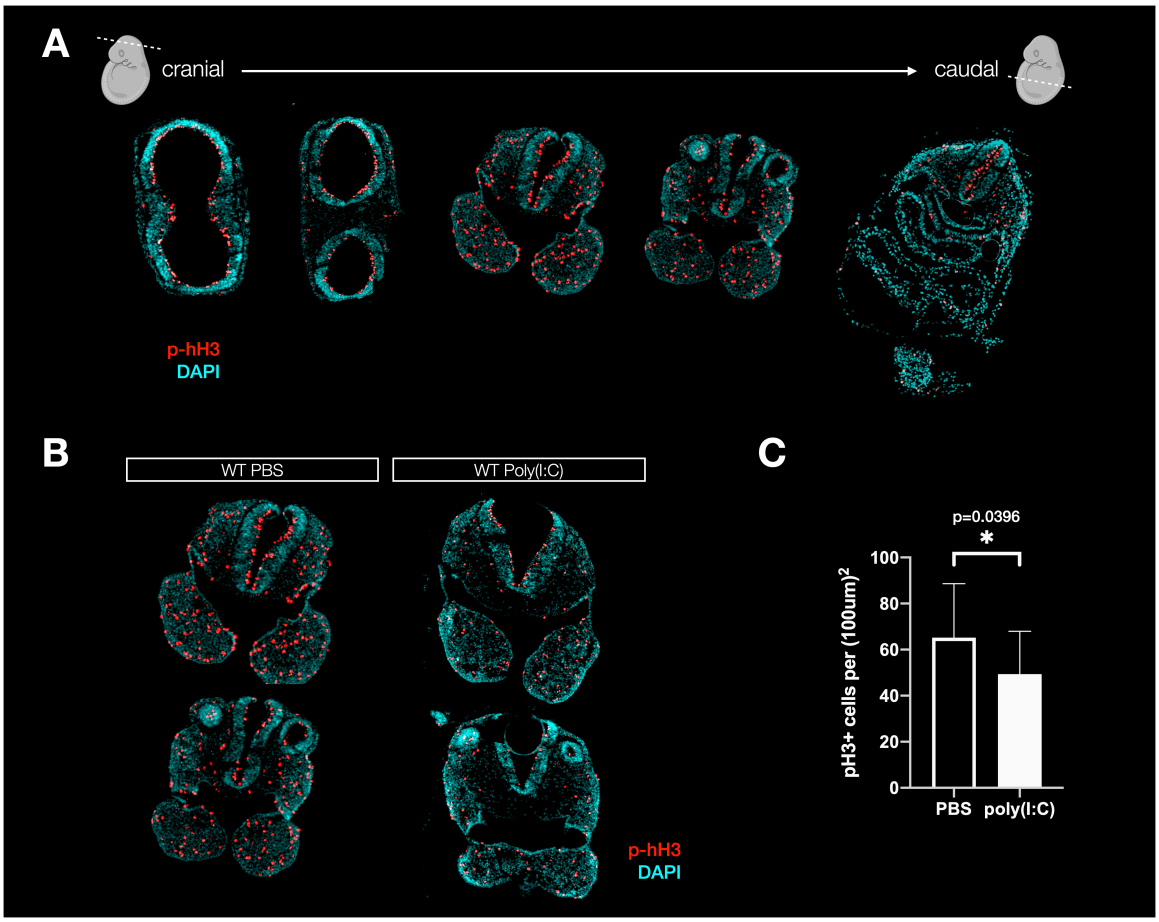

Figure 2.11: MIA is associated with decreased proliferation at the fetal neural tube. (A) Axial sections of the E9.5 fetal neural tube. (B) Representative images of the cranial neural tube in fetuses from either PBS-treated or poly(I:C)-treated pregnancies. (C) Quantitation of p-hH3+ cells in the fetal neural tube of PBS control vs. poly(I:C)-treated litters.

2.4.7 Interrogating γδ T cell-laminin-NTD links using spatial gene expression with 10x Visium

In order to investigate the association between γδ T cell, laminin expression, and fetal neural tube closure in our model of MIA, we used 10x Visium Spatial Gene Expression to investigate gene expression changes in wild-type C57BL/6J vs. *Tcrd*$^{-/-}$ maternal-fetal interfaces. Pregnant dams were injected with either PBS or poly(I:C) at E7.5

and concepti were harvested at E9.5, 48 hours post-treatment (n=2 biological replicates per condition, n=8 capture regions total).

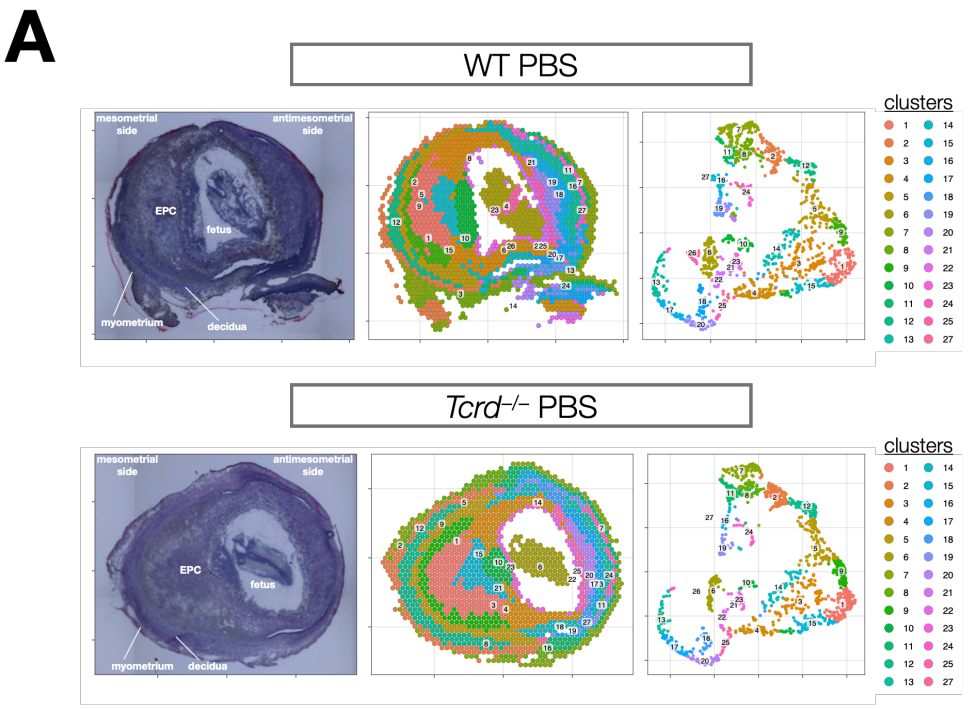

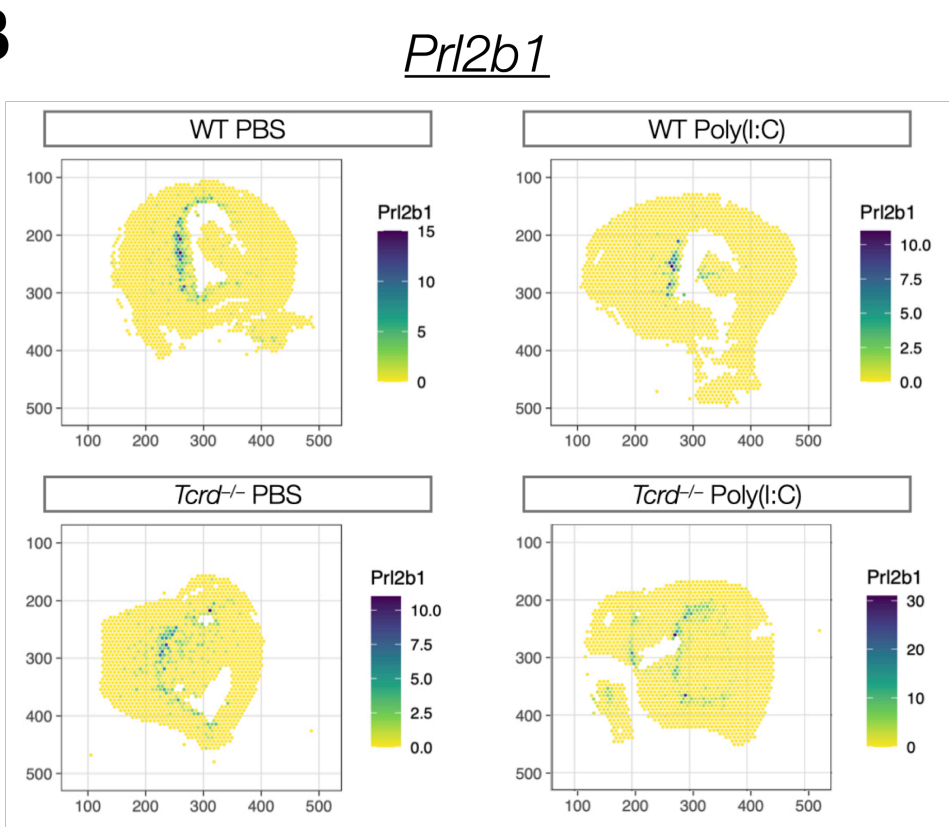

Figure 2.12: Mapping the maternal-fetal interface during MIA with spatial gene expression. (A) Spatial gene expression mapping and clusters of the maternal-fetal interface. Shown are H&E staining, spatially resolved capture spots, and identified clusters for control PBS-treated WT (C57BL/6J) and *Tcrd*$^{-/-}$ sections. Clusters were determined by differentially expressed genes and are represented by color. (B) Plot of spatially mapped Prl2b1 transcripts in the maternal-fetal interface of WT and *Tcrd*$^{-/-}$ crosses treated with either control PBS or poly(I:C) to induce MIA.

Clusters were generated and captured key regions including the ectoplacental cone (cluster 15; Figure 2.12, A). Furthermore, mapped clusters exhibited similar expression patterns across WT and *Tcrd*$^{-/-}$ interfaces and conditions (Figure 2.12, A). While single-gene and interaction analyses of these data are still ongoing, we used this platform to visualize the expression of trophoblast-specific *Prl2b1* (Figure 2.12, B), a placental hormone previously implicated in midgestational MIA[118] and a differentially expressed gene in our bulk dataset analysis.

Cluster	WT			*Tcrd*$^{-/-}$		
	Average log2FC	P_{adj}	Direction of change	Average log2FC	P_{adj}	Direction of change
1	-3.44	1.58×10^{-3}	down	0.27	1.00	unchanged
4	-2.63	2.18×10^{-5}	down	3.52	9.26×10^{-1}	unchanged
13	0.27	4.29×10^{-3}	up	-1.81	1.00	unchanged

Table 2.1: Poly(I:C)-induced MIA is associated with cluster-specific changes in *Lamc2* expression in WT but not *Tcrd*$^{-/-}$ crosses.

Poly(I:C) treatment was associated with significant differences in *Lamc2* expression in clusters 1, 4, and 13 for WT samples, but *Lamc2* expression at the maternal-fetal interface was unchanged in these clusters for *Tcrd*$^{-/-}$ samples (Table 2.1), consistent with results of our bulk sequencing analysis. Future work will focus on localizing key transcriptional changes at the maternal-fetal interface not only to clusters but to capture spots at higher resolution and analyzing interactions patterns in these regions. Among other goals, we plan to locate capture spots exhibiting *Tcrd* expression and determine gene

expression changes in these capture spots across conditions to ultimately link γδ T cell function and the associated gene expression patterns regionally to laminin loss programs and risk of NTD formation.

2.5 Discussion

This work represents the first model of antiviral maternal immune activation leading to NTDs. While there exist other models of NTD formation such as genetic knockout mice and LPS- or CpG-based models, this is the first study to implicate antiviral defenses of innate immunity as a potential driver of poor fetal outcomes including exencephaly, agnathia, and anophthalmia. These findings are thus relevant to the high rate of viral infections, including the majority of TORCH infections, experienced annually during pregnancy that result in significant morbidity and mortality worldwide.

I show that NTD formation following poly(I:C)-induced MIA is maternal TLR3/TRIF-dependent and that the interferon response via STAT1 plays an important role in driving pathogenesis. The TLR3 dependence of this poly(I:C)-driven phenotype is notable for its relevance to vaccine design and safety. I find that i.p. administration of the COVID-19 mRNA vaccine Pfizer-BioNTech BNT162b2 does not induce NTD formation or teratogenesis, likely due to rational design approaches including targeted N1-methylpseudouridine (m1Ψ) substitutions that reduce the activation of TLR3 pathways[164]. These results therefore have the potential to inform investigations of vaccine safety as further described in Chapter 4.

Furthermore, we demonstrate that this model of antiviral MIA operates via pathways distinct from other models of poly(I:C)-induced MIA leading to behavioral

abnormalities. While previously described MIA models demonstrate that the development of behavioral abnormalities is dependent on systemic IL-6 and IL-17a production, our experiments with knockout mice and antibody-mediated depletion of these cytokines shows that NTDs are not eliminated. Maternal SFB status and fetal sex were also not modulating factors for risk of NTD development.

While I focused on NTD phenotypes in this study, a number of crosses demonstrated that the eye defect phenotype seen in poly(I:C)-induced MIA is distinct from that of NTD formation. The eye defect phenotype was observed in crosses protected from NTDs (e.g., STAT1-deficient and γδ T cell-deficient backgrounds) and appears to be driven by pathways distinct from those producing NTDs and CFDs. Without exception, all fetuses derived from homozygous *Ifitm3*$^{-/-}$ crosses subjected to poly(I:C)-induced MIA exhibited anophthalmia or absence of eyes at harvested timepoints E12.5 and beyond, indicating that the interaction of immune pathways and *Ifitm3* transcriptional programs may influence key processes of eye development, particularly in MIA-primed environments.

At the maternal-fetal interface, while there are major shifts in immune populations at the maternal-fetal interface, many prominent populations by size are not required for manifestation of NTD phenotypes in exposed litters. Instead, I find that the small population of γδ T cells at the maternal-fetal interface are linked to NTD outcomes in this MIA model.

Our work thus identifies a novel role for γδ T cells at the maternal-fetal interface in antiviral responses during pregnancy. The female reproductive tract is characterized by a Vγ6^{+} γδ T cell population largely producing IL-17a[165]. During pregnancy, this resident

population is joined by an influx of IL-17a-producing Vγ4^{+} γδ T cells into the placenta[165,166]. Future work is centered on identifying the γ-chain usage of the γδ T cells concentrated at the ectoplacental cone and surrounding regions in our MIA model of NTD development.

The absence of laminin staining at the ectoplacental cone region of the maternal-fetal interface in MIA-exposed C57BL/6J pregnancies is particularly interesting given the association between laminin knockout phenotypes and NTD pathogenesis. Certain laminin deficiencies have been associated with NTDs and craniofacial abnormalities, analogous to our antiviral model of MIA. Mice lacking the laminin α5 chain exhibit exencephaly at a similar rate to our model (~60%) and exhibit defects in neural crest migration[167,168]. Antibody-mediated disruption of laminins also leads to impaired neural crest development[169-171] and laminin isoforms are strikingly expressed throughout the neural tube[172]. Our work suggests that at least one other potential consequence of this MIA-altered landscape on the fetal neural tube could be the observed decrease in neural progenitor proliferation, although it remains to be uncovered whether this proliferative defect is due to direct immune-mediated regulation of mitotic programs, an inability to meet the metabolic demands of development due to altered trophoblast biology, or otherwise. Interestingly, in one model of cancer invasion and metastasis, γδ T cells were found to target laminin receptor-expressing cells for destruction[173]. Future work will investigate whether activated γδ T cells at the maternal-fetal interface are targeting potential laminin- or laminin receptor-expressing subpopulations such as extravillous trophoblasts or developing trophoblast giant cells during MIA in early pregnancy.

Ultimately, we anticipate that this ongoing work will lead to an expanded understanding of the consequences of MIA in early pregnancy and the role of γδ T cells in maternal-fetal biology. Such insight could inform potential strategies toward the prevention of fetal congenital defects including NTDs and the management of both infectious and noninfectious inflammatory states in pregnancy.

Chapter 3: Investigation of SARS-CoV-2 infection during human pregnancy and its impact on the maternal-fetal interface

This chapter contains excerpts from:

Hosier H, Farhadian SF, Morotti RA, Deshmukh U, Lu-Culligan A, et al. 2020. SARS-CoV-2 infection of the placenta. *J. Clin. Invest.* 130(9):4947–53

Lu-Culligan A, Chavan AR, Vijayakumar P, Irshaid L, Courchaine EM, et al. 2021. Maternal respiratory SARS-CoV-2 infection in pregnancy is associated with a robust inflammatory response at the maternal-fetal interface. *Med (N Y)*. 2(5):591–610.e10

3.1 Author Contributions

I designed and conceived of all experiments with the supervision of Akiko Iwasaki and Shelli Farhadian. I collected and processed specimens, performed all experiments, conducted or guided the analysis of the data, and interpreted the results. Arun Chavan analyzed single cell RNA sequencing. Pavithra Vijayakumar assisted with patient identification, consent, and coordination, as well as analyzed clinical and demographic information. Lina Irshaid and Raffaella Morotti analyzed and scored specimens for histopathology. Edward M. Courchaine, Hannah J. Lee, and Karla M. Neugebauer

contributed to in vitro studies. Kristin M. Milano assisted with immunohistochemistry experiments. Zhonghua Tang and Seth Guller performed placental cell isolations. Scott Pope, William J. Lu-Culligan, and Eric Song contributed to processing of sequencing data. Chantal B.F. Vogels and Nathan D. Grubaugh performed and analyzed RT-qPCR on placental tissue. Feimei Liu and Aaron Ring performed plasma antibody assays. The Yale Impact Team, Jessica M. Toothaker, and Liza Konnikova assisted with case identification and biospecimen collection. Albert I. Ko contributed to study design and edited the manuscript. Harvey J. Kliman guided and supported the execution, analysis, and interpretation of histopathological and immunohistochemical data.

3.2 Summary

Pregnant women are at increased risk for severe outcomes associated with COVID-19, but the pathophysiology underlying this increased morbidity and its potential impact on the developing fetus is not well understood. Together with collaborators, I contributed to the identification of one of the first reported cases worldwide of SARS-CoV-2 detected at the placenta in pregnancy. My work was the first to show that SARS-CoV-2 infection localizes to the syncytiotrophoblast layer of the placenta and is associated with an intervillositis containing CD68+ macrophages and T cells. By investigating the expression pattern of the SARS-CoV-2 receptor ACE2 in healthy placentas from the first trimester to term, I determined that ACE2 is also localized to syncytiotrophoblast cells of the placenta and that placental ACE2 levels change over the timeline of gestation, explaining both temporal and spatial patterns of SARS-CoV-2 infection observed in pregnancy. Amongst uninfected women, ACE2 was detected by immunohistochemistry in syncytiotrophoblast

cells of the normal placenta during early pregnancy but was rarely seen in healthy placentas at full term. Term placentas from women infected with SARS-CoV-2, however, displayed a significant increase in ACE2 levels and additionally displayed increased intervillous fibrin on histopathology. Using immortalized cell lines and primary isolated placental cells, I determined the vulnerability of various placental cell types to direct infection by SARS-CoV-2 *in vitro*, showing that cytotrophoblasts are the subset most prone to direct infection.

Expanding this study to pregnant women with and without COVID-19, I assessed viral and immune dynamics at the placenta during maternal SARS-CoV-2 infection. Despite the susceptibility of placental cells to SARS-CoV-2 infection *in vitro*, my analysis of human samples detected viral RNA in the placentas of only a subset (~13%) of pregnancies in this cohort. Through single cell transcriptomic analyses, I found that the maternal-fetal interface of SARS-CoV-2-infected women exhibited markers associated with pregnancy complications, such as preeclampsia, and robust immune responses, including increased activation of placental NK and T cells and increased expression of interferon-related genes. Overall, these data suggest that SARS-CoV-2 is associated with immune activation at the maternal-fetal interface even in the absence of detectable local viral invasion. While this likely represents a protective mechanism shielding the placenta from infection, inflammatory changes in the placenta may also contribute to poor pregnancy outcomes and thus warrant further investigation.

3.3 Introduction

Coronavirus disease 2019 (COVID-19), due to SARS-CoV-2 infection, is a public health emergency that has impacted the lives of millions of people around the world. The

effect of SARS-CoV-2 infection in pregnant women is of particular concern: population-based studies show that pregnant women with COVID-19 are at increased risk for severe illness compared to non-pregnant women with COVID-19[176]. SARS-CoV-2 infection during pregnancy has also been associated with increased risk of pregnancy complications such as preterm birth, premature rupture of membranes, and preeclampsia[177-179]. However, the mechanisms underlying these poor outcomes are unknown, and their dependence on active SARS-CoV-2 infection of the placenta remains poorly understood. Given that pregnancy involves a tightly regulated series of immunological processes, perturbations to this environment may contribute to the development of these pathologies. While systemic inflammatory changes in maternal SARS-CoV-2 infection have been explored[180], the inflammatory changes to the maternal-fetal interface during SARS-CoV-2 infection in pregnancy have yet to be elucidated. Furthermore, the emerging picture of the inflammatory consequences of SARS-CoV-2 infection during pregnancy suggests that exposed neonates could be at potential risk of long-term effects[180,181].

Studies of other coronaviruses suggest the potential for placental pathology during maternal coronavirus infection both through direct viral invasion at the placenta and through a secondary inflammatory reaction. Mouse hepatitis virus (MHV), a coronavirus of laboratory mice, infects placental cells *in vivo*[182], leading to placental inflammation and increased susceptibility to subsequent bacterial infection of the placenta[183]. During the SARS pandemic of 2008, maternal infection with SARS-CoV-1 was associated with histological abnormalities but not with viral invasion of the placenta[184]. While variable findings have been reported[185-189], recent transcriptomic analyses of healthy placentas have suggested limited expression of the canonical SARS-CoV-2 receptor *ACE2* in the placenta

and little to no co-expression of *ACE2* with its classical co-factor *TMPRSS2* at the transcriptional level[185-187]. Thus, it remains unclear whether the placenta is susceptible to SARS-CoV-2 infection under normal physiological conditions or under conditions of systemic inflammation, such as that which occurs with maternal COVID-19. Moreover, it remains unknown whether placental pathology develops in the absence of viral infection of the placenta[174,190,191].

In this chapter, I investigate a case of placental SARS-CoV-2 infection from a pregnant woman presenting with severe COVID-19 disease in the second trimester and study a cohort of pregnant women with mild or asymptomatic COVID-19 disease at term. I characterize the susceptibility of the human placenta to SARS-CoV-2 infection over the course of pregnancy, through *in situ* analysis of ACE2 protein expression and through *in vitro* studies. Furthermore, I describe *in vivo* immune responses at the maternal-fetal interface in response to maternal SARS-CoV-2 infection during pregnancy.

3.4 Results

3.4.1 SARS-CoV-2 is capable of infecting the placenta

A previously healthy 35-year-old woman presented at 22 weeks of gestation with symptoms of COVID-19 infection starting ten days prior to admission (i.e., fever and cough) with an acute worsening four days prior to admission (i.e., fever, cough, malaise, diffuse myalgias, anorexia, nausea, and diarrhea). On the day of admission, patient developed vaginal bleeding and abdominal pain and presented to Yale New Haven Hospital where she was diagnosed with severe preeclampsia. Her blood pressure was 150/100 and laboratory studies revealed elevated liver transaminases, profound thrombocytopenia, and

increased urine protein consistent with preeclampsia, as well as a prolonged partial thromboplastin time and decreased fibrinogen consistent with disseminated intravascular coagulation. SARS–CoV-2 RNA was detected by reverse transcription PCR (RT-PCR) in a nasopharyngeal swab obtained from the patient on admission. Termination of the pregnancy was performed via dilation and evacuation to treat severe preeclampsia and the patient consented to the release of tissues for research-related testing according to our IRB-regulated protocol.

We performed the United States Centers for Disease Control and Prevention quantitative RT-PCR (qRT-PCR) assay, which showed that the placenta (3×10^7 virus copies/mg) and umbilical cord (2×10^3 virus copies/mg) were positive for SARS–CoV-2 RNA (Figure 3.1). Fetal heart and lung tissues were also tested and met the human RNA control (RNase P) standards and were negative for viral RNA (Figure 3.1). Maternal samples were also collected postoperatively, and although the oral and nasal swabs were negative, the saliva and urine were still positive for SARS–CoV-2 (Figure 3.1).

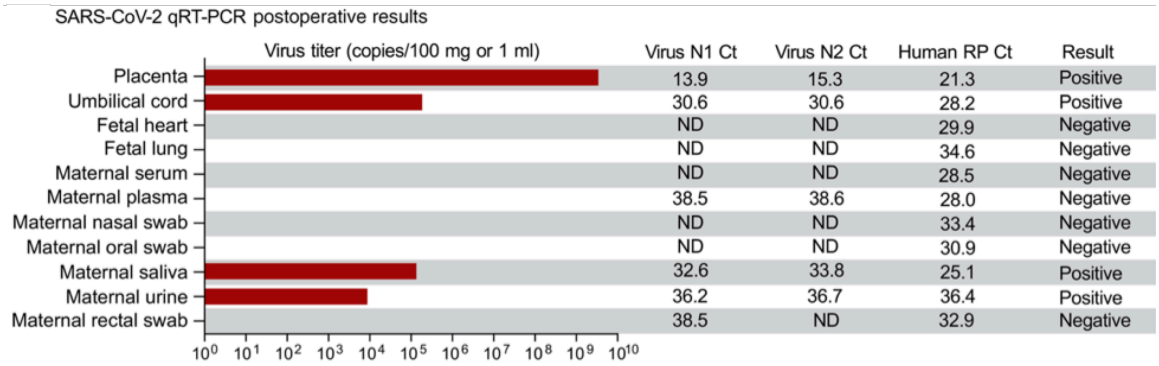

	Virus N1 Ct	Virus N2 Ct	Human RP Ct	Result
Placenta	13.9	15.3	21.3	Positive
Umbilical cord	30.6	30.6	28.2	Positive
Fetal heart	ND	ND	29.9	Negative
Fetal lung	ND	ND	34.6	Negative
Maternal serum	ND	ND	28.5	Negative
Maternal plasma	38.5	38.6	28.0	Negative
Maternal nasal swab	ND	ND	33.4	Negative
Maternal oral swab	ND	ND	30.9	Negative
Maternal saliva	32.6	33.8	25.1	Positive
Maternal urine	36.2	36.7	36.4	Positive
Maternal rectal swab	38.5	ND	32.9	Negative

Figure 3.1: SARS-CoV-2 RNA in maternal and fetal tissues. SARS-CoV-2 qRT-PCR results of fetal and maternal samples using the CDC assay which consists of the N1 and N2 primers and probes targeting the coronavirus nucleocapsid and the RP primers/probe targeting human RNase P as an internal control. Cycle threshold (Ct) values from both N1 and N2 must be below 38 for the result to be positive, as internally validated. Virus titers shown as the average calculation from N1 and N2 Ct values. For the tissues, 80-160 mg were used for extractions; and for the swabs in viral transport media and other liquid samples, 0.25-0.4 ml were used.

On gross examination the placenta showed a marginal adherent blood clot associated with a focal placental infarct supportive of the clinical diagnosis of abruption and was otherwise unremarkable. On histological examination the placenta was remarkable for the presence of diffuse perivillous fibrin and an intervillous inflammatory infiltrate (Figure 3.2, A-C) composed of macrophages as well as T-lymphocytes, as demonstrated by immunohistochemistry for CD68 (Figure 3.2, D-E) and CD3 (Figure 3.2, F). SARS-CoV-2 localized predominantly to the syncytiotrophoblast cells of the placenta, as demonstrated by immunohistochemistry for the SARS-CoV-2 spike protein (Figure 3.2, G-H), and by SARS-CoV-2 RNA *in situ* hybridization (Figure 3.2, I). Maternal vessels did not show features of decidual vasculopathy. The fetal organs were grossly and microscopically unremarkable (Figure 3.3, A-D). SARS-CoV-2 spike protein was not detected in fetal organs.

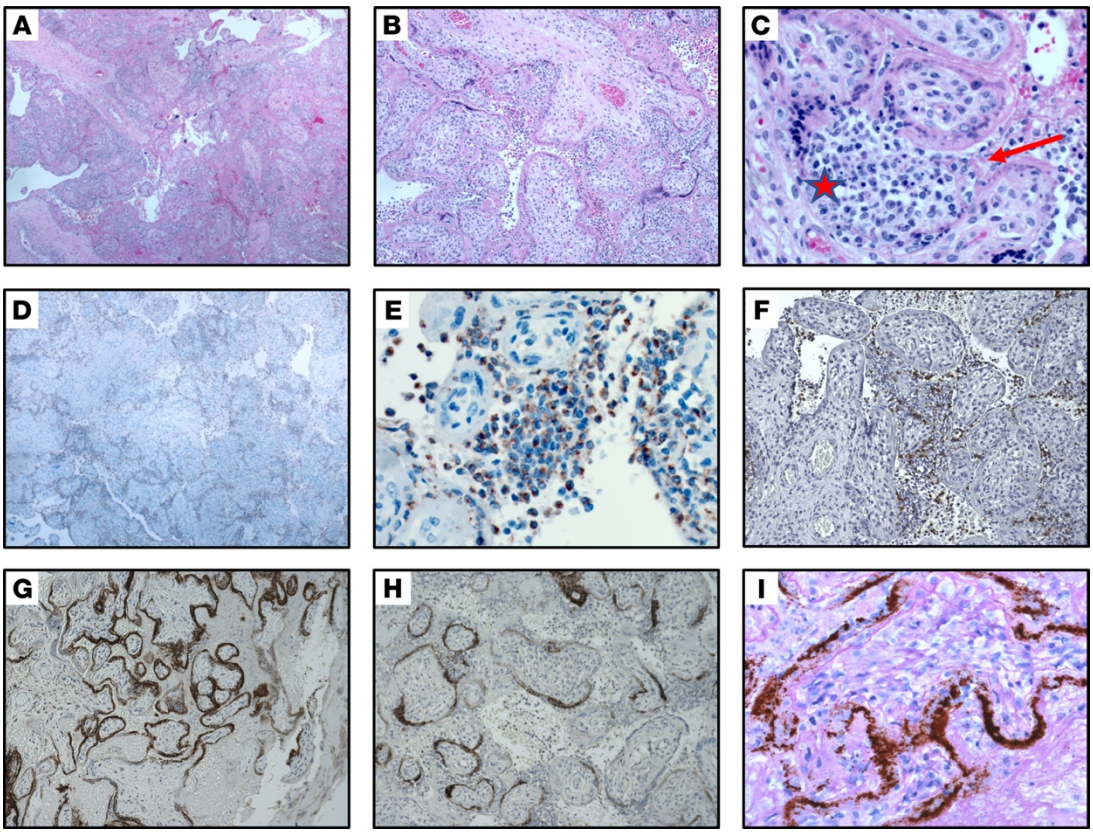

Figure 3.2: SARS-CoV-2-infected placenta exhibits localization of virus to syncytiotrophoblasts and intervillositis with infiltration of CD68 macrophages and T cells. (A-C) Section of placenta stained with H&E showing histiocytic intervillositis. Original magnification, x40 (A), x100 (B), and x400 (C). Star in (C) indicates intervillous space infiltrated by immune cells. Arrow indicated perivillous fibrin. (D-E) Immunohistochemical stain for CD68 showing the majority of intervillous inflammatory infiltrate is positive (brown stain) for this macrophage marker. Original magnification, x40 (D), x400 (E). (F) Staining for CD3, a marker of T lymphocytes. Original magnification, x100. (G and H) Immunohistochemical staining for SARS-CoV-2 spike protein, demonstrating virus localization predominantly in syncytiotrophoblast cells. Original magnification, x50 (G), x400 (H). (I) In situ analysis for the presence of SARS-CoV-2 RNA shows strong positive staining within the placenta. Original magnification, x400.

3.4.2 Most cases of respiratory SARS-CoV-2 infection in pregnancy do not result in placental invasion

After establishing that SARS-CoV-2 is capable of invading the maternal-fetal interface, we sought to determine whether this outcome is commonplace in women with respiratory SARS-CoV-2 infection. We sought to gain a better understanding of how frequently the virus is able to reach the placenta in women with respiratory SARS-CoV-2 infection exhibit placental invasion of the virus. Women who tested positive for SARS-CoV-2 infection by RT-qPCR of nasopharyngeal swab or saliva at the time of delivery (n=12; 80%) or in the 1 month prior to delivery (n=3; 20%) were prospectively enrolled and consented to donation of biospecimens. One participant was identified based on positive SARS-CoV-2 testing at the time of delivery but was also noted to have an initial positive test 2 weeks prior. One pregnancy ended in fetal demise at 22 weeks[174]; the rest were full-term deliveries. Overall, the median time from SARS-CoV-2 upper respiratory testing to placental sampling was 1.5 days (range 0-28 days). One participant (COVID-1) received hydroxychloroquine; none of the other study participants received hydroxychloroquine, remdesivir, dexamethasone or other treatment for COVID-19 prior to delivery. Clinical information about these participants is noted in Table 1.

ID	Maternal Age	gestational age	Days between first positive test and delivery	Symptomatic COVID-19	Days between symptom onset and delivery	treatment	Severe COVID-19*	NP swab SARS-CoV-2 RT-PCR at delivery	NP swab CT-value at delivery***	placenta SARS-CoV-2 RT-qPCR
COVID 1	36	22.857	0	Y	0	HCQ	Y	+	33.8**	+
COVID 2	26	40.714	15	Y	19	no	Y	+	37.3**	-
COVID 3	32	38.143	1	Y	1	no	N	+	26.6	+
COVID 4	20	38.857	2	Y	2	no	Y	+	17.1	-
COVID 5	21	40.714	0	Y	21	no	N	+	43.8	-
COVID 6	35	41	1	N		no	N	+	30.4	-
COVID 7	22	40.286	2	N		no	N	+	39.3	-
COVID 8	31	39.429	1	N		no	N	+	31.9	-
COVID 9	34	41.143	0	N		no	N	+	35.5	-
COVID 10	40	37.714	4	N		no	N	+	37.5	-
COVID 11	36	38.286	27	Y	28	no	N	ND	ND	-
COVID 12	21	38.429	0	Y	7	no	N	+	32.7	-
COVID 13	35	39.714	1	N		no	N	+	22.2	-
COVID 14	36	36.857	24	Y	25	no	N	ND	ND	-
COVID 15	31	40.714	23	Y	40	no	N	ND	ND	-

*ICU or supplemental oxygen

**saliva

***N2 gene

ND= not done

Table 3.1: Clinical features of COVID-19 cases tested by RT-qPCR.

Among the 15 placentas tested by RT-qPCR for the presence of SARS-CoV-2, viral RNA was detected in two of the placentas (Table 3.1 and Table 3.2). One was from the case study of severe preeclampsia at 22 weeks described above in Section 3.4.1. This placenta (COVID-1) was excluded from further cohort analyses due to the mismatch in gestational age compared to the rest of the group of term placentas and since the details of this case were previously reported[174]. The second SARS-CoV-2-positive placenta was obtained from a 32-year-old woman who presented in labor at 38 weeks of gestation with symptoms of pneumonia, not requiring supplemental oxygen, who progressed to a healthy delivery. The neonate tested negative for SARS-CoV-2 by nasopharyngeal swab RT-qPCR at the time of delivery.

Sample_ID	Sample_Type	Replicate	N1	N2	RP	Result
#COVID-1	Placenta Fetal	1	31.6	33.9	17.4	Positive
		2	29.3	31.2	17.2	Positive
	Placenta Maternal	1	37.2	37.7	18.0	Positive
		2	ND	ND	18.6	Negative
	Placenta Membrane	1	33.1	33.8	19.4	Positive
		2	32.0	32.6	18.8	Positive
	Umbilical Cord	1	35.0	35.6	21.2	Positive
		2	35.6	35.2	21.0	Positive
#COVID-3	**Placenta**	**1**	**13.9**	**15.3**	**21.3**	**Positive**
	Umbilical Cord	1	30.6	30.6	28.2	Positive

Table 3.2: RT-qPCR results for placenta samples that tested positive by the modified CDC assay. Total nucleic acid was extracted from each sample and tested by RT-qPCR in duplicate. Reported are Ct values for the primer-probe sets N1, N2, and RP. Samples IDs are related to Table 3.1.

When we restricted our analysis to only those participants with full-term pregnancies who had a positive upper respiratory SARS-CoV-2 RT-qPCR at the time of full-term delivery, 1/11 had detectable viral RNA in the placenta. Plasma available for 12 SARS-CoV-2 infected women at the time of delivery was tested for systemic inflammatory markers and for SARS-CoV-2 spike S1 protein-specific IgG and IgM antibodies (anti-S1 IgG and IgM). No apparent differences in ELISA absorbance values were observed between symptomatic and asymptomatic infected mothers, or between pregnant and non-pregnant SARS-CoV-2 infected hospitalized individuals (Figure 3.3, A). Serum collected from pregnant patients with COVID-19 were also analyzed for systemic inflammatory markers and cytokines (Figure 3.3, B).

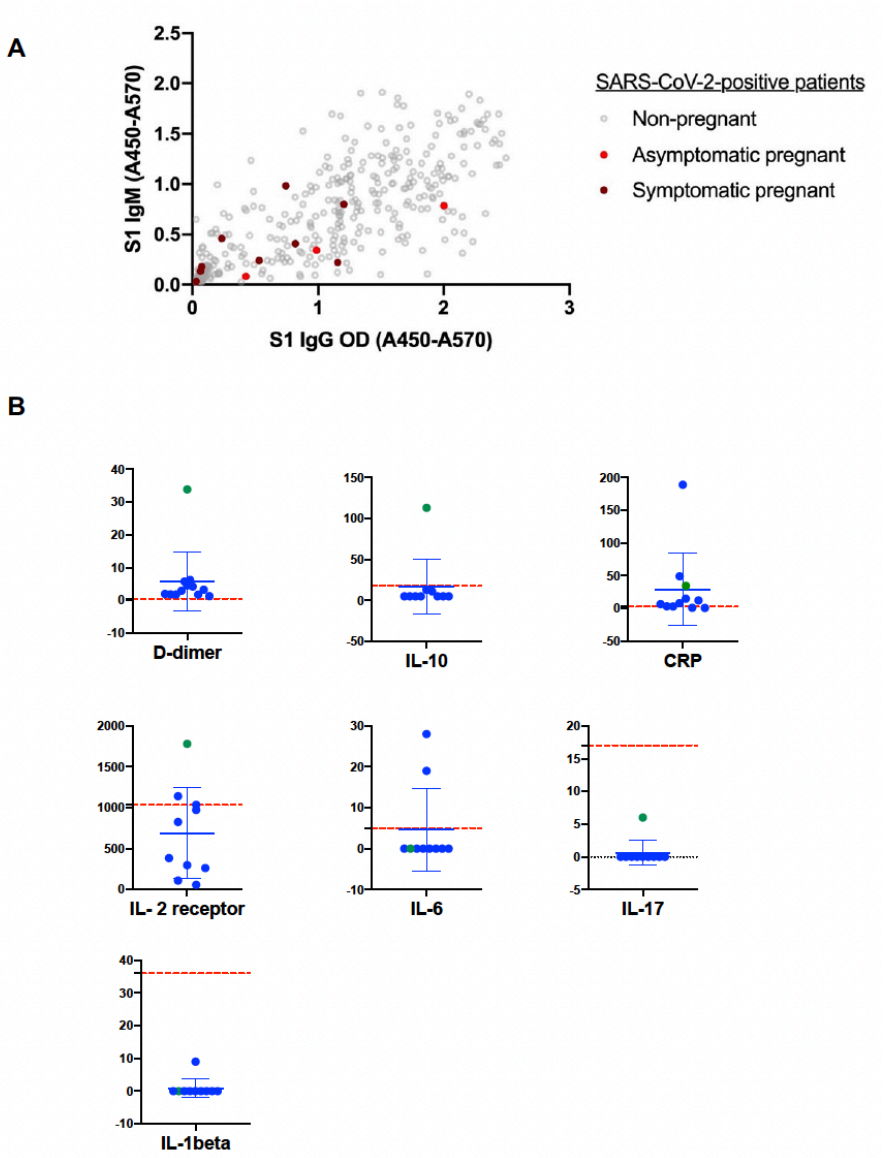

Figure 3.3: Systemic immune responses to SARS-CoV-2 during pregnancy. (A) SARS-CoV-2 spike S1 protein-specific IgG and IgM (anti-S1 IgG and IgM) ELISA absorbance values in 12 pregnant SARS-CoV-2-positive women compared to 355 non-pregnant SARS-CoV-2-positive individuals. (B) Systemic inflammatory markers in pregnant women with acute COVID-19. The following cytokines were not detected in any sample: IL-13, IL-4, IL-8, IFN-gamma, IL-12. The upper limit of normal for each cytokine is shown with a dashed red line. Shown in green is COVID-1 which was the only case of (pre-term) fetal loss in the series.

3.4.3 ACE2 expression decreases over the course of normal pregnancy

I assessed the potential for SARS-CoV-2 infection of the placenta by examining placental expression of ACE2, the canonical receptor required for SARS-CoV-2 infection.

Prior transcriptome studies have suggested that *ACE2* mRNA is absent or expressed at low levels in placenta. Consistent with these previous reports, analyses of bulk and single-cell RNA sequencing data in placenta from COVID-19 cases and controls demonstrate very low levels of *ACE2* gene expression in the term placenta (Figure 3.4).

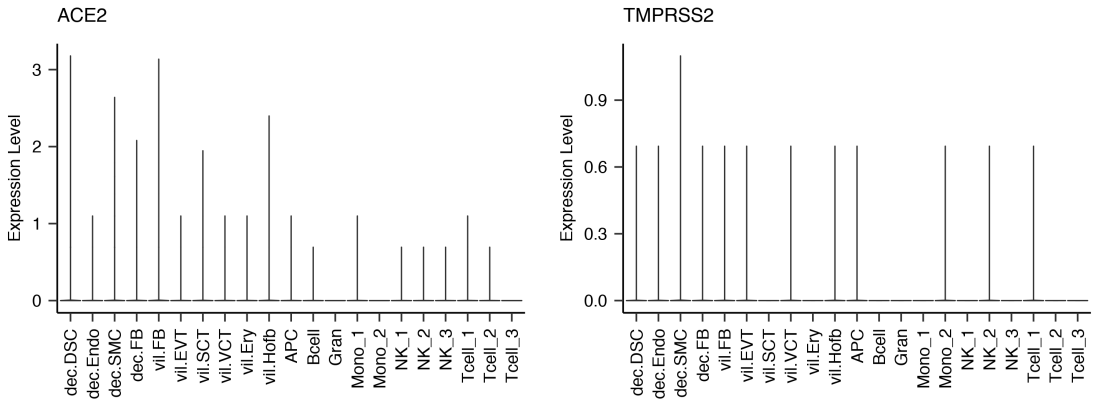

Figure 3.4: Violin plot of ACE2 and TMPRSS2 expression in placenta cell subsets.

However, when protein-level ACE2 expression was examined by immunohistochemistry, I found ACE2 to be highly expressed in syncytiotrophoblast cells in first and second trimester placentas, with ACE2 protein expression virtually absent in normal term placentas obtained from pre-pandemic controls (Figure 3.5, B-F). While the expression pattern of ACE2 in the placenta decreased steadily over gestational age in placentas derived from healthy pregnancies (Figure 3.5, I), I found that ACE2 protein was present at significantly higher levels in term placenta collected from COVID-19 cases (Figure 3.5, J). These findings suggest that detection of *ACE2* mRNA expression is not a reliable surrogate for ACE2 protein expression in the placenta and, importantly, that ACE2-mediated risk for placental infection by SARS-CoV-2 may vary over the course of pregnancy, with the detection of higher ACE2 levels in the first and second trimesters suggesting the most vulnerability may exist prior to term. I detected minimal TMPRSS2

protein expression and no overlap of TMPRSS2 with ACE2 by immunohistochemistry in any term placentas.

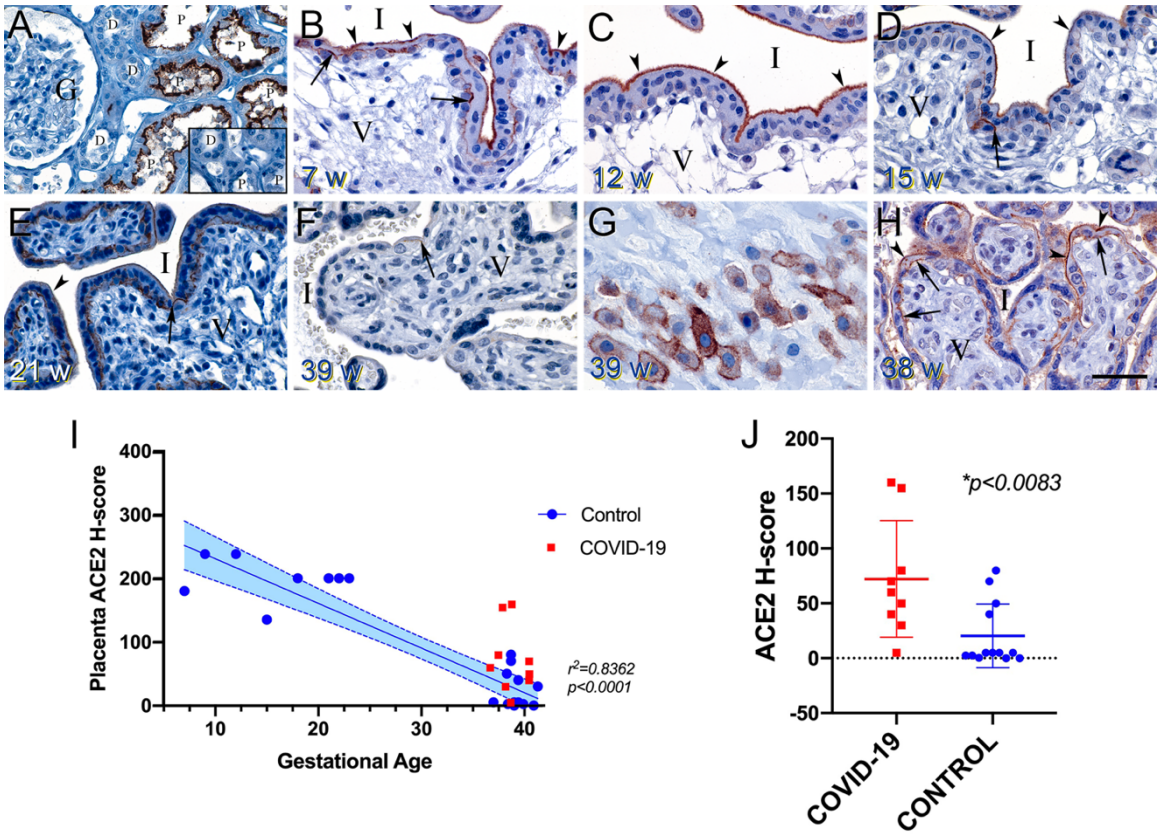

Figure 3.5: ACE2 protein expression in the placenta varies with gestational age. (A) Human kidney used as a positive control revealed strong apical staining of the proximal tubules (P). The distal tubules (D) and glomerulus (G) were negative. Inset shows a serial section of the same kidney stained with non-immune rabbit sera resulting in no staining. (B-D) Placentas derived from normal pregnancies between 7 and 15 weeks of gestation demonstrated strong, uniform, apical microvillus syncytiotrophoblast staining (arrow heads), and patchy strong basolateral staining at the cytotrophoblast–syncytiotrophoblast contact zone (arrows). Intervillous space (I) and villous core (V). (E) A normal 21-week placenta still exhibited syncytiotrophoblast surface staining (arrow head), but to a lesser extent than the earlier samples. Cytotrophoblast–syncytiotrophoblast contact zone staining was still prominent (arrow). (F) A representative normal placenta at 39 weeks revealed almost no ACE2 staining. Occasionally, staining at the cytotrophoblast–syncytiotrophoblast contact zone was noted (arrow) (G) Normal extravillous invasive trophoblasts from a 39-week placenta demonstrated strong surface expression of ACE2, with variable cytoplasmic staining. (H) Representative image of ACE2 expression in a 38-week placenta derived from a case of symptomatic maternal COVID-19. Reappearance of strong apical microvillus syncytiotrophoblast (arrow heads) and cytotrophoblast–syncytiotrophoblast contact zone staining (arrows) was observed. All sections were cut at 5 μM, except panel (E), which was cut at 10 μM. Bar represents 50 μM for images A-H. (I) ACE2 H-score demonstrated steady loss of placental ACE2 with increasing gestational age in healthy pregnancies ($p<0.001$). Linear regression (blue line) was fit to data from healthy controls (circles). 95% confidence interval is shown with dashed lines. Placentas derived from COVID-19 cases are depicted as red squares. (J) ACE2 H-score was significantly increased in term placentas from COVID-19 cases (squares) compared to healthy matched controls (circles).

3.4.4 In vitro *infection of primary isolated cytotrophoblasts by SARS-CoV-2*

To determine whether placental cells dissociated from their native tissue environment exhibit intrinsic resistance to SARS-CoV-2 infection, I performed *in vitro* infections of placental cell subpopulations using a replication-competent infectious clone of SARS-CoV-2 expressing the fluorescent reporter mNeonGreen (icSARS-CoV-2-mNG)[192] for 24 hours.

Immortalized cell lines are commonly used as a model for various placental cell types. The BeWo line, a human choriocarcinoma line, is used to model villous cytotrophoblasts. The HTR-8/SVneo line is derived from invasive extravillous cytotrophoblasts isolated from first trimester placenta and contains two cell populations[193,194]. Neither of these immortalized cell lines, BeWo and HTR-8/SVneo, exhibited significant infection with icSARS-CoV-2-mNG (Figure 3.6, A). BeWo cells, however, were rarely detected (<0.0001%) to exhibit infection, as indicated by viral mNeonGreen fluorescence co-localized with SARS-CoV-2 nucleocapsid (NP) staining.

I also measured the infectious potential of icSARS-CoV-2-mNG in primary placental cells isolated from healthy term deliveries. I observed no detectable infection of Hofbauer cells or primary placental fibroblasts at 24 hours post-infection (Figure 3.6, A-B), nor at 48, 72, and 96 hours post-infection. However, we found infection of primary isolated cytotrophoblasts by mNeonGreen reporter detection and staining for SARS-CoV-2 NP (Figure 3.6, A). These findings were consistent with SARS-CoV-2 N1 detection by RT-qPCR (Figure 3.6, B).

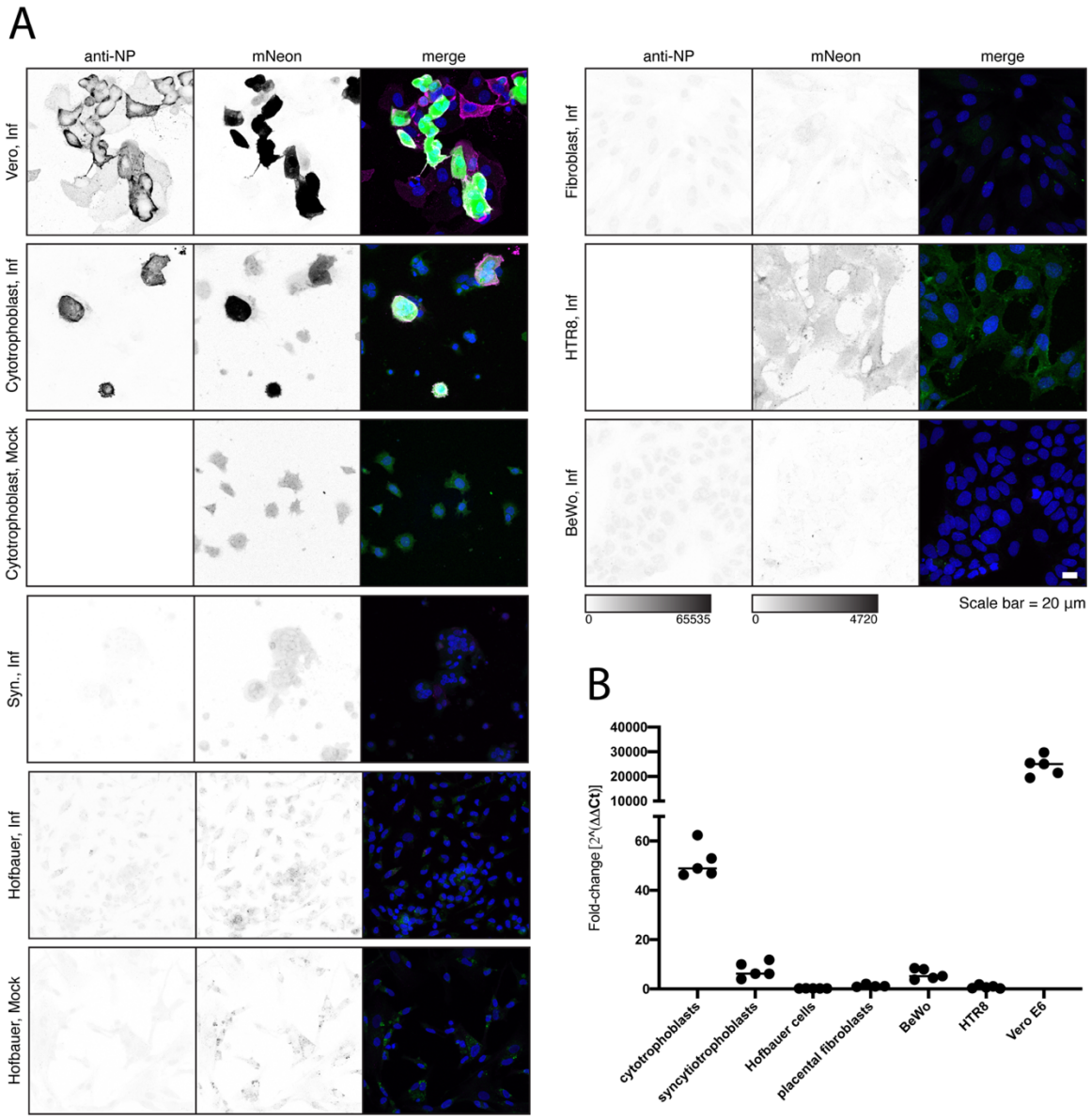

Figure 3.6: SARS-CoV-2 infection of placental cells *in vitro.* (A) Representative images of icSARS-CoV-2-mNG infection of primary placental cells, immortalized placental cell lines, and Vero E6 cells as measured by mNeonGreen expression and immunofluorescence staining of SARS-CoV-2 nucleocapsid (NP). Images are displayed as maximum intensity projections of z-stacks and grayscale bars indicate measured fluorescence intensity in arbitrary digital units. (B) Fold-change quantification of SARS-CoV-2 N1 by RT-qPCR at 24 hours post-infection. Cells were infected at an MOI of 5 for one hour and washed three times with PBS before the addition of fresh media. Cells were washed and collected at 24 hours post-infection. Data presented are representative results from one of three replicates.

Primary isolated syncytiotrophoblasts (derived from cytotrophoblasts allowed to spontaneously differentiate for 72-96 hours) were not as readily infected (Figure 3.6, A-B), showing more limited capacity for infection even at 72 hours post-infection (Figure

3.7, A). By immunofluorescence, only extremely rare individual cells exhibiting viral mNeonGreen fluorescence and NP staining (estimated to be <0.0001%) could be visualized. These infrequent positive cells were notably isolated cells excluded from the syncytialized regions of the culture, an appearance typical of cytotrophoblast cells defective for syncytialization (Figure 3.7, B). These results indicate that cytotrophoblasts are the placental cell type most vulnerable to direct SARS-CoV-2 infection in vitro.

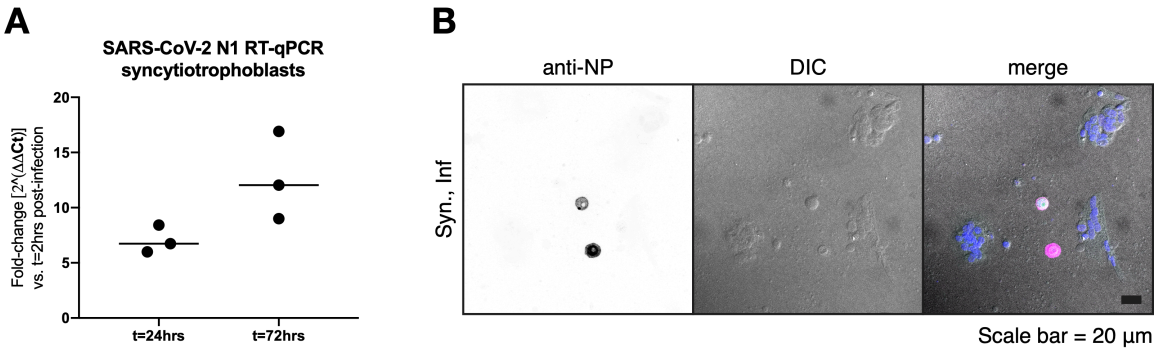

Figure 3.7: SARS-CoV-2 infection of primary syncytiotrophoblasts. Primary syncytiotrophoblasts were derived from primary isolated cytotrophoblasts allowed to spontaneously differentiate for 72-96 hours. Following the differentiation period, cells were infected at an MOI of 5 for one hour and washed three times with PBS before the addition of fresh media. (A) Fold-change quantification of SARS-CoV-2 N1 by RT-qPCR at 24 and 72 hours post-infection in primary syncytiotrophoblasts. (B) Visualization of rare cells (estimated to be <0.0001%) in syncytiotrophoblast culture at 72 hours post-infection. Shown are two individual cells as detected by immunofluorescence following staining with anti-NP antibody (left panel). Differential interference contrast (DIC, center panel) image shows these two cells are excluded from the surrounding syncytia. Merged image (right panel) shows pseudocolor labeling of syncytialized cells in purple and infected NP-labeled individual cells in pink.

3.4.5 Transcriptional changes at the placenta during maternal COVID-19 reflect a localized inflammatory response to systemic SARS-CoV-2 infection

Despite the fact that cytotrophoblasts are permissive to SARS-CoV-2 infection *in vitro*, and that SARS-COV-2 infection of syncytiotrophoblasts has been demonstrated in isolated cases[174,190,195,196], SARS-CoV-2 infection was not detected in the majority of the placentas tested in our case series and in a recent cohort study of pregnant women with

acute COVID-19[197]. This was true even in women with high nasopharyngeal viral loads and with symptomatic SARS-CoV-2 infection, including those with severe complications. This absence of placental infection suggested the presence of a localized and effective anti-viral response in the placenta. I thus used bulk-RNA sequencing of placental villi to examine differences in placental gene expression between pregnant women with COVID-19 (n=5) and uninfected controls matched for maternal age, gestational age, maternal comorbidities, and mode of delivery (n=3).

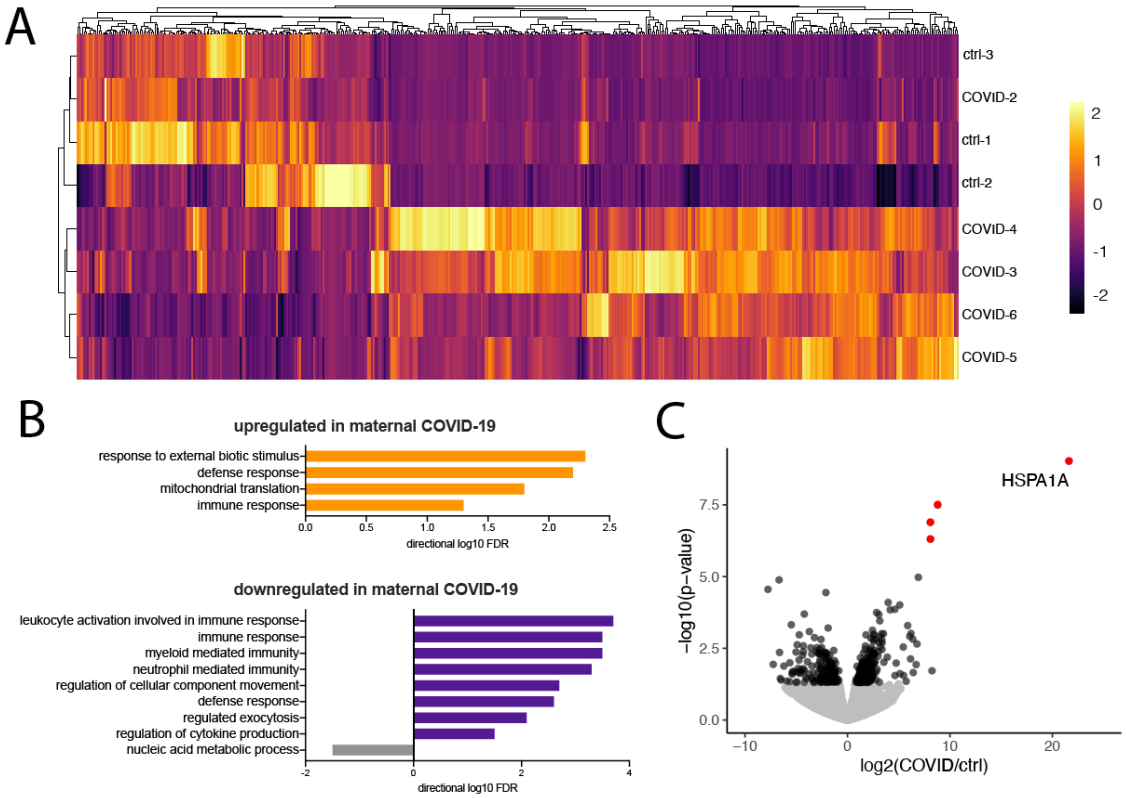

Figure 3.8: HSPA1A is significantly upregulated in maternal COVID-19. (A) Hierarchal clustering and heatmap of differentially expressed genes ($p<0.05$). Bulk RNA-seq was performed on placental villi isolated from control and maternal COVID cases. (B) Gene ontology of differentially expressed genes ($p<0.05$) in bulk RNA-seq. (C) Volcano plot indicating differentially expressed genes between control and maternal COVID-19 groups from bulk RNA-seq. Significant hits are depicted in red ($p_{adj}<0.05$) and black ($p<0.05$). Non-significant genes are shown in gray.

In my comparison of the placental transcriptome in COVID-19 cases to matched controls, COVID-19 cases showed increased expression of genes associated with immune responses, suggesting a robust local response to respiratory infection, even in the absence of localized placental infection ($p<0.05$, Figure 3.8, A). These changes in gene expression were largely shared among COVID-19 cases when compared to controls, as indicated by their grouping upon hierarchical clustering; placental transcriptomes from COVID-19 cases largely clustered together, and separately from healthy controls, with the exception of one case (COVID-2) (Figure 3.8, A). Further analysis of differentially expressed genes by gene ontology indicated an enrichment in defense and immune response categories in COVID-19 cases compared to healthy controls (Figure 3.8, B). The most significantly upregulated gene in the placenta during maternal SARS-CoV-2 infection was *HSPA1A*, which encodes the heat shock protein Hsp70 (Figure 3.8, C), a proposed alarmin that has been previously implicated in placental vascular diseases and preeclampsia[198-200]. Among the top gene hits in the comparison of COVID-19 cases to controls were a significant number of immune genes and markers, including complement factors and interferon-stimulated genes (Figure 3.9).

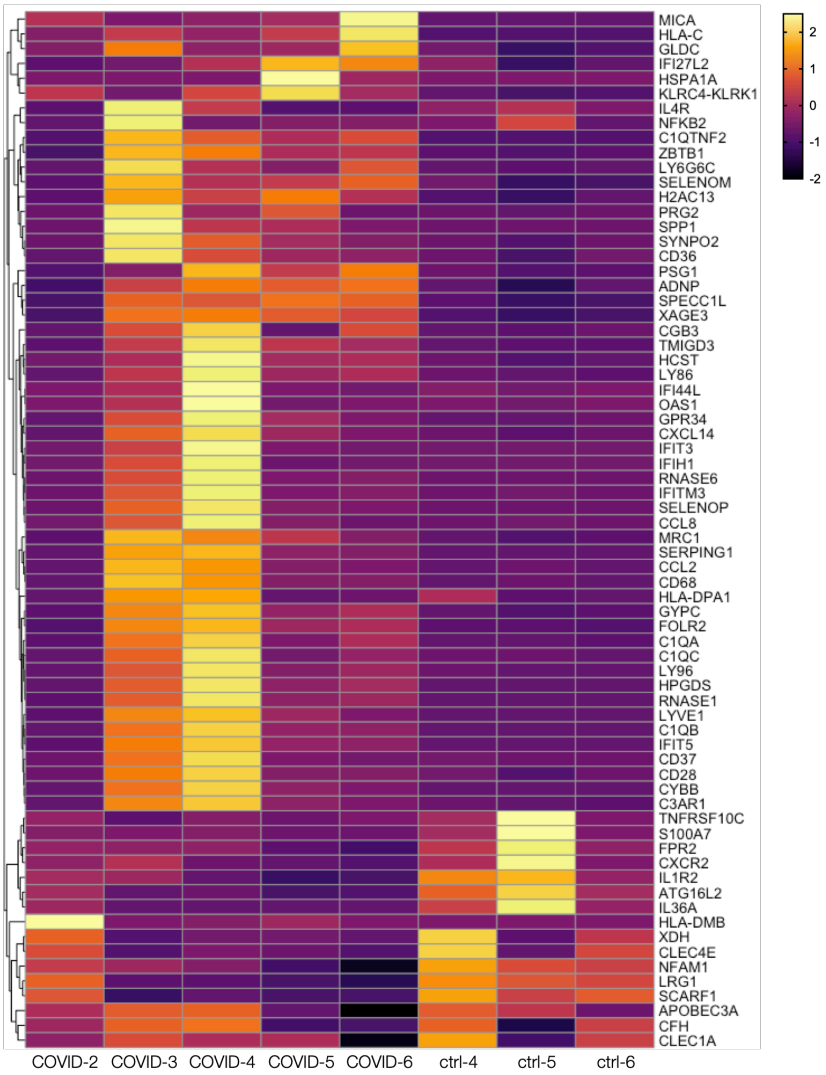

Figure 3.9: Heatmap of selected top genes in bulk RNA sequencing analysis of COVID-19 placentas compared to healthy cases at full term. Bulk RNA-seq was performed on placental villi isolated from control (n=3) and maternal COVID-19 (n=5) cases at term pregnancy and z-scores were calculated from normalized counts.

3.4.6 Single cell transcriptomic profiling of the placenta reveals cell-type specific immune response to maternal SARS-CoV-2 infection

We next assessed COVID-19 associated transcriptomic changes in the placenta in a cell-type specific manner. To do so, we characterized placenta cells derived from placental villi and from decidua parietalis from hospitalized maternal acute COVID-19 cases (n=2) and matched controls (n=3) through unbiased, single cell RNA sequencing.

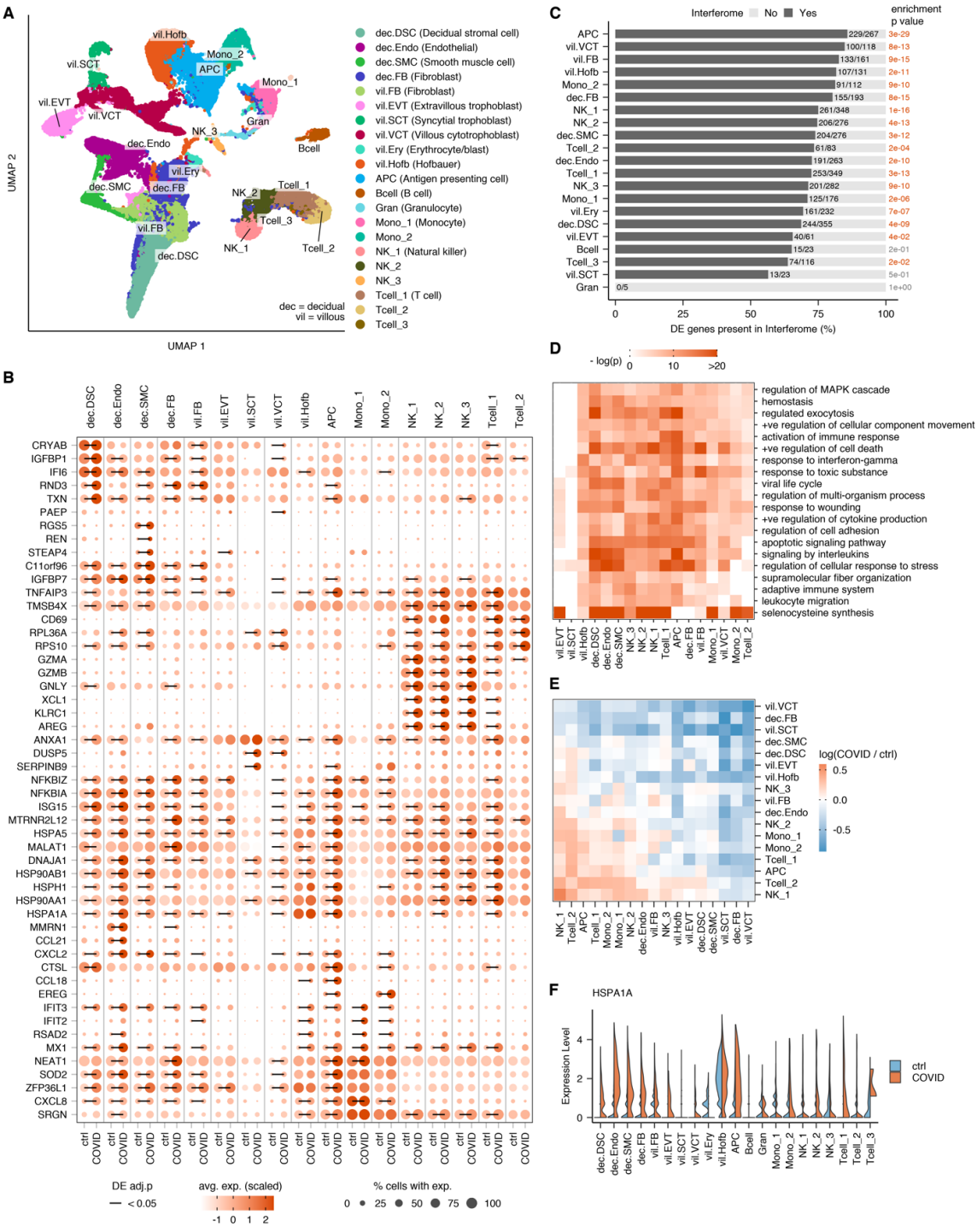

Figure 3.10: Single cell RNA sequencing of placental cells demonstrates gene expression changes in placental immune cells in SARS-CoV-2 infection. (A) UMAP projection of 83378 single placenta cells from COVID-19 cases (n=2 decidual and n=2 villous samples) and uninfected controls (n= 2 decidual and n = 3 villous samples). Cell type annotations based on correlation with reference datasets[29-31] followed by manual examination of marker genes. (B) Dotplot of the top 5 genes that are upregulated between COVID-19 and uninfected control samples for each annotated cell type based on fold-difference. Size of dots represents percent of cells in cluster expressing gene of interest; intensity of color reflects average scaled

expression. Significantly altered expression between COVID-19 cases and controls (Bonferroni-adjusted, two-tailed, Wilcoxon rank-sum test $P < 0.05$) is marked by a solid black line. (C) Interferome analysis demonstrating the fraction of differentially expressed genes in each cell type that are interferon-responsive, in COVID-19 cases compared to controls; with *p* values for enrichment (observed over expected fraction) calculated using hypergeometric distribution. (D) Clustered heatmap showing the top enriched functional terms according to Metascape[86] among differentially expressed genes between COVID-19 and control samples in the annotated placental cell types. Bars are colored to encode *p*-values of increasing statistical significance. (E) Heat map depicting the log-transformed ratio (COVID-19 cases over controls) of number of ligand-receptor interactions between all placental cell type pairs, inferred using the CellphoneDB repository of ligands, receptors and their interactions[36]. Red indicates cell type pairs with more interactions in COVID-19 cases compared to control; blue indicates the opposite. (F) Violin plots of *HSPA1A* expression at the placental villi and maternal decidua obtained by scRNA-seq.

A total of 83,378 cells were included in the analysis, 44,140 from placental villi and 39,238 from decidua parietalis. Placentas from these COVID-19 cases tested negative for SARS-CoV-2 by RT-qPCR. To further test for the presence of intracellular virus, open reading frames of SARS-CoV-2 (spike, ORF3a, envelope, membrane glycoprotein, ORF6, ORF7a, ORF8, nucleocapsid and ORF10) were added to the reference genome before alignment with CellRanger. No viral transcripts were detected in any of the cells surveyed. We next performed unsupervised cluster analysis and represented single cell transcriptome data from COVID-19 cases and controls in UMAP space (Figure 3.10, A).

The classification of subsets at the maternal-fetal interface by single cell RNA sequencing is challenging due to the presence of multiple cell types, of both maternal and fetal origin, in highly active transcriptional states. We overcame this challenge by creating a reference set of cell type-specific transcriptomes for cell types present at the human fetal-maternal interface, using cell type-averaged expression values from three previously published placenta single cell RNA sequencing studies[201-203]. We then compared single cell transcriptomes in our dataset to this composite reference dataset, and, after annotating clusters by comparison with the reference dataset, we manually examined clusters for

marker gene expression and annotated remaining clusters. Through this approach we identified 21 distinct cell types at the maternal-fetal interface (Figure 3.10, A).

Differential gene expression analysis revealed significantly altered gene expression in both immune and non-immune cell types in the placenta from COVID-19 cases (Figure 3.10, B), including markedly increased expression of pro-inflammatory genes and chemokines. In NK cells from pregnancies impacted by COVID-19, we found significant enrichment of genes encoding cytotoxic proteins, including *GZMA, GZMB,* and *GNLY,* as well as a tissue-repair growth factor, *AREG.* T cell subsets from COVID-19 cases upregulated *CD69*, a classical activation marker, as well as genes encoding ribosomal proteins, *RPL36A* and *RPS10.* Among endothelial cells, which have previously been implicated in COVID-19 pathogenesis, including COVID-19 associated thrombosis and vasculopathy[204], we found evidence for increased innate immune responses in COVID-19 cases compared to controls, including significant upregulation of *ISG15*, an interferon-induced protein that has been implicated as a central player in host antiviral responses, and *NFKBIA* and *NFKBIZ,* critical regulators of the NF-KB pathway. Notably, while we do not find significant expression of *ACE2* or *TMPRSS2* in placental and decidual cells in either COVID-19 cases or healthy controls, we do find widespread expression of *CTSL,* an alternative SARS-CoV-2 entry co-receptor, including in immune cells, fibroblasts, and trophoblasts at the maternal-fetal interface, and find that *CTSL* expression is increased in decidual stromal cells and decidual antigen presenting cells in COVID-19.

Given the increasing evidence that hospitalized patients with COVID-19 demonstrate strong type-1 interferon responses[205,206], we used Interferome[207], a database of interferon-regulated genes, to determine whether an interferon-driven inflammatory

signature is displayed by the placenta. We find that cellular subsets at the maternal-fetal interface demonstrate significantly increased expression of interferon-related genes in COVID-19 compared to healthy controls (Figure 3.10, C). Pathway analysis of all differentially expressed genes likewise shows increased engagement of immune-related pathways in placental subsets from COVID-19 cases, as well as increases in synthesis of selenocysteine associated with the anti-oxidative response to oxidative stress (Figure 3.10, D). Finally, we asked whether the transcriptional changes observed in placental and decidual tissue suggested altered cellular interactions at the maternal-fetal interface during COVID-19 compared to healthy conditions. Using CellphoneDB signaling network analysis[208], we found a significant increase in the number of interactions between immune cells at the maternal-fetal interface in COVID-19 cases when compared to controls. Among the strongest enriched relationships identified in COVID-19 cases were the interactions of T cells with monocytes and NK cells (Figure 3.10, E), suggesting innate to adaptive immune cell communication in the local placental environment during maternal COVID-19.

Consistent with the bulk RNA-seq data, analysis of single-cell data indicated significant upregulation of *HSPA1A*, the gene encoding heat shop protein 70. HSPA1A was differentially expressed in select cellular subsets from COVID-19 cases, including decidual APCs, decidual endothelial cells, and extravillous trophoblasts (Figure 3.10, F).

3.5 Discussion

This work is the first to describe the localization of SARS-CoV-2 in the placenta. Additional case reports during the current COVID-19 pandemic have also since

demonstrated that SARS-CoV-2 is capable of infecting the placenta[174,209,210]; however, the mechanism for viral entry remains unclear. Furthermore, immune responses at the maternal-fetal interface can be a double-edged sword. These responses are critical for protecting the developing fetus from pathogen invasion, but, at the same time, placental inflammation itself may lead to pathological changes detrimental to pregnancy and fetal development[1,8,211,212]. In this study, I demonstrate that ACE2, the canonical entry receptor for SARS-CoV-2, is highly expressed during early gestation but exhibits low levels at full term in normal pregnancy; however, term placentas from COVID-19-affected pregnancies displayed increased ACE2 expression. While primary trophoblast cells of the placenta are susceptible to SARS-CoV-2 infection *ex vivo,* SARS-CoV-2 RNA is rarely detected in the term placenta *in vivo.* Through bulk and single cell RNA sequencing, I find evidence for robust immunological defenses mounted at the placenta in women with acute respiratory SARS-CoV-2 infection, even in the absence of viral RNA at the placenta. These findings suggest that placental immune responses during maternal respiratory SARS-CoV-2 infection may contribute to the poor pregnancy outcomes in COVID-19, and that active infection at the maternal-fetal interface is not required for immune activation at this distant site.

While previous studies analyzing transcriptomic data have yielded mixed results regarding placental *ACE2* expression[185-189], our immunohistochemical analysis conclusively demonstrated that ACE2 protein is present in the placenta despite low transcript levels. Recent studies of central nervous system and other tissue likewise confirm that mRNA level of *ACE2* is not a reliable surrogate for ACE2 protein expression[189,213]. Furthermore, ACE2 protein expression is highest in the first trimester and decreases over

the course of healthy pregnancy, indicating potential vulnerability to SARS-CoV-2 infection during early pregnancy. These data are supported by a recent study that reports *ACE2* mRNA levels decreasing with increased gestational age[214]. Surprisingly, I found that ACE2 expression appears to be widely expressed in the placenta of COVID-19 cases at term despite low levels of ACE2 in the placentas of healthy controls at term. The unique modifying factors that drive placental ACE2 expression during COVID-19 remain unknown; however, studies of ACE2 expression during other disease states, including COPD, suggest that ACE2 is upregulated under inflammatory conditions[215]. These data suggest that the hyperinflammatory state associated with COVID-19 may similarly increase ACE2 expression at the term placenta.

Although I found low mRNA expression of *ACE2* and *TMPRSS2,* there is high expression of a number of other proposed alternative SARS-CoV-2 receptors and co-factors, including *CTSL*, the gene encoding the Cathepsin L protease. CSTL regulates SARS-CoV-2 infection[216,217] and in a genome-wide CRISPR screen of SARS-CoV-2 entry factors was a top hit over TMPRSS2, second only to ACE2[218]. While one of many proposed entry factors, this finding suggests that there are other gene candidates may promote entry of SARS-CoV-2 to the placenta.

Given the extremely low rate of placental infection by SARS-CoV-2 observed clinically, it was unknown whether the healthy term placenta is intrinsically susceptible to SARS-CoV-2. Prior case reports of SARS-CoV-2 infection of the placenta presented in the context of severe comorbid conditions and preeclampsia, suggesting that these placentas may have been uniquely capable of supporting infection. By isolating primary placental cells from elective cesarean sections absent of any comorbidities, complications, or

evidence of infection, I show through in vitro experiments that trophoblasts from the healthy term placenta are capable of being infected by SARS-CoV-2.

The presence of ACE2 at the syncytiotrophoblast layer of the placental villi is consistent with the finding that the *in vivo* distribution of SARS-CoV-2 in rare cases of placental infection is intensely concentrated at the syncytiotrophoblast layer[174,190,195,196]. *In vitro*, however, I detected only minimal infection of primary syncytiotrophoblast cultures after 72 hours post-infection, and intriguingly this was visualized most robustly only in isolated, unsyncytialized cells. Cytotrophoblasts were the only placental cell type that we found were reliably infected by SARS-CoV-2 *in vitro*. Given that syncytiotrophoblasts originate from the spontaneous differentiation and fusion of cytotrophoblast stem cells[219], it is possible that removed from their *in vivo* context, these terminally differentiated cells are not as readily capable of supporting a productive viral infection *in vitro*. These findings may together paint a clearer picture of the events leading to the pattern of placental infection observed *in vivo*; namely, that infected cytotrophoblasts could give rise to syncytiotrophoblasts that through fusion create a wall or layer of infected cells in the placenta. Alternatively, differences in susceptibility of primary placental cells to viral infection *in vivo* versus *in vitro* have also been demonstrated for Zika virus[220]. Zika virus has similarly been found to infect cytotrophoblasts[221] but not syncytiotrophoblasts owing to constitutive IFN-λ production[35]. Notably, unlike Zika virus and many other "TORCH" pathogens linked to congenital conditions following *in utero* exposure, SARS-CoV-2 does not appear to productively infect placental Hofbauer cells either *in vivo* or *in vitro*[12,222,223].

Despite the capacity of trophoblasts to be infected *in vitro*, SARS-CoV-2 invasion of the placenta has only rarely been observed *in vivo*. Indeed, despite active respiratory

infections in our cohort, we detected SARS-CoV-2 RNA in the placenta in only one case of maternal COVID-19 at full-term. However, it is important to note that we were only able to test placentas following parturition, with variable time between maternal symptom onset and delivery for each of our cases (Table 1). Thus, our study offers a view of infectious status at only a snapshot in time and does not represent a generalizable view of the vulnerability of the placenta to SARS-CoV-2 infection prior to delivery. Low rates of placental infection may also be due to previously reported low levels of SARS-CoV-2 viremia[224] (i.e., the absence of a direct route of infection to the placenta *in vivo*), to variable ACE2 expression at term, and/or to protective immune responses elicited in the placenta. Unfortunately, I was unable to screen for potential maternal SARS-CoV-2 viremia in our group, but other studies found no detectable viremia in a large cohort of pregnant women[197] and an extremely low rate of detectable viremia in non-pregnant SARS-CoV-2-infected patients (~1%)[225].

I find that the term placenta exhibits an inflammatory profile in the context of maternal upper respiratory infection and that an active, concurrent infection locally is not required. Even in the absence of placental viral RNA, I observed localized gene expression differences in SARS-CoV-2-affected term placental and decidual tissue indicating a marked immune response to maternal respiratory infection distinctly manifesting at the maternal-fetal interface. Gene ontology analyses reveal certain immune pathways with increased expression and others with decreased expression in the placenta in response to maternal respiratory SARS-CoV-2 infection. Viral infection and immune activation likely perturb the maternal-fetal environment both by upregulating pathways developed for pathogen response, while downregulating the physiological immune pathways intricately

involved in supporting normal pregnancy. The majority of these differentially expressed genes are interferon-regulated genes, demonstrating the capacity of the placenta to sense and respond to even distal infection.

Our cell-cell interaction analysis of transcriptomic changes observed at the maternal-fetal interface uncovered novel interactions, including between NK cells and T cells, that are features of the gene expression changes in placentas from COVID-19-infected women but not in uninfected controls. Decidual NK cells predominate at the maternal-fetal interface early in pregnancy where they promote trophoblast invasion of the decidua and vascular remodeling, but decline to their lowest numbers at term. NK cells are known to play a distinct role in controlling human cytomegalovirus infection at the maternal-fetal interface[226], but it is unknown whether they play a role in responding to non-TORCH infections[227]. Their activation is associated with the release of cytokines and proangiogenic factors[228] and dysregulation of these NK populations is associated with poor outcomes such as preeclampsia[229-232]. I hypothesize that inappropriate activation of NK cells late in pregnancy may contribute to increased risk for complications in COVID-affected pregnancies. This hypothesis is further supported by the bulk sequencing data, in which top gene hits included genes involved in shaping NK and T cell tolerance at the maternal-fetal interface such as HLA-C[233].

I found that *HSPA1A* (Hsp70), is highly upregulated at the maternal-fetal interface during maternal COVID-19. Notably, Hsp70 has been proposed as a potential alarmin that has been shown *in vitro* to stimulate proinflammatory processes associated with parturition and pre-term birth[198,234,235]. Hsp70 is associated with endothelial activation in placental vascular disease[200] and serum levels are increased in cases of preeclampsia[199,236,237].

Extracellular Hsp70 is known to stimulate proinflammatory cytokines such as TNF-α, IL-1β, and IL-6[199]. Hsp70 levels are furthermore significantly elevated in patients exhibiting hemolysis, elevated liver enzymes, and low platelet count (HELLP syndrome) compared to patients with severe preeclampsia without HELLP syndrome[199,238]. Intriguingly, there have been multiple reports of HELLP or HELLP-like syndrome in pregnant women affected by SARS-CoV-2 infection and COVID[174,239,240]. While the interplay between COVID-19 and HELLP-like syndrome remains incompletely understood, these results suggest a potential common pathway for COVID-19 associated maternal morbidity and placental vascular diseases, including HELLP and preeclampsia.

By characterizing changes at the maternal-fetal interface in the context of systemic infection, this study indicates that maternal respiratory SARS-CoV-2 infection at term is associated with an inflammatory state in the placenta that may contribute to poor pregnancy outcomes in COVID-19. These immune responses at the maternal-fetal interface may serve to protect the placenta and fetus from infection, but they also have the potential to drive pathological changes with adverse consequences for developing embryos and fetuses, since *in utero* inflammation is associated with multisystemic defects and developmental disorders in affected offspring[1,241]. Mouse models of congenital viral infection have also shown that type I IFN signaling during early embryonic development can cause fetal demise[242], through the upregulation of IFITM proteins that interfere with cytotrophoblast fusion[243,244]. Further studies are therefore needed to assess the long-term consequences of SARS-CoV-2 associated immune activation in pregnant women regardless of local infectious status of the placenta.

Chapter 4: Challenging COVID-19 vaccine misinformation about pregnancy and fertility

This chapter contains excerpts from:

Lu-Culligan A, Tabachnikova A, Pérez-Then E, Tokuyama M, Lee HJ, Lucas C, Monteiro VS, Miric M, Brache V, Cochon L, Muenker MC, Mohanty S, Huang J, Kang I, Dela Cruz C, Farhadian S, Campbell M, Yildirim I, Shaw AC, Ma S, Vermund SH, Ko AI, Omer SB, Iwasaki A. 2022. No evidence of fetal defects or anti-syncytin-1 antibody induction following COVID-19 mRNA vaccination. *PLOS Biology.* (In revision)

4.1 Author Contributions

I designed and conceived of all experiments with Sasha Tabachnikova under the supervision of Akiko Iwasaki. I performed all mouse experiments including the collection and processing of tissues, conducted or guided the analysis of the data, and interpreted the results. Hannah Lee contributed to mouse tissue harvest and fetal measurements. Carolina Lucas and Valter Silva Monteiro performed SARS-CoV-2 ELISAs. Sasha Tabachnikova performed anti-syncytin-1 antibody ELISAs. The IMPACT Team and DR Team were responsible for human sample cohort selection, consent, and sample collection.

4.2 Summary

The impact of coronavirus disease 2019 (COVID-19) mRNA vaccination on pregnancy and fertility has become a major topic of public interest. I investigated two of the most widely propagated claims to determine 1) whether COVID-19 mRNA vaccination of mice during early pregnancy is associated with an increased incidence of birth defects or growth abnormalities, and 2) whether COVID-19 mRNA-vaccinated human volunteers exhibit elevated levels of antibodies to the human placental protein syncytin-1. Using a mouse model, I found that intramuscular COVID-19 mRNA vaccination during early pregnancy at gestational age E7.5 did not lead to differences in fetal size by crown-rump length or weight at term, nor did I observe any gross birth defects. In contrast, injection of the TLR3 agonist and double-stranded RNA mimic polyinosinic-polycytidylic acid, or poly(I:C), impacted growth *in utero* leading to reduced fetal size. No overt maternal illness following either vaccination or poly(I:C) exposure was observed. I also found that term fetuses from vaccinated murine pregnancies exhibit high circulating levels of anti-Spike and anti-RBD antibodies to SARS-CoV-2 consistent with maternal antibody status, indicating transplacental transfer. Finally, I did not detect increased levels of circulating anti-syncytin-1 antibodies in a cohort of COVID-19 vaccinated adults compared to unvaccinated adults by ELISA. These findings contradict popular claims associating COVID-19 mRNA vaccination with infertility and adverse neonatal outcomes.

4.3 Introduction

Pregnant women are at increased risk for severe coronavirus disease 2019 (COVID-19) with higher rates of hospitalization, intensive care, and death compared to nonpregnant women[176,245-250]. However, pregnant women were not included in the initial COVID-19

vaccine trials, leading to a lack of data on vaccine-associated benefits or adverse events in this population[251]. While the first COVID-19 vaccine trials in pregnant women are now underway, over 158,000 women in the United States have self-identified to the Centers for Disease Control and Prevention (CDC) v-safe COVID-19 Pregnancy Registry as having received some form of the vaccine during pregnancy. The mRNA vaccines, Pfizer-BioNTech's BNT162b2 and Moderna's mRNA-1273, represent the majority of these immunization events as they were the first to receive emergency use authorization in the United States. Preliminary studies of these data found no serious safety concerns to maternal or fetal health associated with mRNA vaccination but these early analyses were most limited in their assessment of vaccination events during the first and second trimesters due to ongoing pregnancies[252,253]. These findings from the CDC are notably consistent with the conclusions from other studies supporting the safety of COVID-19 mRNA vaccination during pregnancy[254,255].

Even as more data accumulate supporting the safety of the mRNA COVID-19 vaccines in pregnant and nonpregnant individuals alike[256,257], public perception of the risk surrounding vaccination has been impacted by the rapid proliferation of numerous theories that lack confirmatory data or overtly misrepresent the current evidence. Women are more likely than men to be vaccine hesitant[258], and a number of these unconfirmed speculations target women's health issues specifically, spreading fear about pregnancy, breastfeeding, and fertility post-vaccination. Concerns about safety and efficacy remain the most highly cited reasons for COVID-19 vaccine hesitancy in reproductive age and pregnant women[259-261]. Meanwhile, public health recommendations for pregnant women in particular continue to evolve with more data, further complicating the process of vaccine acceptance[262].

Concerns about the impact of mRNA COVID-19 vaccination on future fertility are a major source of vaccine hesitancy in non-pregnant women. One of the most frequently noted concerns is that maternal antibodies generated against the severe acute respiratory syndrome coronavirus 2 (SARS-CoV-2) spike protein in response to vaccination could result in cross-reactivity to the retrovirus-derived placental protein, syncytin-1[263]. Syncytin-1 is encoded by the human endogenous retrovirus W (*HERV-W*) gene and is involved in trophoblast fusion during placental formation[264]. There is limited homology between syncytin-1 and spike protein of SARS-CoV-2, and this is likely not sufficient to mediate cross-reactivity of vaccine-induced anti-spike antibodies to syncytin-1. Furthermore, many women at this stage in the pandemic have conceived following both COVID-19 infection and COVID-19 vaccination, with no reports of reduced fertility. Despite the absence of supporting evidence[265-269], the link between the COVID-19 mRNA vaccines and infertility persists, undermining mass vaccination campaigns worldwide.

Amidst public pressure and media scrutiny surrounding the potential risks of vaccination during pregnancy, the beneficial effects of vaccination on the fetus *in utero* have received far less attention. Recent evidence has linked COVID-19 vaccination during the third trimester with improved maternal and neonatal outcomes[270]. Following natural infection with SARS-CoV-2, maternal antibodies against SARS-CoV-2 proteins readily cross the placenta[197,271]. Likewise, recent studies have found antibodies against the Spike and RBD domains of SARS-CoV-2 in human infant cord blood samples following vaccination during pregnancy, suggesting vaccine-induced protection by maternal antibodies is conferred across the maternal-fetal interface[272-275]. Maternal transfer of

antibody-mediated protection following vaccination against SARS-CoV-2 to the infant can additionally occur via breastmilk in nursing women[276-279].

Mouse models permit an investigation of vaccine effects at defined points of organogenesis at the earliest periods of pregnancy, timepoints at which many women do not yet know they are pregnant. Vaccine doses can also be administered to mice at concentrations many times greater than that used in humans to maximize the probability of eliciting and observing any potential teratogenic effects. In this study, I investigated the impact of mRNA-1273 vaccination during early pregnancy using a mouse model to screen for birth defects and quantified circulating antibodies in mother and fetus at the end of gestation. Finally, using human samples, I analyzed the effect of mRNA-1273 (Moderna) and BNT162b2 (Pfizer-BioNTech) vaccination on circulating anti-syncytin-1 antibody levels to address infertility speculation.

4.4 Results

4.4.1 Vaccination of pregnant mice during early pregnancy with mRNA-1273 does not lead to fetal birth defects or differences in fetal size

To determine whether COVID-19 mRNA vaccination during early pregnancy leads to birth defects in mice, pregnant dams were subjected to intramuscular (i.m.) injection of 2 μg mRNA-1273 at E7.5 and fetuses were harvested at term but prior to birth at E18.5 to assess phenotypes. I chose this early timepoint of pregnancy for vaccination, as previous studies have demonstrated particular vulnerability to the development of fetal defects by stimulating maternal innate immune responses during this gestational period[7,156,160,280-282]. I injected a very large dose of mRNA vaccine, 2 μg mRNA-1273 in an average mouse

weighing 25 g corresponding to over 50 times the µg vaccine per g weight administered to humans, to ensure we detect impact of vaccine on the developing fetus, if any. I did not observe any birth defects in either vaccine-exposed or PBS-treated control litters (Figure 4.1, A-B). Fetal length and weight measured directly prior to birth at E18.5, or term prior to parturition, were also not impacted by maternal vaccination during early gestation (Figure 4.1, C-D).

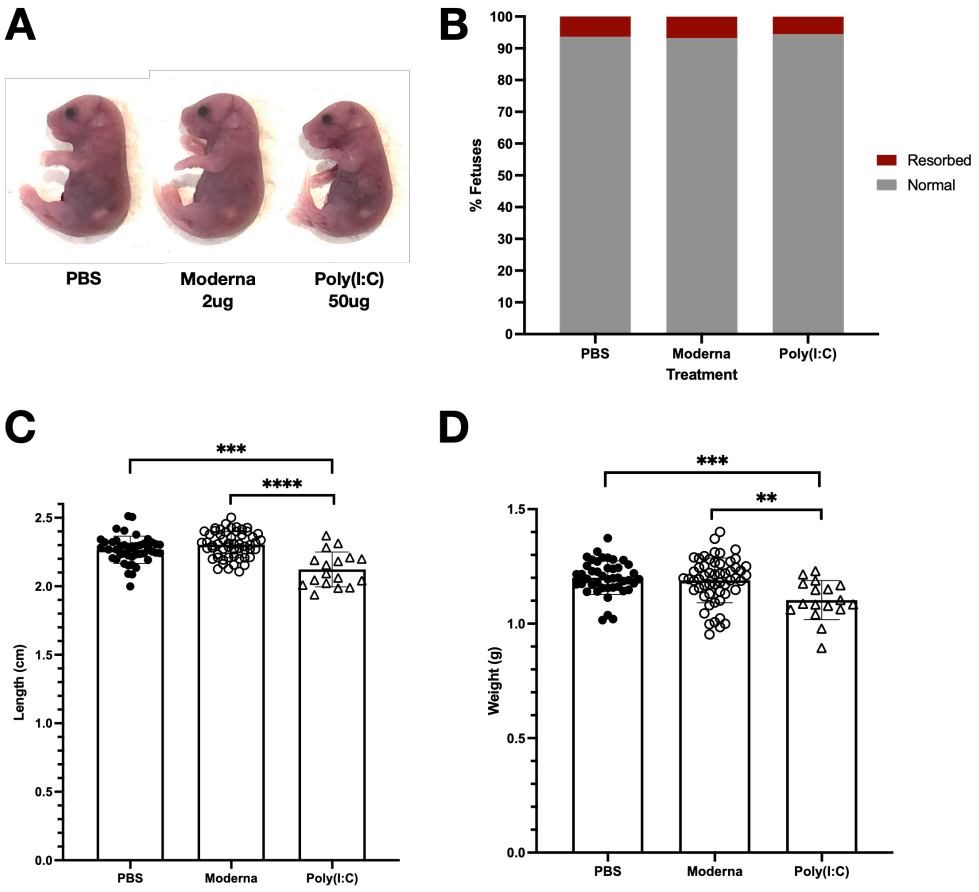

Figure 4.1: Maternal vaccination with mRNA-1273 at E7.5 in early pregnancy does not impact fetal viability or size at term. Pregnant dams were injected intramuscularly with 50ul of PBS (n=6 litters, 44 fetuses), 2 µg Moderna vaccine (n=7 litters, 55 fetuses), or 50 µg poly(I:C) (n=3 litters, 17 fetuses) at E7.5 and fetuses were harvested at E18.5. (A) Normal phenotypes observed in fetuses from PBS-treated and Moderna-vaccinated pregnancies. (B) Fetal resorption rates in PBS-treated, Moderna-vaccinated, and Poly(I:C)-treated pregnancies. (C) Crown-rump length and (D) weight of dissected fetuses. Mean values and standard deviation are represented. Shapiro-Wilk normality tests were used to confirm Gaussian distribution of fetal weights and crown-rump lengths. Brown-Forsythe and Welch ANOVA tests were used to calculate statistical significance (∗: $p \leq 0.05$; ∗∗: $p \leq 0.01$; ∗∗∗: $p \leq 0.001$; ∗∗∗∗: $p \leq 0.0001$).

Administration of poly(I:C), a double-stranded RNA mimic and potent TLR3 agonist, induces maternal immune activation and results in fetal growth restriction and fetal demise in rodents[7,283,284]. Compared to mRNA-vaccinated and control groups, maternal injection i.m. with a high dose of 50 µg poly(I:C) at E7.5 resulted in decreased fetal crown-rump length and weight at E18.5. No birth defects were seen following i.m. delivery of poly(I:C).

4.4.2 Anti-SARS-CoV-2 antibodies are found in fetal circulation at term following maternal vaccination in early pregnancy

In order to test whether vaccine-induced antibodies against SARS-CoV-2 can cross the maternal-fetal interface, we quantified anti-Spike and anti-RBD antibodies in the fetal sera by ELISA following vaccination of dams during early pregnancy. Pregnant dams were vaccinated i.m. with mRNA-1273 at E7.5 and both maternal and fetal sera were analyzed 12 days post-vaccination at E18.5, prior to birth. Both maternal and fetal sera from vaccinated pregnancies contained high levels of circulating antibodies against SARS-CoV-2 Spike and RBD by ELISA as compared sera from PBS-injected mice (Figure 4.2).

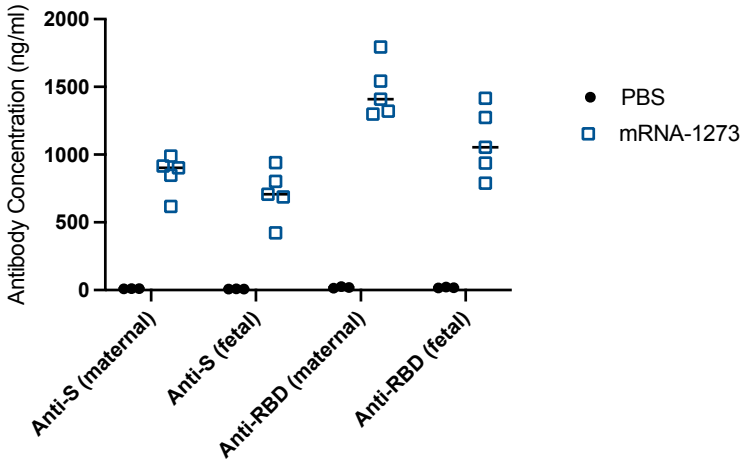

Figure 4.2: Maternal vaccination against SARS-CoV-2 in early pregnancy induces an antibody response that crosses the maternal-interface and is detectable in fetal sera at term. Pregnant dams were injected intramuscularly with 50µl of PBS (n=3 litters) or 2µg Moderna vaccine (n=5 litters) at E7.5. Maternal serum and pooled fetal serum from each litter were collected at E18.5, 12 days post-treatment. Anti-Spike (anti-S) and anti-Receptor-Binding Domain (anti-RBD) levels were measured by ELISA and antibody concentration was calculated based on a standard curve. Horizontal bars represent mean values.

4.4.3 COVID-19 mRNA vaccination does not lead to an increase in anti-syncytin-1 antibodies

We quantified levels of anti-syncytin-1 antibodies in human sera from a cohort of unvaccinated and vaccinated adult volunteers[285] to determine whether vaccination status is associated with anti-syncytin-1 antibodies. Samples from healthy, unvaccinated healthcare workers who tested negative for SARS-CoV-2 by PCR (HCW[PCR-, Pre-Vax]) were used to assess anti-syncytin-1 levels in a healthy, normal population prior to vaccination. Using a kernel distribution estimate to determine the normal range of anti-syncytin-1 antibodies in these healthy controls, the upper limit of normal anti-syncytin-1 levels was found to be 28.8 ng/ml in this group.

We then analyzed anti-syncytin-1 levels in a previously collected cohort of patients with systemic lupus erythematosus (SLE)[286]. SLE is a complex disease with variable presentation that is associated with ERV dysregulation and elevation in anti-ERV envelope antibodies[286]. We detected two SLE patients with highly elevated anti-syncytin-1 antibody levels above the normal range, while the remainder were negative (Figure 4.3).

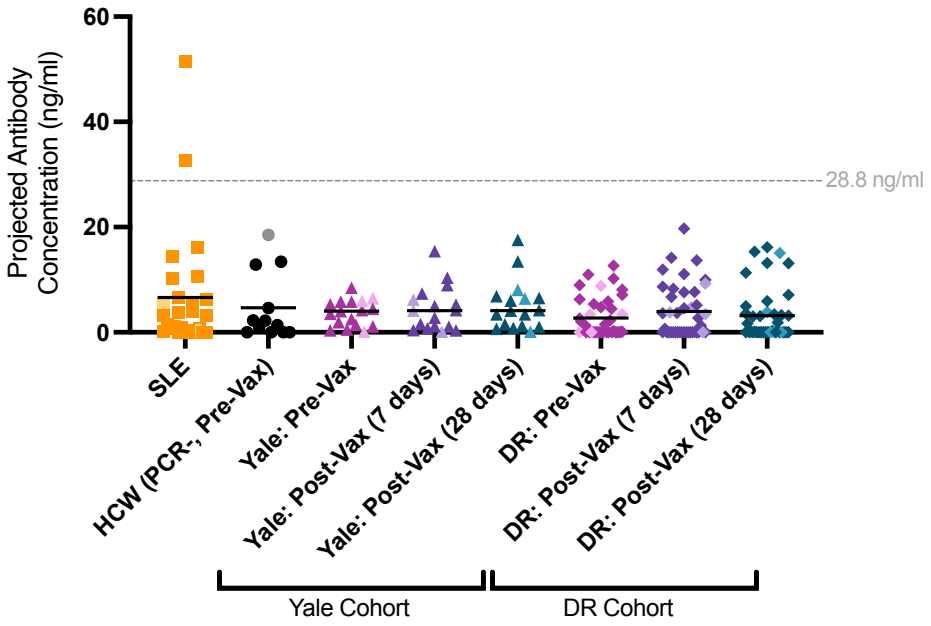

Figure 4.3: mRNA vaccination against COVID-19 is not associated with increased levels of circulating anti-syncytin-1/HERV-W IgG antibodies in humans. Plasma reactivity to syncytin-1 protein was assessed using ELISA. SLE samples (n=27) and uninfected, unvaccinated HCW controls (SARS-COV-2 PCR negative, pre-vaccination; n=12) are shown alongside a cohort (Yale Cohort) of matched samples from individuals pre-vaccination, 7 days post-second vaccine dose, and 28 days post-second vaccine dose of mRNA-1273 or BNT162b2 (n=17). A second cohort (DR Cohort) of matched samples from individuals who had previously received the CoronaVac inactivated virion vaccine and received booster vaccination with BNT162b2 is also shown at timepoints prior to booster vaccination, and at 7- and 28 days post-booster vaccination with BNT162b2. All antibody concentrations were calculated based on a standard curve generated using a monoclonal antibody against syncytin-1. Each dot represents a single individual and male subjects are lightened in color. Horizontal bars represent mean values. Statistical significance was assessed using nonparametric Kruskal-Wallis tests and Mann-Whitney tests. No groups were significantly elevated. Horizontal dashed line (drawn at 28.8168 ng/ml) represents maximum of kernel distribution estimate for HCW (PCR-, Pre-Vax) control samples, indicating the upper limit of the normal range in healthy, unvaccinated individuals.

Next, we compared serum levels of anti-syncytin-1 antibodies in matched samples from individuals in two independent COVID-19 vaccination cohorts, before and after receiving an mRNA vaccine. The first cohort (Yale HCW) was analyzed at three timepoints: 1) pre-vaccination, 2) 7 days post-vaccination (second dose), and 3) 28 days post-vaccination (second dose) with either mRNA-1273 or BNT162b2. The two latter timepoints correspond with the highest titers of anti-SARS-CoV-2 antibodies, peaking at

7 days post-vaccination with the second dose[285]. The second cohort (DR) had already received two doses of the CoronaVac inactivated whole-virion vaccine and was evaluated for anti-syncytin-1 levels before and after a booster vaccination with BNT162b2 using three timepoints: 1) pre-booster vaccination (previously CoronaVac-vaccinated), 2) 7 days post-booster vaccination, and 3) 28 days post-booster vaccination.

In both cohorts examined, administration of mRNA vaccine (either primary series or as a booster to CoronaVac) was not associated with any differences in anti-syncytin-1 IgG levels at 7 and 28 days post-vaccination as compared to matched samples pre-vaccination and unvaccinated SARS-CoV-2-negative controls (Figure 4.3). No samples from either the unvaccinated and COVID-19 mRNA vaccinated groups exhibited anti-syncytin-1 antibody levels outside of the normal range.

We also compared levels of anti-syncytin-1 IgG during acute COVID-19 disease in pregnant and non-pregnant patients. We did not detect significant levels of anti-syncytin-1 antibodies during the acute phase of SARS-CoV-2 infection in either group (Figure 4.4).

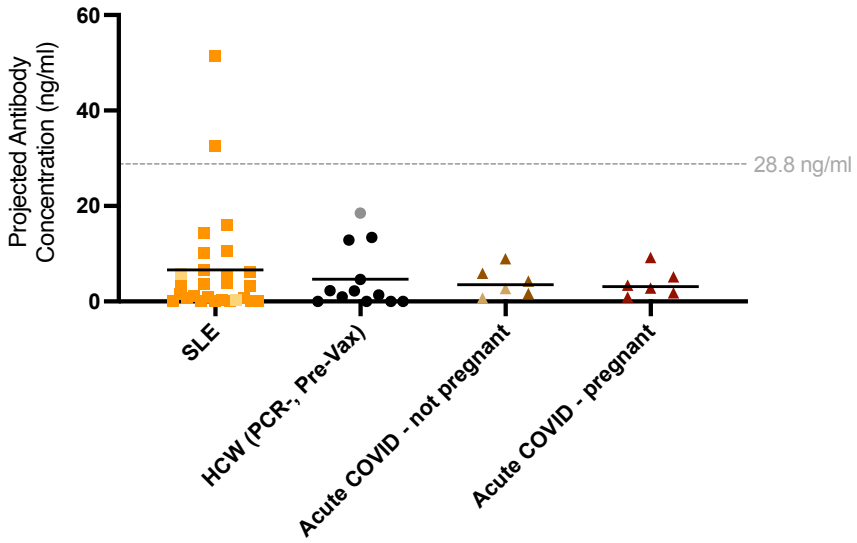

Figure 4.4: Acute COVID-19 disease is not associated with increased levels of circulating anti-syncytin-1/HERV-W antibodies in humans. Plasma reactivity to syncytin-1 protein was assessed by ELISA in SLE samples (n=27), unvaccinated HCW samples (n=12), non-pregnant patients with acute COVID-19 disease (n=7), and pregnant patients with acute COVID-19 disease (n=6). Each dot represents a single individual. Male subjects are lightened in color. Horizontal bars represent mean values. Statistical significance was assessed using nonparametric Mann-Whitney tests. No groups were significantly elevated as compared to HCW controls. Horizontal dashed line (drawn at 28.8168 ng/ml) represents maximum of kernel distribution estimate for HCW (PCR-, Pre-Vax) control samples, indicating the upper limit of the normal range in healthy, unvaccinated individuals.

4.5 Discussion

Public fear surrounding the consequences of vaccination on pregnancy and fertility remains an ongoing source of vaccine hesitancy during the COVID-19 pandemic. Here, we demonstrate in a mouse model that intramuscular injection of the mRNA-1273 vaccine during early pregnancy does not induce birth defects and does not lead to differences in fetal size at birth. These findings are consistent with CDC data in humans that found no congenital anomalies following vaccination in the first trimester or periconception periods, although these numbers were limited[252]. More extensive data on vaccination during the second and third trimesters have similarly shown a high safety profile with no increase in adverse outcomes[252]. Our results did not uncover overt fetal defects in mice exposed to early pregnancy vaccination with an mRNA-1273 dose approximately 50 times greater than that used in humans. The vaccine dosage used in these murine studies (2 μg total, or 0.08 μg mRNA-1273 per gram weight in a 25 g mouse) are over 50 times the dose by weight used in humans (100 μg regardless of weight, or 0.00125 μg mRNA-1273 per gram weight for average individual of 80 kg in the U.S.). We specifically chose this high dose to test whether COVID-19 mRNA vaccine has any potential deleterious effects on pregnancy. Our data demonstrated no negative impact of the vaccine on the pregnant mother or the developing fetus.

Intramuscular administration of poly(I:C), a synthetic double-stranded RNA, to pregnant dams at the same timepoint in early pregnancy also did not result in birth defects. However, poly(I:C)-treated pregnancies were associated with decreased fetal size by crown-rump length and weight at the end of gestation.

The observed differences in fetal outcomes for mRNA vaccine-treated pregnancies and poly(I:C)-treated pregnancies may be attributed to key differences in the immune response induced. The mRNA vaccines, including mRNA-1273, are designed to exhibit reduced immunogenicity with targeted modifications such as N1-methylpseudouridine (m1Ψ) substitutions that decrease TLR3 activation[164]. In contrast, poly(I:C) leads to the robust activation of innate immune sensors such as TLR3. It is well established that poly(I:C) or viral infection during early pregnancy in mice leads to fetal growth restriction and demise[283,287,288]. In contrast, even at high doses, mRNA vaccine resulted in no negative impact on the developing fetus. These findings further suggest that the immune response generated after mRNA vaccination is safer in pregnancy than the immune response to SARS-CoV-2 infection, which is known to elicit a robust inflammatory signature at the maternal-fetal interface[175].

Our data also demonstrated that pregnant dams vaccinated during early pregnancy, prior to the establishment of fetal circulation, subsequently confer protective antibodies to the *in utero* fetus up to the time of birth. These findings are consistent with human studies showing the presence of SARS-CoV-2 vaccine-induced antibodies in cord blood following delivery and currently limited data on first trimester vaccination[272-275].

Recent studies suggest that the timing of vaccination during pregnancy may be important for the efficiency of transplacental transfer of antibodies from mother to fetus,

with some pointing to a beneficial impact of vaccination earlier in pregnancy during the second or early third trimester compared to later in the third trimester[289-294]. Though many women have now received COVID-19 vaccinations in the first trimester, few studies had previously been able to focus on immunization during these early timepoints. Given this interest, continuation of this work is thus necessary to comprehensively investigate both the safety and potential of earlier vaccination schedules.

Limitations of our mouse model of vaccination include the use of a single dose of mRNA-1273 during pregnancy whereas the full vaccine schedule in humans is two doses approximately 28 days apart, longer than the murine gestation period. While this study provides the first step in establishing safety for early vaccine approaches in pregnancy, we surveyed litters only for overt birth defects and size at E18.5. Findings of this work await validation with results from the ongoing human studies of vaccination during the first trimester. Our study does not capture potential effects of mRNA vaccination timing during late gestation.

Finally, using human data we demonstrated that circulating anti-syncytin-1 antibodies are not increased following COVID-19 mRNA vaccination with either mRNA-1273 or BNT162b2 in two independent cohorts with a total of 96 subjects, using matched samples collected over time. Notably, we did not detect elevated anti-syncytin-1 antibody levels in any samples from our vaccinated cohorts and the prevalence of anti-syncytin-1 autoimmunity appears to be low. Even in a population at high risk for anti-ERV autoimmunity, only two out of 27 individuals with SLE were found to exhibit anti-syncytin-1 levels above the normal threshold. These findings represent the largest study of anti-syncytin-1 antibody status in individuals receiving the COVID-19 mRNA vaccines to

date and add to the mounting evidence that a syncytin-1-based mechanism of infertility by mRNA vaccination against SARS-CoV-2 Spike protein is not supported by scientific observations[263,265,266].

Millions of women and pregnancies continue to be impacted by the ongoing COVID-19 pandemic and by vaccine hesitancy. In the absence of complete clinical trial data, many women are choosing to vaccinate during pregnancy after weighing the risks and benefits of their situation. Thus, filling in gaps in knowledge, particularly surrounding vaccination in early pregnancy, and combatting misinformation are more imperative than ever. This study thus provides a reassuring view of the safety and protection provided following COVID-19 mRNA vaccination during early pregnancy within a mouse model. We demonstrate the absence of anti-syncytin-1 antibodies in our cohort of vaccinated adults, discrediting one of the most widespread infertility myths surrounding COVID-19 vaccination. Future work must be expanded to examine the impact of vaccination at all gestational ages and continue to provide data that can address public concerns about vaccine safety in all populations.

Appendix 1: Methods and Data Analysis

A1.1 Methods and Data Analysis for Chapter 2: Establishment and characterization of a novel model of maternal immune activation leading to fetal neural tube defects

Animals

All animal procedures were completed in compliance with approved Yale Institutional Animal Care and Use Committee protocols. C57BL/6J and knockout mice were purchased from Jackson Laboratory or bred in-house from Jackson Laboratory stocks.

Maternal immune activation

Mice were mated overnight and females were checked for the presence of seminal plugs each morning, designated E0.5. On E7.5, pregnant mice were injected intraperitoneally with 100 ul of either PBS or 100 μg poly(I:C) (Invivogen #vac-pic). Vaccigrade HMW poly(I:C) (Invivogen #vac-pic) was prepared at 1 mg/ml at room temperature and stored at -20°C, then thawed to room temperature prior to injection. Pregnant mice were left undisturbed in their cages until collection at the specified embryonic date. All females used were 6-12 weeks of age.

Flow cytometry

At E9.5, pregnant uterus was collected and for each conceptus the myometrium was dissected away from decidua and fetal tissues in clean PBS. Tissues were pooled and collected in digestion buffer containing cold HBSS with Ca^{2+} and Mg^{2+} with 26 WU/ml of Liberase TM and 4 mg/ml DNase I at no more than 100 mg tissue/ml digestion buffer. Concepti from the same litter were pooled together. Tissue was minced before incubation in a 37°C water bath for 60 minutes, pipetting samples every 10 minutes. Samples were then centrifuged at 1000 x g for 4 minutes and supernatant removed. Red blood cell lysis was performed by resuspending pellet in 1 ml PBS and 1 ml ACK lysis buffer and incubating at room temperature for 3 minutes before quenching with RPMI. Cells were washed and strained through a 70-μm nylon mesh cell strainer prior to incubation in Fc blocking buffer for 15 minutes at 4°C. After washing, cocktail of primary antibodies was added to cells for 30 minutes at 4°C. For stimulation experiments, cells were first incubated with Cell Stimulation Cocktail and Protein Transport Inhibitors (eBioscience) in complete RPMI for 4 hours at 37°C before antibody staining and detection of intracellular expression levels of transcription factors and cytokines using the Foxp3/Transcription Factor Staining Buffer Set (eBioscience). Samples were analyzed on an Attune NXT (ThermoFisher). Data were analyzed using FlowJo software (version 10.7, Tree Star).

Antibody-mediated depletions

Timed matings were set up as described above. For IL-17a depletion, pregnant dams were injected with 500 μg anti-IL-17a antibody (BioXCell, clone 17F3) or 500 μg mouse IgG1 isotype control antibody (BioXCell, clone MOPC-21), 8 hours prior to poly(I:C) injection at E7.5 as previously described[119,121]. For NK cell depletion, pregnant

dams were injected with 200 µg anti-NK1.1 (BioXCell, clone PK136) or mouse IgG2a isotype control antibody (BioXCell, clone C1.18.4) at E6.5, 24 hours prior to poly(I:C) injection at E7.5. For CD4 and CD8 T cell depletion, pregnant dams were injected with 300 µg of anti-CD4 (clone GK1.5, BioXCell) and 300 µg of anti-CD8 (clone 2.43, BioXCell), or 600 µg of rat IgG2b isotype control antibody (clone LTF-2, BioXCell) at E6.5, 24 hours prior to poly(I:C) injection at E7.5. Depletion of >95% was confirmed by flow cytometry at E9.5.

Serum cytokine measurements

Maternal blood was collected and sera was isolated by two rounds of centrifugation at 10,000 x g for 10 minutes in a benchtop centrifuge at 4°C. Sera was aliquoted and stored at -80°C. Samples were shipped to Eve Technologies (Calgary, Alberta, Canada) on dry ice, and levels of cytokines and chemokines were measured using the Mouse Cytokine Array/Chemokine Array 31-Plex Panel. All samples were measured after a maximum of 1-2 freeze-thaw cycles.

Immunofluorescence

Samples in OCT were cut in 20um sections using a Leica cryostat. After sectioning, samples were blocked for 2 hours at RT in PBS with 1% BSA, 0.3% Triton-X 100, and 1% Fc Block (anti-CD16/CD32, clone 93, ThermoFisher). Samples were then stained overnight at 4°C at 5 µg/mL with TCRγδ, BV421 (GL3, Biolegend) or 2.5 µg/mL for other markers. Antibodies used are as follows: Laminin, DyLight 550 (polyclonal, ThermoFisher Cat# PA5-2903); Vimentin, AF647 (clone D21H3, CellSignaling Technologies); pan-

Cytokeratin (clone C-11, Biolegend) conjugated with CF405L Mix-n-Stain Antibody conjugation kit (Biotium). Slides were washed with PBS and mounted with Fluoromount G (ThermoFisher).

Confocal immunofluorescence microscopy was acquired with a Leica SP8-STED or Leica Stellaris 8 microscope. Image processing and quantification was performed using Imaris software (Bitplane).

For the quantification of γδ T cells, Imaris software (Bitplane) was used to segment cells based on BV421-gdTCR (clone GL3) staining. Segmented γδ T cells were verified manually during counting. Identified γδ T cells were categorized by tissue location using tissue morphology as well as staining patterns for laminin (myometrium, yolk sac), cytokeratin (yolk sac, EPC), and vimentin (decidua is vimentin-positive, EPC is vimentin-negative) staining patterns. Quantified γδ T cells were compared between PBS- and poly(I:C)-treated conditions using student's t-test in R software.

Bulk RNA sequencing

Pregnant uteri were collected and concepti were dissected to separate the 1) myometrium, 2) decidua and extraembryonic tissues, and 3) fetus. All tissues were transferred into 600 ul Trizol (Invitrogen) in Lysing Matrix D tubes (MP Biomedicals) and homogenized using a FastPrep-24 Classic Instrument (MP Biomedicals). Samples were centrifuged at 10,000 x g for 10 min on a benchtop centrifuge at 4°C. RNA was extracted with the Qiagen RNeasy Kit and stored at -80°C. Depletion of rRNA, library preparation, and sequencing on the Illumina HiSeq 2500 platform were performed at the Yale Center for Genome Analysis (YCGA).

FASTQ files from HiSeq 2500 were analyzed using Kallisto v0.46.1[95] using the "-b 100 and -t 20" options to obtain transcript abundances in TPM and estimated counts. The kallisto index used during transcript quantification was built (31bp k-mer length) from the *Mus musculus* transcriptome GRCm39 downloaded as a FASTA file from Ensembl (Ensembl.org). Transcripts were annotated using the Bioconductor package biomaRt v2.40.5[96] in R v3.6.2.

Read counts for individual transcripts were summarized for gene-level analysis using the Bioconductor package tximport v1.12.3 with default parameters[97]. Differential expression analysis was performed using DESeq2 v1.24.0 with default parameters[98].

10x Visium Spatial Gene Expression and analysis

Concepti were collected at E9.5 following MIA and flash frozen in an isopentane bath in liquid nitrogen as described in 10x Visium protocol. Frozen tissue was sectioned at 10 μm per section onto 10x Visium Capture Slides and subjected to the complete 10x Visium Spatial Gene Expression Protocol. Depletion of rRNA, library preparation, and sequencing on the Illumina NovaSeq platform were performed at the Yale Center for Genome Analysis (YCGA).

Output of Space Ranger was read into R version 4.0.2 (R Core Team 2020) with Load10x_Spatial function from Seurat version 4.0.5[295]. Counts were normalized using regularized negative binomial regression with Seurat function SCTransform[296] with default parameters. The data from all 8 Visium sections were integrated using the Seurat integration workflow as follows: top 3000 variable features to use for integration were selected with SelectIntegrationFeatures, the data were prepared with PrepSCTIntegration,

anchors were determined with FindIntegrationAnchors, and integration was performed with IntegrateData. All subsequent steps up to clustering were performed using the integrated dataset. Dimensionality reduction, UMAP projection, nearest neighbor graph creation, and clustering were performed using RunPCA, RunUMAP, FindNeighbors, and FindClusters respectively. For clustering resolution parameter was set to 1. Marker genes specific to each cluster were identified with FindConservedMarkers.

For each cluster, we compared PBS- and poly(I:C)-treated groups by performing differential gene expression analysis separately for WT (C57BL/6J) and *Tcrd*$^{-/-}$ samples. The two lists of differentially expressed genes were examined for candidates that exhibited a divergent response to poly(I:C) treatment depending on WT or *Tcrd*$^{-/-}$ genetic background (i.e., genes regulated by an interaction between functional *Tcrd* gene status and poly(I:C) treatment status). We identified our targets as those genes in which the direction of change (up, down, or unchanged in response to poly(I:C) treatment) in WT mice is different from that in *Tcrd*$^{-/-}$ mice. For these analyses, we used two types of differential expression tests: (1) Wilcoxon Rank Sum test as implemented in Seurat, and (2) a modified version of Welch's *t*-test such that the sample size is calibrated based on the Intraclass Correlation Coefficient (ICC) of normalized gene expression values of a given gene[297]. The latter method accounts for the nested experimental design and helps moderate the risk of false discoveries[298]. Gene set enrichment analyses were performed using the Metascape web tool, version 3.5[299].

A1.2 Methods and Data Analysis for Chapter 3: Investigation of SARS-CoV-2 infection during human pregnancy and its impact on the maternal-fetal interface

Human subjects

All women who presented to Yale New Haven hospital for delivery underwent routine clinical testing for SARS-CoV-2 during the study period (March 27, 2020 to June 1, 2020). Women who were admitted to Yale New Haven Hospital Labor and Birth during the study period and who were positive for SARS-CoV-2 by nasopharyngeal swab RT-qPCR at the time of or in the one month prior to delivery hospitalization were approached for consent to donate additional tissue for research studies through the Yale IMPACT study (Implementing Medical and Public Health Action Against Coronavirus in CT). These participants provided informed consent for research studies of donated placental and blood tissue. They provided additional clinical information and were included in RNA sequencing and PCR analyses of placenta. In addition, for the histological analyses, we performed chart review to retrospectively identify all women who were diagnosed with SARS-CoV-2 infection by NP swab RT-qPCR at the time of or in the one month prior to delivery during the study period, and who had placental sections available for histological review. Pre-pandemic (before 2019) histological controls were selected from pathology files at Yale New Haven Hospital and matched to the COVID-19 placental cases by maternal age, gestational age, and maternal co-morbidities. Additional SARS-CoV-2 uninfected women (as determined by negative RT-qPCR testing of nasopharyngeal swab)

were recruited during the study period and provided informed consent to donate placenta tissue to serve as uninfected controls for transcriptomic studies. Placentas from uninfected controls were confirmed negative by RT-qPCR. The study was approved by the Yale Institutional Review Board (protocol #2000027690 and 2000028550).

Pathology files at Yale New Haven Hospital were searched for placentas corresponding to cases of maternal COVID-19 during the study period. All available placental cases were included in the histological study. Additionally, pathology files were searched for placentas from mothers without SARS-CoV-2 infection (pre-June 2019) to serve as historical controls. These controls were matched to study cases for maternal age, gestational age and maternal comorbidities. A total of 27 cases and 10 matched controls were assessed histologically. Of those, one case was of a dichorionic diamniotic twin pregnancy. The placentas of this twin pregnancy demonstrated extremely similar microscopic features and identical pathologic scores; thus, they were together considered as a single case in the statistical analysis.

For healthy control tissues and placental cell isolation, samples from normal term placentas were collected anonymously from healthy patients undergoing elective repeat Cesarean sections. All women who provided term placental samples signed an informed consent (Yale IRB protocol 1208010742).

First and second trimester specimens from the elective termination of pregnancy, ranging from 7 to 15 weeks of gestation (based on last menstrual period), were collected from otherwise healthy women with no known genetic or other abnormalities, as previously described[300]. All women who provided first and second trimester placentas signed an informed consent (protocol #021-06-972) approved by the ethical committee of the Bnai

Zion Medical Center, Haifa, Israel under Helsinki convention guidelines. Placentas of gestational age 18 to 23 weeks were obtained from non-genetic healthy terminations through the University of Pittsburgh Biospecimen Core (IRB#: PRO18010491).

Primary cell cultures

Isolation of Hofbauer cells and cytotrophoblasts from healthy term placentas was performed as previously described[301]. Placentas from uncomplicated term pregnancies were brought to the laboratory within 30 minutes following elective cesarean section without labor at Yale-New Haven Hospital and processed immediately. Inclusion criteria included maternal BMI <40, singleton pregnancy, neonatal birth weight >2500g, and >10th percentile for neonatal weight. Exclusion criteria included multiple gestations, evidence of infection, any significant comorbidities (i.e., chronic hypertension, diabetes mellitus, autoimmune disease, congenital heart disease, chronic severe asthma, thrombophilia), placental abruption or vaginal bleeding during pregnancy, psychiatric conditions, use of medications associated with preterm delivery, and substance use during delivery. Primary placental cells were maintained in F12:DMEM with 10% FBS supplemented with antibiotic/antimycotic.

Cell lines

BeWo cells were maintained in F12K Kaighn's modified media, HTR-8/SVneo cells in RPMI media, and Vero E6 cells in F12:DMEM media, all with 10% FBS and antibiotic/antimycotic.

SARS-CoV-2 detection in placenta by RT-qPCR

Placenta samples were homogenized and centrifuged before nucleic acid was extracted using the MagMax Viral/Pathogen Nucleic Acid Isolation Kit. RNA was isolated from cells infected with SARS-CoV-2 *in vitro* using the Qiagen RNeasy Mini Kit.

SARS-CoV-2 was detected using a modified RT-qPCR assay with the N1, N2, and human RNase P (RP) primer-probe sets developed by the CDC and the NEB Luna Universal Probe One-Step RT-qPCR kit on the Bio-Rad CFX96 Touch Real-Time PCR Detection System[302]. Each sample was extracted and tested in duplicate to confirm results. Placenta samples were considered positive by RT-qPCR if cycle threshold (CT) values for N1 and N2 were both <38, and with any value of RP. Samples were considered negative if N1 and N2 >38, and RP <38. Samples were considered invalid if N1 and N2 >38 and RP >38.

SARS-CoV-2 S1 spike protein IgM and IgG serology testing

ELISA assays for IgG and IgM antibodies towards SARS-CoV-2 were performed on plasma as described by Amanat et al. [303]. Screening was conducted on a total of 367 plasma samples from all SARS-CoV-2-positive patients enrolled.

In short, Triton X-100 and RNase A were added to serum samples at final concentrations of 0.5% and 0.5 mg/ml respectively and incubated at room temperature for 30 min before use to reduce risk from any potential virus in serum. Then, 96-well MaxiSorp plates (Thermo Scientific 442404) were coated with 50 µl per well of recombinant SARS-CoV-2 S1 protein (ACROBiosystems S1N-C52H3-100 µg) at a concentration of 2 µg/ml in PBS and were incubated overnight at 4°C. The coating buffer was removed, and plates

were incubated for one hour at room temperature with 200 µl of blocking solution (PBS with 0.1% Tween-20, 3% milk powder). Serum was diluted 1:50 in dilution solution (PBS with 0.1% Tween-20, 1% milk powder) and 100 µl of diluted serum was added for two hours at room temperature. Plates were washed three times with PBS-T (PBS with 0.1% Tween-20) and 50 µl of HRP anti-Human IgG Antibody (GenScript A00166, 1:5000) or anti-Human IgM-Peroxidase Antibody (Sigma-Aldrich A6907, 1:5000) prepared in dilution solution were added to each well. After one hour of incubation at room temperature, plates were washed six times with PBS-T. Plates were developed with 100 µl of TMB Substrate Reagent Set (BD Biosciences 555214) and the reaction was stopped after 12 minutes by the addition of 100ul of 2 N sulfuric acid. Plates were then read at a wavelength of 450 nm and 570 nm.

The cut-off values for seropositivity were determined as 0.392 and 0.436 for anti-S1-IgG and anti-S1-IgM, respectively. Eighty pre-pandemic plasma samples were assayed to establish the negative baselines, and these values were statistically determined with confidence level of 99%.

Histopathological analysis of placenta

Freshly collected specimens were fixed in 10% neutral buffered formalin (NBF) for at least 24-48 hours and embedded in paraffin, after which 5 µm sections were placed on coated glass slides designed for H&E staining and immunohistochemistry (IHC) processing.

For historical specimens, pathology files at Yale New Haven Hospital were searched for placentas corresponding to cases of maternal COVID-19 during the study

period. All available placental cases were included in the histological study. Additionally, pathology files were searched for placentas from mothers without SARS-CoV-2 infection (pre-June 2019) to serve as historical controls. These controls were matched to study cases for maternal age, gestational age and maternal comorbidities. A total of 27 cases and 10 matched controls were assessed histologically. Of those, one case was of a dichorionic diamniotic twin pregnancy. The placentas of this twin pregnancy demonstrated extremely similar microscopic features and identical pathologic scores; thus, they were together considered as a single case in the statistical analysis. All placentas received with a requisition form for pathologic evaluation were immediately fixed in 10% neutral buffered formalin for three days. A total of six sections inclusive of at least two full thickness sections, peripheral membranes and umbilical cord were submitted for histologic examination.

Two pathologists (LI and RM) blinded to patient information and diagnostic report independently scored all H&E stained placental tissue for villitis (absent, low-grade or high-grade; if low-grade, focal or multifocal and if high-grade, patchy or diffuse), intervillositis (absent or present), increased intervillous fibrin (absent or present, defined as intervillous fibrin occupying >10% of a full thickness section on 20x low-power magnification), chorioamnionitis (absent or present; if present, maternal and fetal inflammatory responses were staged and graded), fetal and/or maternal vascular malperfusion (absent or present; if present, a histologic description was recorded) and increased decidual lymphocytes (absent or present, defined as clusters of >10 lymphocytes in >3 foci in the placental disc and/or peripheral membranes). Diagnostic criteria for villitis, chorioamnionitis, fetal vascular malperfusion (FVM) and maternal vascular malperfusion

(MVM) followed those reported in the Amsterdam placental workshop group consensus statement[304]. Cases with discrepant scoring results were reviewed and re-scored by both pathologists simultaneously. Results were correlated with maternal, fetal and placental COVID-19 status.

ACE2 immunohistochemistry

Following dissection, placental tissue was rinsed in PBS and fixed in 10% neutral buffered formalin for 48-72 hours. Tissues were paraffin-embedded and cut into 5 μm thickness sections by Yale Pathology Tissue Services. The following rabbit polyclonal antibodies were used: anti-ACE2 (Abcam, Cambridge, MA, ab108252, used at 1 μg IgG/ml); and, as a negative control, normal rabbit serum (Sigma-Aldrich, St. Louis, MO, R9133, used at 1 μg IgG/ml). Antibody concentrations were chosen to produce strong staining in the positive cellular structures without background staining.

Slides were immunohistochemically stained as previously described[305] using the MACH2 Rabbit HRP-Polymer system (Biocare Medical, RHRP520L, Pacheco, CA) to mark the sites of antibody binding with a brown deposit. All buffers contained Tween20 (Sigma-Aldrich, P1379) to facilitate uniform application of all reagents and 0.1% bovine serum albumin (Sigma-Aldrich, A9647) to block background staining. Paraffin sections were heated for 30 minutes at 60°C and treated with xylenes followed by rehydration in decreasing concentrations of ethanol (100%, 90%, 80%, 70%). After deparaffinization, antigen retrieval was performed by heating the slides in citrate buffer (pH 6.0) to ≥95˚C for 60 minutes using an Oster model 5712 food steamer. The citrate buffer was then allowed to cool to a temperature of 28˚C before the slides were removed. Endogenous

peroxidase activity was blocked by incubation in 0.03% hydrogen peroxide in ddH_2O for 30 minutes. The slides were drained and primary antibody was applied overnight at 4˚C. After washing, the secondary polymer was applied according the Biocare MACH2 system instructions. The chromagen step utilized the Biocare Betazoid DAB Chromagen kit (BDB2004) for exactly 5 minutes at room temperature. Slides were counterstained with hematoxylin, decolorized with 4% acetic acid, and fixed with Li_2CO_3 for 40 seconds. The slides were then dehydrated in increasing concentrations of ethanol, cleared with xylenes, and mounted with VectaMount permanent mounting medium (Vector Laboratories H-5000). To minimize run-to-run variability, replicate samples were stained simultaneously with one antibody. Positive control sections from a de-identified normal human kidney were analyzed concurrently with each batch of slides.

For quantification of immunoreactivity, slides were inspected microscopically using a raster pattern to ensure that the entire histologic section was examined. A modified histology score[306] was calculated by multiplying the percentage of trophoblasts that stained by the average staining intensity (ranging from 0-3), resulting in H-scores from 0 and 300.

Primary cell isolations from placentas

Isolation of Hofbauer cells and cytotrophoblasts from healthy term placentas was performed as previously described[301]. Placentas from uncomplicated term pregnancies were brought to the laboratory within 30 minutes following elective cesarean section without labor at Yale-New Haven Hospital and processed immediately. Inclusion criteria included maternal BMI <40, singleton pregnancy, neonatal birth weight >2500g, and >10th percentile for neonatal weight. Exclusion criteria included multiple gestations, evidence of

infection, any significant comorbidities (i.e., chronic hypertension, diabetes mellitus, autoimmune disease, congenital heart disease, chronic severe asthma, thrombophilia), placental abruption or vaginal bleeding during pregnancy, psychiatric conditions, use of medications associated with preterm delivery, and substance use during delivery.

Villous tissue was dissected, minced, and rinsed with PBS. Minced tissue was subjected to sequential enzymatic digestions in a solution of 0.25% trypsin and 0.2% DNase I at 37°C. Undigested tissue was removed by passage through gauze and a 100-μm sieve. Cells were resuspended in DMEM:F12 media with 10% FBS and 1% antibiotic/antimycotic.

Cytotrophoblasts were separated on a discontinuous gradient of Percoll (50%/45%/35%/30%) by centrifugation at 1000 x g for 20 minutes at room temperature. Cells migrating to the 35%/45% Percoll interface were recovered by centrifugation at 300 x g for 10 minutes at room temperature and immunopurified by negative selection using mouse anti-human CD9 antibody and mouse anti-human CD45 antibody. Following incubation with goat anti-mouse IgG-conjugated Dynabeads, contaminating cells were removed by exposure to a magnet.

Hofbauer cells were isolated from further digestion of trypsin-treated tissue with collagenase A and DNase I. Cells were pelleted, resuspended in RPMI, and loaded onto a discontinuous Percoll gradient (40%/35%/30%/20%) and centrifuged for 30 minutes. Cells from the 20%/25% to 30%/35% interfaces were combined and immunopurified by negative selection using sequential treatment with anti-EGFR and anti-CD10 antibodies conjugated to magnetic beads. Cells from the supernatant were plated and after 1 hour of incubation, floating and weakly adherent cells were removed.

Fibroblasts were obtained from cells removed during negative immunoselection of cytotrophoblasts and Hofbauer cells. Bead-cell mixtures were washed and cultured in media until confluency was reached. Following trypsinization of first passage cells, magnetic beads with attached cells (~10% of population) were removed with a magnet. Passage 3 fibroblasts were used for experiments.

SARS-CoV-2 infections in vitro

Primary placental cells were with icSARS-CoV-2 mNG[192] infected at an MOI of 5 for one hour at 37°C. Following infection, cells were washed three times in PBS before adding fresh media. At the indicated timepoints, cells were washed three times in PBS and collected in Trizol (Invitrogen).

Immunofluorescence sample preparation and imaging

Placental cells on coverslips were fixed in fixed in 4% paraformaldehyde for 24 hours. Coverslips were blocked and permeabilized in 3% BSA (Sigma) and 0.1 % Triton X-100 (American Bioanalytical). Each sample was incubated overnight with anti-SARS-CoV-2-NP rabbit polyclonal antibody (GeneTex # GTX135357) at a dilution of 1:200. After washing in PBS, coverslips were incubated for 1 hour in a 1:500 dilution of Alexa 594 anti rabbit secondary antibody (Jackson ImmunoResearch 711-585-152), washed again in PBS and treated with 1 μg/mL Hoechst 33342 for 10 min and washed a final time in PBS. Samples were then mounted in DABCO/glycerol mounting media (Sigma) and imaged on a Leica Sp8 Laser Scanning Confocal Microscope equipped with a 40x N.A.

1.3 HC PL APO CS2 objective. Images are displayed as maximum intensity projections of z-stacks and a color bar is given in arbitrary digital units.

Preparation of decidua and placental villi for bulk and single-cell sequencing

Placentas were collected from Yale-New Haven Hospital and transferred to the laboratory for processing. Placental villi were isolated by sampling from midway between the chorionic and basal plates of the placenta. The decidua parietalis was isolated from the chorioamniotic membranes as previously described[307]. The chorioamniotic membranes were dissected, rinsed in PBS, and placed with the chorion facing upward. Blood clots were removed using fine-point forceps and membranes were rinsed in PBS. A disposable cell scraper was used to gently remove the decidual layer from the membrane.

Dissected tissues were rinsed thoroughly in PBS and minced with scissors in a tissue digestion buffer of Liberase TM (0.28 WU/ml) and DNase I (30 μg/ml) in HBSS with Ca^{2+} and Mg^{2+}. Finely minced tissue was enzymatically digested at 37°C for 1 hour with agitation, pipetting, and further mincing every 10 minutes until disaggregated. The suspension was passed through sterile gauze, centrifuged at 1000 x g for 5 minutes at 4°C to pellet cells, and washed with fresh digestion buffer. After centrifugation, the supernatant was aspirated and the cell pellet was resuspended in ACK lysing buffer for 5 minutes. Cells were centrifuged and resuspended in RPMI media before filtering through a 70-μm mesh cell strainer.

Bulk RNA sequencing

Total RNA was prepared from freshly isolated placental villi dissected from clinical specimens and rinsed three times in PBS. Homogenization and nucleic acid extraction were performed using the MagMax Viral/Pathogen Nucleic Acid Isolation Kit. RNA was isolated from cells infected with SARS-CoV-2 *in vitro* using the Qiagen RNeasy Mini Kit. Depletion of rRNA, library preparation, and sequencing on the Illumina HiSeq 2500 platform were performed at the Yale Center for Genome Analysis (YCGA).

FASTQ files from HiSeq 2500 were analyzed using Kallisto v0.46.1[308] using the "-b 100 and -t 20" options to obtain transcript abundances in TPM and estimated counts. The kallisto index used during transcript quantification was built (31bp k-mer length) from the *Homo sapiens* transcriptome GRCh38 downloaded as a FASTA file from Ensembl (Ensembl.org). Transcripts were annotated using the Bioconductor package biomaRt v2.40.5[309] in R v3.6.2.

Read counts for individual transcripts were summarized for gene-level analysis using the Bioconductor package tximport v1.12.3 with default parameters[310]. Differential expression analysis was performed using DESeq2 v1.24.0 with default parameters, comparing all 3rd trimester samples by maternal status.

Single-cell RNA sequencing

Library preparation: Single-cell suspensions were loaded onto the Chromium Controller (10x Genomics) for droplet formation. scRNA-seq libraries were prepared using the Chromium Single Cell 3′ Reagent Kit (10x Genomics). Samples were sequenced using the Illumina NovaSeq platform.

Data preprocessing and clustering: Sequencing results were demultiplexed into FASTQ files using the Cell Ranger (10x Genomics; v3.0.2) mkfastq function. Samples were aligned to GRCh38 10x genome and the count matrix was generated using the count function with default settings. Low quality cells containing <500 or >6000 genes detected were removed, as well cells with >20% of transcripts mapping to mitochondrial genes. Genes that were present in less than 3 cells were excluded from analysis. Gene expression values were then normalized, log-transformed, and scaled. Single cell transcriptomes from COVID-19 cases and healthy controls were pooled prior to unsupervised cluster analysis. Seurat version 3.1.5 with R version 3.4.2 was used for normalization, dimensionality reduction, clustering, and UMAP visualization, while Seurat version 3.2.2[311] with R version 4.0.2 was used for all downstream analyses.

Cluster annotation: Preliminary annotation of all clusters was performed by the similarity of their gene expression to annotated cell types in published single cell RNA-seq datasets of human maternal-fetal interface[201-203]. For each cluster, mean of SCTransform-normalized[296] gene expression across cells was calculated using Seurat function AverageExpression and used as the cluster's average gene expression. Spearman correlation coefficients between the cluster's average expression and averaged expression of annotated cell types from all three reference datasets were calculated using the R function cor, and top three cell types with highest correlation coefficient were assigned as preliminary annotations of the clusters (Supplementary Figure 7). These annotations were further refined through manual examination of cluster marker genes (identified using Seurat function FindAllMarkers with options only.pos = TRUE and logfc.threshold = 0.25). During manual refinement of annotation, tissue origin of the cells was also taken

into account, i.e., whether majority of cells in a cluster come from villi samples or decidua samples. Clusters that are highly similar to each other and have the same final cell type annotation, were then merged, resulting in the final set of 21 annotated clusters.

Differential gene expression: For each annotated cluster, differentially expressed genes between control and COVID-19 samples were identified using Wilcoxon rank-sum test as implemented in the Seurat function FindMarkers. Genes that meet the following criteria were considered differentially expressed: absolute log (natural) fold-change of 0.4 (corresponding to at least 50% change in expression) and Bonferroni-adjusted two-tailed *p*-value less than 0.05.

Functional enrichment analyses: Two types of functional gene set enrichment analyses were performed, Interferome[207] and Metascape[299]. For Interferome analysis, lists of differentially expressed genes in each cluster were searched against Interferome (version 2.01) with the default parameters except that the search was limited to human genes. Enrichment score for each cluster was calculated as the ratio between the observed fraction of differentially expressed genes found in Interferome database and the expected fraction, where the expected fraction is the ratio of total number of genes in the Interferome database over the total number of genes used in differential expression analysis. Enrichment *p*-values were calculated from the hypergeometric distribution using the R function phyper. Functional enrichment with Metascape was performed on lists of differentially expressed genes using the web application.

Ligand-receptor interactions: Ligand-receptor interactions were inferred using CellPhoneDB[208] separately for cells from control and COVID-19 samples. CellPhoneDB version 2.1.4 was used with Python version 3.6. For computational efficiency both control

and COVID-19 data were subsampled to 5000 cells each. CellPhoneDB output was read into R for data visualization. CellPhoneDB output file count_network.txt was used for visualization of number of interactions between pairs of cell types in Figure 5E. For visualization of individual ligand pair interactions in Supplementary Figure 6, we selected interactions that are present in COVID samples (adjusted p value < 0.01) but absent in control samples.

Quantification and statistical analyses

Statistical details can also be found in figures legends. One-way ANOVA was used to compare clinical and demographic features between the three groups presented in Table 3.3. Chi-square tests were used for statistical comparisons of histologic features of cases versus controls. Differences were designated statistically significant when the p value was less than 0.05.

In Figure 3.5, ACE2 H-score was compared between cases and controls using the Mann-Whitney test. The linear regression line for ACE2 H score vs. gestational age was fit using Prism (v8.0.1), which was also used to calculate 95% confidence intervals. The equation for the best fit line is $y = -6.149x + 287.6$.

For bulk RNA sequencing analysis, differential expression analysis was performed using DESeq2 v1.24.0 with default parameters.

For single-cell RNA sequencing analysis of each annotated cluster, differentially expressed genes between control and COVID-19 samples were identified using Wilcoxon rank-sum test as implemented in the Seurat function FindMarkers. Genes that meet the following criteria were considered differentially expressed: absolute log (natural) fold-

change of 0.4 (corresponding to at least 50% change in expression) and Bonferroni-adjusted two-tailed *p*-value less than 0.05.

For Interferome analysis, enrichment p-values were calculated from the hypergeometric distribution using the R function phyper. For Metascape analysis, functional enrichment was performed using the Metascape web application.

Data and code availability

Datasets for bulk (GSE171995) and single cell (GSE171381) RNA sequencing in the paper are available at GEO. The code generated during this study are available at: https://github.com/archavan/covid-placenta. Additional supplemental items are available from Mendeley Data at: https://dx.doi.org/10.17632/v6bgbwf3td.1

Resources

Oligonucleotides		
nCOV_N1 forward primer GACCCCAAAATCAGCGAAAT	IDT	Cat#10006830
nCOV_N1 reverse primer TCTGGTTACTGCCAGTTGAATCTG	IDT	Cat#10006831
nCOV_N1 probe FAM-ACCCCGCATTACGTTTGGTGGACC-IBFQ	IDT	Cat#10006832
nCOV_N2 forward primer TTACAAACATTGGCCGCAAA	IDT	Cat#10006833
nCOV_N2 reverse primer GCGCGACATTCCGAAGAA	IDT	Cat#10006834
nCOV_N2 probe FAM-ACAATTTGCCCCCAGCGCTTCAG-IBFQ	IDT	Cat#10006835
RNAse P forward primer AGATTTGGACCTGCGAGCG	IDT	Cat#10006836
RNAse P reverse primer GAGCGGCTGTCTCCACAAGT	IDT	Cat#10006837
RNAse P probe FAM-TTCTGACCTGAAGGCTCTGCGCG-IBFQ	IDT	Cat#10006838

A1.3 Methods and Data Analysis for Chapter 4: Challenging COVID-19 vaccine misinformation about pregnancy and fertility

Ethics Statement

Animal care and protocol were approved by the Yale University Office of Animal Research Support (Protocol #2021-10365), with an approved Animal Welfare Assurance (A3230-01) on file with the Office of Laboratory Animal Welfare.

All research involving human participants was conducted according to the principles expressed in the Declaration of Helsinki with written consent provided. Protocols were approved by the Yale Human Research Protection Program Institutional Review Board in the United States and by the National Bioethics Committee of the Dominican Republic (CONABIOS) in the Dominican Republic.

Timed matings and injections

C57BL/6J mice were mated overnight and females were checked for the presence of seminal plugs each morning, designated E0.5. On E7.5, pregnant mice were anesthetized and subjected to a single intramuscular (i.m.) injection into the thigh muscle of the hind limb with 50 µl volume of PBS, 2 µg of mRNA-1273, or 50 µg poly(I:C). Vaccigrade HMW poly(I:C) (Invivogen #vac-pic) was prepared at 1 mg/ml at room temperature and stored at -20°C, then thawed to room temperature prior to injection.

Harvest of fetuses, fetal serum collection, and fetal measurements

On E18.5, prior to birth, pregnant dams were anesthetized by isofluorane inhalation and cervical dislocation was performed. Fetuses were individually dissected from the pregnant uterus, rinsed three times in PBS, and patted dry on Kimwipes. During harvest, fetuses remained intact and were separated from the placenta. Fetuses were then measured, weighed, and assessed for birth defects such as missing eye(s) and neural tube defects. Fetal blood was collected from the trunk following decapitation and allowed to clot for 1 hour at room temperature before two rounds of centrifugation at 10000 x g for 10 minutes at 4°C. Serum was collected and stored at -80°C.

All statistical analyses comparing fetal viability and growth measurements were performed with GraphPad Prism 8.4.3 software. Before assessing the statistical significance, Shapiro-Wilk normality test was used to confirm Gaussian distribution of the fetal weights and crown-rump lengths. Afterwards, the data were analyzed with Brown-Forsythe and Welch ANOVA tests for multiple comparisons between the PBS, Poly(I:C), and Moderna treatments (∗: $p \leq 0.05$; ∗∗: $p \leq 0.01$; ∗∗∗: $p \leq 0.001$; ∗∗∗∗: $p \leq 0.0001$).

SARS-CoV-2-specific antibody measurements

ELISAs were performed as previously described[303]. In short, Triton X-100 and RNase A were added to serum samples at final concentrations of 0.5% and 0.5mg/ml respectively and incubated at room temperature (RT) for 30 minutes before use, to reduce risk from any potential virus in serum. 96-well MaxiSorp plates (Thermo Scientific #442404) were coated with 50 µl/well of recombinant SARS Cov-2 STotal (ACROBiosystems #SPN-C52H9-100ug), S1 (ACROBiosystems #S1N-C52H3-100ug), and RBD (ACROBiosystems #SPD-S52H6-100ug) at a concentration of 2 µg/ml in PBS

and were incubated overnight at 4°C. The coating buffer was removed, and plates were incubated for 1 hour at RT with 200 µl of blocking solution (PBS with 0.1% Tween-20, 3% milk powder). Plasma was diluted serially 1:100, 1:1000, and 1:10000 in dilution solution (PBS with 0.1% Tween-20, 1% milk powder) and 100 µl of diluted serum was added for two hours at RT. Human anti-Spike (anti-S) and anti-Receptor-Binding Domain (anti-RBD) antibodies were serially diluted to generate a standard curve. Plates were washed three times with PBS-T (PBS with 0.1% Tween-20) and 50 µl of HRP anti-Human IgG Antibody (GenScript #A00166, 1:5,000) diluted in dilution solution added to each well. After 1 h of incubation at RT, plates were washed six times with PBS-T. Plates were developed with 100 µl of TMB Substrate Reagent Set (BD Biosciences #555214) and the reaction was stopped after 5 min by the addition of 2 N sulfuric acid. Plates were then read at a wavelength of 450 nm and 570 nm.

Human plasma collection and cohort selection

Plasma was collected from healthcare worker (HCW) volunteers who received the mRNA vaccine (Moderna mRNA-1273 or Pfizer-BioNTech BNT162b2) between November 2020 and January 2021 as approved by the Yale Human Research Protection Program Institutional Review Board (IRB Protocol ID 2000028924). None of the participants experienced serious adverse effects after vaccination. HCWs were followed serially post-vaccination, and samples were collected at baseline (prior to vaccination), and 7- and 28-days post second vaccination dose. Blood acquisition was performed and recorded by a separate team. Female HCWs age 55 and under were selected, along with 3 male controls. Plasma samples from patients experiencing acute infection with SARS-

CoV-2 ranging from asymptomatic to severe disease, including six pregnant patients, were selected from the previously described Yale IMPACT study, approved by the Yale Human Research Protection Program Institutional Review Board (FWA00002571, IRB Protocol ID 2000027690)[312]. Matched uninfected, unvaccinated HCW were also analyzed.

Plasma was collected from adult participants who received the mRNA vaccine Pfizer-BioNTech BNT162b2 between July 30 and August 27, 2021, at least four weeks after two doses of CoronaVac inactivated whole-virion vaccine, as approved by the National Bioethics Committee of the Dominican Republic (CONABIOS). All participants provided written consent to enroll in this observational study. None of the participants experienced serious adverse effects after vaccination. Participants were followed serially post-vaccination, and samples were collected at baseline (prior to mRNA-booster, after two CoronaVac doses), and 7- and 28-days post mRNA booster. Demographic information was aggregated through a systematic review and blood acquisition was performed and recorded by a separate team. Plasma samples were sourced from Dominican Republican participants and were shipped to Yale University. 36 female participants age 50 and under were selected for this study, along with 5 male controls.

Finally, plasma from previously described[286] patients with systemic lupus erythematosus (SLE), was used as a positive control. Female patients under the age of 60 were selected, as well as one male SLE patient. SLE patients were recruited from the rheumatology clinic of Yale School of Medicine and Yale New Haven Hospital in accordance with a protocol approved by the Yale Human Research Protection Program Institutional Review Board (IRB Protocol ID 0303025105). The diagnosis of SLE was established according to the 1997 update of the 1982 revised American College of

Rheumatology criteria[313,314]. After obtaining informed consent, peripheral blood was collected in EDTA tubes from human subjects, and plasma was extracted upon centrifugation. Plasma were stored at −80°C. All patients had SLE according to the American College of Rheumatology criteria for classification of SLE.

Isolation of human plasma

Whole blood from HCW was collected in heparinized CPT blood vacutainers (BD #BDAM362780) and kept on gentle agitation until processing. All blood was processed on the day of collection in a single step standardized method. Plasma samples were collected after centrifugation of whole blood at 600 x g for 20 minutes at room temperature without brake. The undiluted plasma was transferred to 15-ml polypropylene conical tubes, and aliquoted and stored at −80 °C for subsequent analysis.

Anti-HERV-W/Syncytin-1 antibody measurements

96-well MaxiSorp plates (Thermo Scientific #442404) were coated with 20 ng per well of human Syncytin-1 recombinant protein (Abnova #H00030816-Q01) in PBS and were incubated overnight at 4°C. The coating buffer was removed, and plates were blocked overnight at 4°C with 250 µl of blocking solution (PBS with 0.1% Tween-20, 3% milk powder). Plasma was diluted 1:800 in dilution solution (PBS with 0.1% Tween-20, 1% milk powder) and 100 µl of diluted plasma was added for one hour at room temperature. Mouse Anti-HERV-W monoclonal antibody (Abnova #H00030816-M06) was serially diluted to generate a standard curve. All samples were plated in duplicate. Plates were washed three times with PBS-T (PBS with 0.1% Tween-20) and 50 µl of HRP anti-Human

IgG Antibody (GenScript #A00166) diluted 1:5000 in dilution solution were added to each well. 50 ul of HRP anti-Mouse IgG1 Antibody (Southern Biotech #1070-05) diluted 1:3000 in dilution solution were added to each standard well. After one hour of incubation at room temperature, plates were washed six times with PBS-T. Plates were developed with 50 µl of TMB Substrate (Invitrogen #00-4201-56) and the reaction was stopped after 10 minutes by the addition of 50 µl 2 N sulfuric acid. Plates were then read at a wavelength of 450 nm and 570nm. To fit the standard curve, mean absorbance (OD450nm) was plotted known antibody concentration to generate a standard curve. Best fit was determined using asymmetrical sigmoidal five-parameter least-squares fit in GraphPad Prism 9.2.0. Projected antibody concentrations were interpolated using this fit.

To determine the normal range of anti-syncytin-1 antibodies found in healthy, pre-vaccination individuals, a kernel distribution estimate curve was plotted on a histogram of all anti-syncytin-1 antibody levels found in the HCW (PCR-, Pre-Vax) group. The maximum of this distribution was found to be 28.8168, and plotted accordingly.

Statistical significance (p) was determined using nonparametric Kruskal-Wallis test followed by Dunn's multiple comparisons test for matched samples across vaccination time points (Figure 3), and by nonparametric Mann-Whitney test to compare each individual cohort to uninfected, unvaccinated HCW controls or to SLE patients (Figure 3, Supplementary Figure 2). All analyses were two-tailed and carried out in GraphPad Prism 9.2.0.

Appendix 2: Science Writing & Public Communication

A2.1 Article on Covid-19 misinformation surrounding the impacts of vaccination on fertility and pregnancy

The following was written with Akiko Iwasaki and originally published as:

Lu-Culligan, A & Iwasaki, A. The False Rumors About Vaccines That Are Scaring Women. *The New York Times* (26 Jan 2021).

"The False Rumors About Vaccines That Are Scaring Women"

The Covid-19 pandemic has taken a disproportionate toll on women's careers, finances and home lives. Although the vaccines may represent a solution, as scientists studying coronavirus infection and immune responses in women, we are now hearing from young women who say they might skip the shots out of fear for their fertility or nursing child. We are concerned about how inaccurate, extreme and widespread these theories have become, because getting vaccinated is the best way for women to protect themselves and their families.

The confusion is understandable: Early clinical trials of Pfizer/BioNTech and Moderna's coronavirus vaccines failed to include pregnant and lactating women, so safety data is not available for these populations. But the valid concerns about this information void have been eclipsed by targeted misinformation campaigns led by vaccine skeptics who are weaponizing women's health issues to advance their agenda. These falsehoods are being spread to amplify our legitimate anxieties and undermine trust in vaccination.

We empathize with the fear stemming from a lack of data. Many women are being bombarded with social media posts that falsely claim that coronavirus vaccines cause infertility. They do not want to take chances. These women need reassurance of the benefits of getting vaccinated, and they need clear explanations of why declining the vaccine would be a bigger gamble.

One myth claims that the vaccines cause infertility by generating antibodies that not only target the coronavirus spike protein, as designed, but also inadvertently react with a protein in the placenta called syncytin-1. Supposedly, the viral protein and human protein are so similar in structure that the protective antibodies against the coronavirus will also prevent the placenta from developing properly, causing infertility.

This is completely false.

Our team compared the coronavirus's spike protein to placental syncytin-1, and we found no notable similarity between their amino acid sequences. We analyzed serum from women

with Covid-19 and did not detect any reaction between patients' antibodies and the syncytin-1 protein. There is also no evidence or reports so far of infertility among women who have recovered from Covid-19, despite the millions who have been infected. To the contrary, women have conceived after coronavirus infection and vaccination. They include vaccinated women who became pregnant while participating in clinical trials of the vaccines. It is exceedingly unlikely that vaccine materials representing a small portion of the virus would impair fertility.

With little data and weak public messaging on coronavirus immunization during breastfeeding, women have been left to draw their own conclusions and are naturally assuming the worst. But the immunization of lactating women is practically guaranteed to benefit both mother and baby. After all, vaccines induce protective immune responses in the mother, creating antibodies that are passed to infants via breast milk and serve to protect them. And it is unlikely that the vaccine can cross into breast milk. Even if they did, they would not pose a threat to the health of a nursing baby; if ingested, these components would be digested and degraded in the gastrointestinal tract. Neither mother nor infant is at any risk for coronavirus infection from the vaccines.

The decision to get vaccinated for the coronavirus during pregnancy asks women to assess their own risk. If a pregnant woman is not in any danger of being exposed to the virus, then it may make sense for her to wait to vaccinate until the baby is born or until more data is available. But the decision may be very different for essential workers who are at much higher risk of exposure.

Any immune response during pregnancy, whether from an infection or a vaccine, could have unknown consequences. However, studies of coronavirus vaccination in animals have shown no impact on pregnancy, and human studies are in the works. Of course, vaccines for the flu and for tetanus, diphtheria and pertussis are routinely and safely administered to pregnant women.

While we do not yet know everything about Covid-19 in human pregnancy, we do know that pregnant women who contract the disease are at higher risk for severe illness. The infection may also be associated with potentially life-threatening complications of pregnancy, such as pre-eclampsia, a condition characterized in part by dangerously high maternal blood pressure. In rare cases, the coronavirus can invade the placenta.

In contrast, there is zero chance that someone can get Covid-19 disease from the vaccines, which contain no live virus. We worry that women who hesitate to get immunized are underestimating the risk of Covid-19 and overestimating the risk of the vaccines.

Unfortunately, women are absorbing rumors much more quickly than they are getting answers from scientists. If vaccine hesitancy leads to deeper mistrust of the medical establishment, there will be no way to convince those we most need to protect, even once more data is available. The scientific community needs to demonstrate that we are listening to and addressing the public's concerns. Women will of course make their own decisions,

but they cannot do so in an informed way without knowing the true risks and benefits of vaccination.

For any woman who is pregnant, nursing or trying to conceive, contracting Covid-19 is almost certainly more dangerous than getting immunized. And ultimately, mass vaccination, combined with physical distancing and wearing masks, provides the only way that we can end the pandemic and protect all women, men and children from the disease.

A2.2 Article on Covid-19 vaccination and menstruation

The following was written with Randi Hutter Epstein and originally published as:

Lu-Culligan, A & Epstein, RH. No, We Don't Know if Vaccines Change Your Period. *The New York Times* (20 Apr 2021).

"No, We Don't Know if Vaccines Change Your Period"

It took a pandemic to get people to talk about menstruation.

A spate of reports from women stating that their periods changed after they got their coronavirus vaccines has left many women worried that the jab is affecting their cycle.

So far, there's no data linking the vaccines to changes in menstruation. Even if there is a connection, one unusual period is no cause for alarm. There is a long list of triggers that can cause changes to the menstrual cycle, including stress, illness and changes in diet and physical activity.

But that raises the question: If so many things can affect periods, why don't we know more about how these vaccines — or any others — affect menstruation? It's part of a long history of medicine not taking women's bodies seriously.

Clinical trials should track and document menstrual changes as they do other possible side effects. Like the fevers reported after the vaccines, a transient change in one's period may not be bad for your overall health or have any lasting effects, but it's still informative.

An unexpected side effect like an unusually heavy period can prompt fear and undermine the public's trust in the vaccines. This is particularly important now, when ending the pandemic requires widespread acceptance of coronavirus vaccination.

Many people with regular periods use their monthly bleeds as a signpost of their overall health. Changes to their normal cycle can seem especially worrying in the wake of false rumors about the shots causing infertility, as well as news of rare blood clots possibly linked to the Johnson & Johnson vaccine.

There are many reasons vaccination could alter menstruation. As many people learn in sex education class or just before puberty, the menstrual cycle is an exquisitely timed series of hormones, including estrogen and progesterone, spiking and falling in preparation for a potential pregnancy.

Every month the lining of the uterus thickens, driven by a steady increase in estrogen, so that a fertilized egg can implant. If there is no conception, levels of progesterone plummet, causing most of the uterine layer to slough off, causing the bleeding.

But periods also involve the immune system. The thickening and thinning of the uterine lining are facilitated by different teams of immune cells and signals moving in and out of the reproductive tract; one wave helps to build, others help to dismantle. The process of shedding this lining during menstruation is in part an inflammatory response, which is why women often experience cramping and pain during this stage.

Since the cycle is supported by the immune system at every turn, it is possible that the vaccines, which are designed to ignite an immune response, temporarily change the normal course of events. For example, an activated immune system might interfere with the usual balance of immune cells and molecules in the uterus. These types of disturbances have been found in studies to contribute to changes in periods, including heavy menstrual flows. But no one can say whether this may explain potential postvaccine disruptions to the menstrual cycle. To find out, we would need a controlled study with a placebo group. Clinical trials, including those for vaccines, typically omit the tracking of menstrual cycles, so we lack the evidence required to put these reports in context. (It should be noted that few mammals menstruate, which makes the subject harder to study in animals.)

“Menstruation is something we don’t know enough about,” said Dr. Hugh Taylor, chair of the department of obstetrics, gynecology and reproductive sciences at Yale School of Medicine. “It’s an important indicator of a person’s health, like any other bodily function.” For much of modern medical history, women were not included in medical trials because of their periods or because they might be pregnant. Investigators worried that fluctuating hormones would add too many variables, confounding their studies. In essence, they

thought that the female body would ruin the research. In 1993, a federal law mandated the inclusion of women in government-funded trials because, as activists pointed out, too little was known about how new drugs and treatments affected women's health.

Even today, menstruation research tends to focus on fertility or contraception. Otherwise, periods have been considered an inconvenience. Researchers now routinely include women in clinical trials, but they often neglect to ask about menstrual cycles unless that's the focus of the study.

Rather than treat menstrual cycles as unimportant or too complicated, researchers should view tracking periods in future studies as a potential opportunity. Such work could help us to better understand the ways in which women respond differently to many diseases, treatments and interventions, not just the ones surrounding Covid-19. It could also inform our approach to the management of long-overlooked conditions known to be affected by the menstrual cycle, such as endometriosis.

For now, scientists are still in the dark about so much of female health. But a conversation has begun, thanks to women openly sharing their concerns. Let's take menstruation more seriously.

Bibliography

1. Lu-Culligan, A. & Iwasaki, A. The Role of Immune Factors in Shaping Fetal Neurodevelopment. *Annu Rev Cell Dev Biol* **36,** 441–468 (2020).

2. PrabhuDas, M. *et al.* Immune mechanisms at the maternal-fetal interface: perspectives and challenges. in **16,** 328–334 (Nature Publishing Group, 2015).

3. Mor, G., Aldo, P. & Alvero, A. B. The unique immunological and microbial aspects of pregnancy. *Nat. Rev. Immunol.* **17,** 469–482 (2017).

4. Abrahams, V. M. & Mor, G. Toll-like receptors and their role in the trophoblast. *Placenta* **26,** 540–547 (2005).

5. Coulthard, L. G., Hawksworth, O. A. & Woodruff, T. M. Complement: The Emerging Architect of the Developing Brain. *Trends in Neurosciences* **41,** 373–384 (2018).

6. Knuesel, I. *et al.* Maternal immune activation and abnormal brain development across CNS disorders. *Nat Rev Neurol* **10,** 643–660 (2014).

7. Yockey, L. J. & Iwasaki, A. Interferons and Proinflammatory Cytokines in Pregnancy and Fetal Development. *Immunity* **49,** 397–412 (2018).

8. Yockey, L. J., Lucas, C. & Iwasaki, A. Contributions of maternal and fetal antiviral immunity in congenital disease. *Science* **368,** 608–612 (2020).

9. Chess, S. Autism in children with congenital rubella. *J Autism Child Schizophr* **1,** 33–47 (1971).

10. Desmond, M. M. *et al.* Congenital rubella encephalitis. Course and early sequelae. *J. Pediatr.* **71,** 311–331 (1967).

11. Nahmias, A. J., Walls, K. W., Stewart John A, Herrmann, K. L. & Flynt, W. J. The ToRCH complex-perinatal infections associated with toxoplasma and rubella, cytomegol- and herpes simplex viruses. *Pediatr Res* **5,** 405–406 (1971).

12. Coyne, C. B. & Lazear, H. M. Zika virus - reigniting the TORCH. *Nat. Rev. Microbiol.* **14,** 707–715 (2016).

13. Estes, M. L. & McAllister, A. K. Immune mediators in the brain and peripheral tissues in autism spectrum disorder. 1–18 (2015). doi:10.1038/nrn3978

14. Deshmukh, H. & Way, S. S. Immunological Basis for Recurrent Fetal Loss and Pregnancy Complications. *Annu Rev Pathol* **14,** 185–210 (2019).

15. Erlebacher, A. Immunology of the maternal-fetal interface. *Annu. Rev. Immunol.* **31,** 387–411 (2013).

16. Ander, S. E., Diamond, M. S. & Coyne, C. B. Immune responses at the maternal-fetal interface. *Sci Immunol* **4,** eaat6114 (2019).

17. Bulmer, J. N., Morrison, L., Longfellow, M., Ritson, A. & Pace, D. Granulated lymphocytes in human endometrium: histochemical and immunohistochemical studies. *Hum. Reprod.* **6,** 791–798 (1991).

18. Bulmer, J. N., Williams, P. J. & Lash, G. E. Immune cells in the placental bed. *Int. J. Dev. Biol.* **54,** 281–294 (2010).

19. Mor, G., Aldo, P. & Alvero, A. B. The unique immunological and microbial aspects of pregnancy. *Nat. Rev. Immunol.* **17,** 469–482 (2017).

20. Liu, S. *et al.* The role of decidual immune cells on human pregnancy. *J. Reprod. Immunol.* **124,** 44–53 (2017).

21. Williams, P. J., Searle, R. F., Robson, S. C., Innes, B. A. & Bulmer, J. N. Decidual leucocyte populations in early to late gestation normal human pregnancy. *J. Reprod. Immunol.* **82,** 24–31 (2009).

22. Davies, N. P. *et al.* Blood leucocyte count in the human fetus. *Arch. Dis. Child.* **67,** 399–403 (1992).

23. Holt, P. G. & Jones, C. A. The development of the immune system during pregnancy and early life. *Allergy* **55,** 688–697 (2000).

24. Rechavi, E. *et al.* Timely and spatially regulated maturation of B and T cell repertoire during human fetal development. *Sci Transl Med* **7,** 276ra25 (2015).

25. Lenz, K. M. & Nelson, L. H. Microglia and Beyond: Innate Immune Cells As Regulators of Brain Development and Behavioral Function. *Front. Immunol.* **9,** 13–13 (2018).

26. Paolicelli, R. C. & Ferretti, M. T. Function and Dysfunction of Microglia during Brain Development: Consequences for Synapses and Neural Circuits. *Front. Synaptic Neurosci.* **9,** 163–17 (2017).

27. Bilimoria, P. M. & Stevens, B. Microglia function during brain development: New insights from animal models. *Brain Res.* **1617,** 7–17 (2015).

28. Thomas, J. R. *et al.* Phenotypic and functional characterization of first-trimester human placental macrophages, Hofbauer cells. *The Journal of Experimental Medicine* **218,** (2021).

29. Bowen, J. M., Chamley, L., Mitchell, M. D. & Keelan, J. A. Cytokines of the Placenta and Extra-placental Membranes: Biosynthesis, Secretion and Roles in Establishment of Pregnancy in Women. *Placenta* **23,** 239–256 (2002).

30. Bulla, R. *et al.* Complement production by trophoblast cells at the feto-maternal interface. *J. Reprod. Immunol.* **82,** 119–125 (2009).

31. Delorme-Axford, E. *et al.* Human placental trophoblasts confer viral resistance to recipient cells. *Proc. Natl. Acad. Sci. U.S.A.* **110,** 12048–12053 (2013).

32. Hsi, B. L., Hunt, J. S. & Atkinson, J. P. Differential expression of complement regulatory proteins on subpopulations of human trophoblast cells. *J. Reprod. Immunol.* **19,** 209–223 (1991).

33. Saito, S. Cytokine network at the feto-maternal interface. *J. Reprod. Immunol.* **47,** 87–103 (2000).

34. Bayer, A. *et al.* Human trophoblasts confer resistance to viruses implicated in perinatal infection. *American Journal of Obstetrics and Gynecology* **212,** 71.e1–71.e8 (2015).

35. Bayer, A. *et al.* Type III Interferons Produced by Human Placental Trophoblasts Confer Protection against Zika Virus Infection. *Cell Host and Microbe* **19,** 705–712 (2016).

36. Stefanski, A. L. *et al.* Murine trophoblast-derived and pregnancy-associated exosome-enriched extracellular vesicle microRNAs: Implications for placenta driven effects on maternal physiology. *PLoS ONE* **14,** e0210675–23 (2019).

37. Abrahams, V. M. *et al.* Divergent trophoblast responses to bacterial products mediated by TLRs. *J Immunol* **173,** 4286–4296 (2004).

38. Abrahams, V. M. *et al.* A role for TLRs in the regulation of immune cell migration by first trimester trophoblast cells. *J Immunol* **175,** 8096–8104 (2005).

39. Abrahams, V. M. *et al.* Expression and secretion of antiviral factors by trophoblast cells following stimulation by the TLR-3 agonist, Poly(I : C). *Hum. Reprod.* **21,** 2432–2439 (2006).

40. Hoffmann, J. A. The immune response of Drosophila. *Nature* **426,** 33–38 (2003).

41. Medzhitov, R. Toll-like receptors and innate immunity. *Nature Publishing Group* **1,** 135–145 (2001).

42. Hanke, M. L. & Kielian, T. Toll-like receptors in health and disease in the brain: mechanisms and therapeutic potential. *Clin. Sci.* **121,** 367–387 (2011).

43. Rolls, A. *et al.* Toll-like receptors modulate adult hippocampal neurogenesis. *Nat. Cell Biol.* **9,** 1081–1088 (2007).

44. Okun, E., Griffioen, K. J. & Mattson, M. P. Toll-like receptor signaling in neural plasticity and disease. *Trends in Neurosciences* **34,** 269–281 (2011).

45. Lathia, J. D. *et al.* Toll-like receptor 3 is a negative regulator of embryonic neural progenitor cell proliferation. *J. Neurosci.* **28,** 13978–13984 (2008).

46. Okun, E. *et al.* Toll-like receptor 3 inhibits memory retention and constrains adult hippocampal neurogenesis. *Proc. Natl. Acad. Sci. U.S.A.* **107,** 15625–15630 (2010).

47. Liu, H. Y. *et al.* TLR7 Negatively Regulates Dendrite Outgrowth through the Myd88-c-Fos-IL-6 Pathway. *Journal of Neuroscience* **33,** 11479–11493 (2013).

48. Hung, Y.-F. *et al.* Endosomal TLR3, TLR7, and TLR8 control neuronal morphology through different transcriptional programs. *The Journal of Cell Biology* **217,** 2727–2742 (2018).

49. Hung, Y.-F., Chen, C.-Y., Li, W.-C., Wang, T.-F. & Hsueh, Y.-P. Tlr7 deletion alters expression profiles of genes related to neural function and regulates mouse behaviors and contextual memory. *Brain Behavior and Immunity* **72,** 101–113 (2018).

50. Ubeda, C. *et al.* Familial transmission rather than defective innate immunity shapes the distinct intestinal microbiota of TLR-deficient mice. *The Journal of Experimental Medicine* **209,** 1445–1456 (2012).

51. Yu, P. *et al.* Nucleic acid-sensing Toll-like receptors are essential for the control of endogenous retrovirus viremia and ERV-induced tumors. *Immunity* **37,** 867–879 (2012).

52. Young, G. R. *et al.* Resurrection of endogenous retroviruses in antibody-deficient mice. *Nature* **491,** 774–778 (2012).

53. Deverman, B. E. & Patterson, P. H. Cytokines and CNS development. *Neuron* **64,** 61–78 (2009).

54. Bilbo, S. D. & Schwarz, J. M. The immune system and developmental programming of brain and behavior. *Frontiers in Neuroendocrinology* **33,** 267–286 (2012).

55. Borsini, A., Zunszain, P. A., Thuret, S. & Pariante, C. M. The role of inflammatory cytokines as key modulators of neurogenesis. *Trends in Neurosciences* **38,** 145–157 (2015).

56. Jiang, N. M., Cowan, M., Moonah, S. N. & Petri, W. A. The Impact of Systemic Inflammation on Neurodevelopment. *Trends in Molecular Medicine* **24,** 794–804 (2018).

57. Pronovost, G. N. & Hsiao, E. Y. Perinatal Interactions between the Microbiome, Immunity, and Neurodevelopment. *Immunity* **50,** 18–36 (2019).

58. Burns, T. M., Clough, J. A., Klein, R. M., Wood, G. W. & Berman, N. E. Developmental regulation of cytokine expression in the mouse brain. *Growth Factors* **9,** 253–258 (1993).

59. Pousset, F. Developmental expression of cytokine genes in the cortex and hippocampus of the rat central nervous system. *Brain Res. Dev. Brain Res.* **81,** 143–146 (1994).

60. Zhao, B. & Schwartz, J. P. Involvement of cytokines in normal CNS development and neurological diseases: recent progress and perspectives. *J. Neurosci. Res.* **52,** 7–16 (1998).

61. Roussa, E. *et al.* Transforming growth factor beta is required for differentiation of mouse mesencephalic progenitors into dopaminergic neurons in vitro and in vivo: ectopic induction in dorsal mesencephalon. *Stem Cells* **24,** 2120–2129 (2006).

62. Heupel, K. *et al.* Loss of transforming growth factor-beta 2 leads to impairment of central synapse function. *Neural Dev* **3,** 25 (2008).

63. Hegarty, S. V., O'Keeffe, G. W. & Sullivan, A. M. BMP-Smad 1/5/8 signalling in the development of the nervous system. *Progress in Neurobiology* **109,** 28–41 (2013).

64. Goumans, M. J. & Mummery, C. Functional analysis of the TGFbeta receptor/Smad pathway through gene ablation in mice. *Int. J. Dev. Biol.* **44,** 253–265 (2000).

65. Sedel, F., Béchade, C., Vyas, S. & Triller, A. Macrophage-derived tumor necrosis factor alpha, an early developmental signal for motoneuron death. *J. Neurosci.* **24,** 2236–2246 (2004).

66. Barker, V., Middleton, G., Davey, F. & Davies, A. M. TNFalpha contributes to the death of NGF-dependent neurons during development. *Nat. Neurosci.* **4,** 1194–1198 (2001).

67. Yoshimatsu, T. Non-cell-autonomous action of STAT3 in maintenance of neural precursor cells in the mouse neocortex. *Development* **133,** 2553–2563 (2006).

68. Hong, S. & Song, M.-R. Signal transducer and activator of transcription-3 maintains the stemness of radial glia at mid-neurogenesis. *J. Neurosci.* **35,** 1011–1023 (2015).

69. Hatta, T., Moriyama, K., Nakashima, K., Taga, T. & Otani, H. The Role of gp130 in cerebral cortical development: in vivo functional analysis in a mouse exo utero system. *J. Neurosci.* **22,** 5516–5524 (2002).

70. Gregg, C. & Weiss, S. CNTF/LIF/gp130 receptor complex signaling maintains a VZ precursor differentiation gradient in the developing ventral forebrain. *Development* **132,** 565–578 (2005).

71. Pollen, A. A. *et al.* Molecular Identity of Human Outer Radial Glia during Cortical Development. *Cell* **163,** 55–67 (2015).

72. Nakashima, K. *et al.* Developmental requirement of gp130 signaling in neuronal survival and astrocyte differentiation. *Journal of Neuroscience* **19,** 5429–5434 (1999).

73. Koblar, S. A. *et al.* Neural precursor differentiation into astrocytes requires signaling through the leukemia inhibitory factor receptor. *Proc. Natl. Acad. Sci. U.S.A.* **95,** 3178–3181 (1998).

74. Barnabé-Heider, F. *et al.* Evidence that Embryonic Neurons Regulate the Onset of Cortical Gliogenesis via Cardiotrophin-1. *Neuron* **48,** 253–265 (2005).

75. Wang, Y. *et al.* IL-34 is a tissue-restricted ligand of CSF1R required for the development of Langerhans cells and microglia. *Nat. Immunol.* **13,** 753–760 (2012).

76. Erblich, B., Zhu, L., Etgen, A. M., Dobrenis, K. & Pollard, J. W. Absence of Colony Stimulation Factor-1 Receptor Results in Loss of Microglia, Disrupted Brain Development and Olfactory Deficits. *PLoS ONE* **6,** e26317–13 (2011).

77. Dohi, E. *et al.* Behavioral Changes in Mice Lacking Interleukin-33. *eNeuro* **4,** (2017).

78. Yasuoka, S. *et al.* Production and functions of IL-33 in the central nervous system. *Brain Res.* **1385,** 8–17 (2011).

79. Fairlie-Clarke, K. *et al.* Expression and Function of IL-33/ST2 Axis in the Central Nervous System Under Normal and Diseased Conditions. *Front. Immunol.* **9,** 479–16 (2018).

80. Vainchtein, I. D. *et al.* Astrocyte-derived interleukin-33 promotes microglial synapse engulfment and neural circuit development. *Science* **359,** 1269–1273 (2018).

81. Lazarini, F., Tham, T. N., Casanova, P., Arenzana-Seisdedos, F. & Dubois-Dalcq, M. Role of the alpha-chemokine stromal cell-derived factor (SDF-1) in the developing and mature central nervous system. *Glia* **42,** 139–148 (2003).

82. Klein, R. S. *et al.* SDF-1 alpha induces chemotaxis and enhances Sonic hedgehog-induced proliferation of cerebellar granule cells. *Development* **128,** 1971–1981 (2001).

83. Zhu, Y. *et al.* Role of the chemokine SDF-1 as the meningeal attractant for embryonic cerebellar neurons. *Nat. Neurosci.* **5,** 719–720 (2002).

84. Bagri, A. *et al.* The chemokine SDF1 regulates migration of dentate granule cells. *Development* **129,** 4249–4260 (2002).

85. Lu, M., Grove, E. A. & Miller, R. J. Abnormal development of the hippocampal dentate gyrus in mice lacking the CXCR4 chemokine receptor. *Proc. Natl. Acad. Sci. U.S.A.* **99,** 7090–7095 (2002).

86. Schwarting, G. A., Henion, T. R., Nugent, J. D., Caplan, B. & Tobet, S. Stromal cell-derived factor-1 (chemokine C-X-C motif ligand 12) and chemokine C-X-C motif receptor 4 are required for migration of gonadotropin-releasing hormone neurons to the forebrain. *J. Neurosci.* **26,** 6834–6840 (2006).

87. Zhu, Y., Matsumoto, T., Mikami, S., Nagasawa, T. & Murakami, F. SDF1/CXCR4 signalling regulates two distinct processes of precerebellar neuronal migration and its depletion leads to abnormal pontine nuclei formation. *Development* **136,** 1919–1928 (2009).

88. Dziembowska, M. *et al.* A role for CXCR4 signaling in survival and migration of neural and oligodendrocyte precursors. *Glia* **50,** 258–269 (2005).

89. Ödemis, V. *et al.* Mice deficient in the chemokine receptor CXCR4 exhibit impaired limb innervation and myogenesis. *Molecular and Cellular Neuroscience* **30,** 494–505 (2005).

90. Chalasani, S. H., Sabelko, K. A., Sunshine, M. J., Littman, D. R. & Raper, J. A. A chemokine, SDF-1, reduces the effectiveness of multiple axonal repellents and is required for normal axon pathfinding. *J. Neurosci.* **23,** 1360–1371 (2003).

91. Lieberam, I., Agalliu, D., Nagasawa, T., Ericson, J. & Jessell, T. M. A Cxcl12-CXCR4 chemokine signaling pathway defines the initial trajectory of mammalian motor axons. *Neuron* **47,** 667–679 (2005).

92. Lee, J. D., Coulthard, L. G. & Woodruff, T. M. Complement dysregulation in the central nervous system during development and disease. *Seminars in Immunology* **45,** 101340 (2019).

93. Stephan, A. H., Barres, B. A. & Stevens, B. The complement system: an unexpected role in synaptic pruning during development and disease. *Annu. Rev. Neurosci.* **35,** 369–389 (2012).

94. Jeanes, A., Coulthard, L. G., Mantovani, S., Markham, K. & Woodruff, T. M. Co-ordinated expression of innate immune molecules during mouse neurulation. *Molecular Immunology* **68,** 253–260 (2015).

95. Denny, K. J. *et al.* C5a Receptor Signaling Prevents Folate Deficiency–Induced Neural Tube Defects in Mice. *J Immunol* **190,** 3493–3499 (2013).

96. Coulthard, L. G. *et al.* Complement C5aR1 Signaling Promotes Polarization and Proliferation of Embryonic Neural Progenitor Cells through PKCζ. *J. Neurosci.* **37,** 5395–5407 (2017).

97. Gong, B. *et al.* IVIG immunotherapy protects against synaptic dysfunction in Alzheimer's disease through complement anaphylatoxin C5a-mediated AMPA-CREB-C/EBP signaling pathway. *Molecular Immunology* **56,** 619–629 (2013).

98. Coulthard, L. G., Hawksworth, O. A., Conroy, J., Lee, J. D. & Woodruff, T. M. Complement C3a receptor modulates embryonic neural progenitor cell proliferation and cognitive performance. *Molecular Immunology* **101,** 176–181 (2018).

99. Shinjyo, N., Ståhlberg, A., Dragunow, M., Pekny, M. & Pekna, M. Complement-derived anaphylatoxin C3a regulates in vitro differentiation and migration of neural progenitor cells. *Stem Cells* **27,** 2824–2832 (2009).

100. Gorelik, A. *et al.* Developmental activities of the complement pathway in migrating neurons. *Nature Communications* **8,** 1–12 (2017).

101. Carmona-Fontaine, C. *et al.* Complement Fragment C3a Controls Mutual Cell Attraction during Collective Cell Migration. *Developmental Cell* **21,** 1026–1037 (2011).

102. Atladóttir, H. Ó. *et al.* Maternal infection requiring hospitalization during pregnancy and autism spectrum disorders. *J Autism Dev Disord* **40,** 1423–1430 (2010).

103. Abdallah, M. W. *et al.* Amniotic fluid chemokines and autism spectrum disorders: An exploratory study utilizing a Danish Historic Birth Cohort. *Brain Behavior and Immunity* **26,** 170–176 (2012).

104. Brown, A. S. *et al.* Elevated maternal C-reactive protein and autism in a national birth cohort. *Molecular Psychiatry* **19,** 259–264 (2014).

105. Keil, A. *et al.* Parental autoimmune diseases associated with autism spectrum disorders in offspring. *Epidemiology* **21,** 805–808 (2010).

106. Krakowiak, P. *et al.* Maternal Metabolic Conditions and Risk for Autism and Other Neurodevelopmental Disorders. *Pediatrics* **129,** e1121–e1128 (2012).

107. Xiang, A. H. *et al.* Association of Maternal Diabetes With Autism in Offspring. *JAMA* **313,** 1425–10 (2015).

108. Consortium, C.-D. G. O. T. P. G. *et al.* Genomic Relationships, Novel Loci, and Pleiotropic Mechanisms across Eight Psychiatric Disorders. *Cell* **179,** 1469–1482.e11 (2019).

109. Kentner, A. C. *et al.* Maternal immune activation: reporting guidelines to improve the rigor, reproducibility, and transparency of the model. *Neuropsychopharmacology* **44,** 245–258 (2019).

110. Solek, C. M., Farooqi, N., Verly, M., Lim, T. K. & Ruthazer, E. S. Maternal immune activation in neurodevelopmental disorders. *Dev. Dyn.* **247,** 588–619 (2017).

111. Careaga, M., Murai, T. & Bauman, M. D. Maternal Immune Activation and Autism Spectrum Disorder_ From Rodents to Nonhuman and Human Primates. *Biological Psychiatry* **81,** 391–401 (2017).

112. Smith, S. E. P., Li, J., Garbett, K., Mirnics, K. & Patterson, P. H. Maternal immune activation alters fetal brain development through interleukin-6. *J. Neurosci.* **27,** 10695–10702 (2007).

113. Graham, A. M. *et al.* Maternal Systemic Interleukin-6 During Pregnancy Is Associated With Newborn Amygdala Phenotypes and Subsequent Behavior at 2 Years of Age. *Biological Psychiatry* **83,** 109–119 (2018).

114. Shin Yim, Y. *et al.* Reversing behavioural abnormalities in mice exposed to maternal inflammation. *Nature* **549,** 482–487 (2017).

115. Dahlgren, J., Samuelsson, A.-M., Jansson, T. & Holmäng, A. Interleukin-6 in the maternal circulation reaches the rat fetus in mid-gestation. *Pediatr Res* **60,** 147–151 (2006).

116. Zaretsky, M. V., Alexander, J. M., Byrd, W. & Bawdon, R. E. Transfer of inflammatory cytokines across the placenta. *Obstet Gynecol* **103,** 546–550 (2004).

117. Hsiao, E. Y. & Patterson, P. H. Activation of the maternal immune system induces endocrine changes in the placenta via IL-6. *Brain Behavior and Immunity* **25,** 604–615 (2011).

118. Wu, W.-L., Hsiao, E. Y., Yan, Z., Mazmanian, S. K. & Patterson, P. H. The placental interleukin-6 signaling controls fetal brain development and behavior. *Brain Behavior and Immunity* **62,** 11–23 (2017).

119. Choi, G. B. *et al.* The maternal interleukin-17a pathway in mice promotes autism-like phenotypes in offspring. *Science* **351,** 933–939 (2016).

120. Kim, S. *et al.* Maternal gut bacteria promote neurodevelopmental abnormalities in mouse offspring. *Nature* **549,** 528–532 (2017).

121. Lammert, C. R. *et al.* Cutting Edge: Critical Roles for Microbiota-Mediated Regulation of the Immune System in a Prenatal Immune Activation Model of Autism. *J Immunol* **201,** 845–850 (2018).

122. Schizophrenia Working Group of the Psychiatric Genomics Consortium. Biological insights from 108 schizophrenia-associated genetic loci. *Nature* **511,** 421–427 (2014).

123. Sekar, A. *et al.* Schizophrenia risk from complex variation of complement component 4. *Nature* **530,** 177–183 (2016).

124. Nimgaonkar, V. L., Prasad, K. M., Chowdari, K. V., Severance, E. G. & Yolken, R. H. The complement system: a gateway to gene-environment interactions in schizophrenia pathogenesis. *Molecular Psychiatry* **22,** 1554–1561 (2017).

125. Brown, A. S. Prenatal infection as a risk factor for schizophrenia. *Schizophr Bull* **32,** 200–202 (2006).

126. Benros, M. E., Mortensen, P. B. & Eaton, W. W. Autoimmune diseases and infections as risk factors for schizophrenia. *Annals of the New York Academy of Sciences* **1262,** 56–66 (2012).

127. Canetta, S. *et al.* Elevated maternal C-reactive protein and increased risk of schizophrenia in a national birth cohort. *Am J Psychiatry* **171,** 960–968 (2014).

128. Severance, E. G., Gressitt, K. L., Buka, S. L., Cannon, T. D. & Yolken, R. H. Maternal complement C1q and increased odds for psychosis in adult offspring. *Schizophrenia Research* **159,** 14–19 (2014).

129. Brown, A. S. *et al.* Elevated maternal interleukin-8 levels and risk of schizophrenia in adult offspring. *Am J Psychiatry* **161,** 889–895 (2004).

130. Buka, S. L. *et al.* Maternal cytokine levels during pregnancy and adult psychosis. *Brain Behavior and Immunity* **15,** 411–420 (2001).

131. Ellman, L. M. *et al.* Structural brain alterations in schizophrenia following fetal exposure to the inflammatory cytokine interleukin-8. *Schizophrenia Research* **121,** 46–54 (2010).

132. Fineberg, A. M. & Ellman, L. M. Inflammatory Cytokines and Neurological and Neurocognitive Alterations in the Course of Schizophrenia. *Biological Psychiatry* **73,** 951–966 (2013).

133. Miller, B. J., Culpepper, N., Rapaport, M. H. & Buckley, P. Prenatal inflammation and neurodevelopment in schizophrenia: A review of human studies. *Progress in Neuropsychopharmacology & Biological Psychiatry* **42,** 92–100 (2013).

134. Meyer, U. *et al.* Adult behavioral and pharmacological dysfunctions following disruption of the fetal brain balance between pro-inflammatory and IL-10-mediated anti-inflammatory signaling. *Molecular Psychiatry* **13,** 208–221 (2008).

135. Li, M. *et al.* Integrative functional genomic analysis of human brain development and neuropsychiatric risks. *Science* **362,** (2018).

136. Zhong, S. *et al.* A single-cell RNA-seq survey of the developmental landscape of the human prefrontal cortex. *Nature* **555,** 524–528 (2018).

137. Polioudakis, D. *et al.* A Single-Cell Transcriptomic Atlas of Human Neocortical Development during Mid-gestation. *Neuron* **103,** 785–801.e8 (2019).

138. Meyer, U. Neurodevelopmental Resilience and Susceptibility to Maternal Immune Activation. *Trends in Neurosciences* **42,** 793–806 (2019).

139. Haida, O. *et al.* Sex-dependent behavioral deficits and neuropathology in a maternal immune activation model of autism. *Translational Psychiatry* 1–12 (2019). doi:10.1038/s41398-019-0457-y

140. Klein, S. L. & Flanagan, K. L. Sex differences in immune responses. *Nat. Rev. Immunol.* **16,** 626–638 (2016).

141. Gomez-Lopez, N., StLouis, D., Lehr, M. A., Sanchez-Rodriguez, E. N. & Arenas-Hernandez, M. Immune cells in term and preterm labor. *Cell Mol Immunol* **11,** 571–581 (2014).

142. Romero, R., Dey, S. K. & Fisher, S. J. Preterm labor: one syndrome, many causes. *Science* **345,** 760–765 (2014).

143. Gilman-Sachs, A. *et al.* Inflammation induced preterm labor and birth. *J. Reprod. Immunol.* **129,** 53–58 (2018).

144. Berry, S. M. *et al.* Premature parturition is characterized by in utero activation of the fetal immune system. *The American Journal of Obstetrics & Gynecology* **173,** 1315–1320 (1995).

145. Romero, R. *et al.* A fetal systemic inflammatory response is followed by the spontaneous onset of preterm parturition. *The American Journal of Obstetrics & Gynecology* **179,** 186–193 (1998).

146. Miller, D., Gershater, M., Slutsky, R., Romero, R. & Gomez-Lopez, N. Maternal and fetal T cells in term pregnancy and preterm labor. *Cell Mol Immunol* **17,** 693–704 (2020).

147. Maric-Bilkan, C. *et al.* Research Recommendations From the National Institutes of Health Workshop on Predicting, Preventing, and Treating Preeclampsia. *Hypertension* **73,** 757–766 (2019).

148. Staff, A. C. The two-stage placental model of preeclampsia: An update. *J. Reprod. Immunol.* **134-135,** 1–10 (2019).

149. Rana, S., Lemoine, E., Granger, J. P. & Karumanchi, S. A. Preeclampsia: Pathophysiology, Challenges, and Perspectives. *Circ Res* **124,** 1094–1112 (2019).

150. Moffett, A. & Hiby, S. E. How Does the maternal immune system contribute to the development of pre-eclampsia? *Placenta* **28 Suppl A,** S51–6 (2007).

151. Lokki, A. I., Heikkinen-Eloranta, J. K. & Laivuori, H. The Immunogenetic Conundrum of Preeclampsia. *Front. Immunol.* **9,** 2630 (2018).

152. Copp, A. J., Stanier, P. & Greene, N. D. E. Neural tube defects: recent advances, unsolved questions, and controversies. *Lancet Neurol* **12,** 799–810 (2013).

153. Greene, N. D. E. & Copp, A. J. Neural Tube Defects. *Annu. Rev. Neurosci.* **37,** 221–242 (2014).

154. Holladay, S. D. *et al.* Nonspecific stimulation of the maternal immune system. I. Effects On teratogen-induced fetal malformations. *Teratology* **62,** 413–419 (2000).

155. Prater, M. R., Johnson, V. J., Germolec, D. R., Luster, M. I. & Holladay, S. D. Maternal treatment with a high dose of CpG ODN during gestation alters fetal craniofacial and distal limb development in C57BL/6 mice. *Vaccine* **24,** 263–271 (2006).

156. Thaxton, J. E., Romero, R. & Sharma, S. TLR9 Activation Coupled to IL-10 Deficiency Induces Adverse Pregnancy Outcomes. *J Immunol* **183,** 1144–1154 (2009).

157. Lanning, J. C., Hilbelink, D. R. & Chen, L. T. Teratogenic effects of endotoxin on the golden hamster. *Teratog., Carcinog. Mutagen.* **3,** 145–149 (1983).

158. Collins, J. G., Smith, M. A., Arnold, R. R. & Offenbacher, S. Effects of Escherichia coli and Porphyromonas gingivalis lipopolysaccharide on pregnancy outcome in the golden hamster. *Infect. Immun.* **62,** 4652–4655 (1994).

159. Ornoy, A. & Altshuler, G. Maternal endotoxemia, fetal anomalies, and central nervous system damage: a rat model of a human problem. *The American Journal of Obstetrics & Gynecology* **124,** 196–204 (1976).

160. Taubeneck, M. W. *et al.* Tumor necrosis factor-alpha alters maternal and embryonic zinc metabolism and is developmentally toxic in mice. *J. Nutr.* **125,** 908–919 (1995).

161. Alexopoulou, L., Holt, A. C., Medzhitov, R. & Flavell, R. A. Recognition of double-stranded RNA and activation of NF-kappaB by Toll-like receptor 3. *Nature* **413,** 732–738 (2001).

162. Kato, H. *et al.* Differential roles of MDA5 and RIG-I helicases in the recognition of RNA viruses. *Nature* **441,** 101–105 (2006).

163. Yockey, L. J. *et al.* Type I interferons instigate fetal demise after Zika virus infection. *Sci Immunol* **3,** (2018).

164. Andries, O. *et al.* N(1)-methylpseudouridine-incorporated mRNA outperforms pseudouridine-incorporated mRNA by providing enhanced protein expression and reduced immunogenicity in mammalian cell lines and mice. *J Control Release* **217,** 337–344 (2015).

165. Ribot, J. C., Lopes, N. & Silva-Santos, B. γδ T cells in tissue physiology and surveillance. *Nat. Rev. Immunol.* **21,** 221–232 (2021).

166. Pinget, G. V. *et al.* The majority of murine γδ T cells at the maternal-fetal interface in pregnancy produce IL-17. *Immunol Cell Biol* **94,** 623–630 (2016).

167. Miner, J. H., Cunningham, J. & Sanes, J. R. Roles for laminin in embryogenesis: exencephaly, syndactyly, and placentopathy in mice lacking the laminin alpha5 chain. *The Journal of Cell Biology* **143,** 1713–1723 (1998).

168. Coles, E. G., Gammill, L. S., Miner, J. H. & Bronner-Fraser, M. Abnormalities in neural crest cell migration in laminin alpha5 mutant mice. *Developmental Biology* **289,** 218–228 (2006).

169. Bronner-Fraser, M. & Lallier, T. A monoclonal antibody against a laminin-heparan sulfate proteoglycan complex perturbs cranial neural crest migration in vivo. *The Journal of Cell Biology* **106,** 1321–1329 (1988).

170. Bronner-Fraser, M. An antibody to a receptor for fibronectin and laminin perturbs cranial neural crest development in vivo. *Developmental Biology* **117,** 528–536 (1986).

171. Heaton, M. B. Influence of laminin on the responsiveness of early chick embryo neural tube neurons to nerve growth factor. *J. Neurosci. Res.* **22,** 390–396 (1989).

172. Copp, A. J. *et al.* Regional differences in the expression of laminin isoforms during mouse neural tube development. *Matrix Biol* **30,** 301–309 (2011).

173. Ferrarini, M., Heltai, S., Pupa, S. M., Mernard, S. & Zocchi, R. Killing of laminin receptor-positive human lung cancers by tumor infiltrating lymphocytes bearing gammadelta(+) t-cell receptors. *J Natl Cancer Inst* **88,** 436–441 (1996).

174. Hosier, H. *et al.* SARS-CoV-2 infection of the placenta. *J. Clin. Invest.* **130,** 4947–4953 (2020).

175. Lu-Culligan, A. *et al.* Maternal respiratory SARS-CoV-2 infection in pregnancy is associated with a robust inflammatory response at the maternal-fetal interface. *Med (N Y)* **2,** 591–610.e10 (2021).

176. Zambrano, L. D. *et al.* Update: Characteristics of Symptomatic Women of Reproductive Age with Laboratory-Confirmed SARS-CoV-2 Infection by Pregnancy Status - United States, January 22-October 3, 2020. *MMWR Morb Mortal Wkly Rep* **69,** 1641–1647 (2020).

177. Ahlberg, M. *et al.* Association of SARS-CoV-2 Test Status and Pregnancy Outcomes. *JAMA* (2020). doi:10.1001/jama.2020.19124

178. Abasse, S. *et al.* Neonatal COVID-19 Pneumonia: Report of the First Case in a Preterm Neonate in Mayotte, an Overseas Department of France. *Children (Basel)* **7,** 87 (2020).

179. Zimmermann, P. & Curtis, N. COVID-19 in Children, Pregnancy and Neonates: A Review of Epidemiologic and Clinical Features. *Pediatr Infect Dis J* **39,** 469–477 (2020).

180. Sherer, M. L. *et al.* Dysregulated immunity in SARS-CoV-2 infected pregnant women. *medRxiv* 2020.11.13.20231373 (2020). doi:10.1101/2020.11.13.20231373

181. Prochaska, E., Jang, M. & Burd, I. COVID-19 in pregnancy: Placental and neonatal involvement. *Am J Reprod Immunol* **84,** e13306 (2020).

182. Barthold, S. W., Beck, D. S. & Smith, A. L. Mouse hepatitis virus and host determinants of vertical transmission and maternally-derived passive immunity in mice. *Arch Virol* **100,** 171–183 (1988).

183. Cardenas, I. *et al.* Viral infection of the placenta leads to fetal inflammation and sensitization to bacterial products predisposing to preterm labor. *J Immunol* **185,** 1248–1257 (2010).

184. Ng, W. F. *et al.* The placentas of patients with severe acute respiratory syndrome: a pathophysiological evaluation. *Pathology* **38,** 210–218 (2006).

185. Pique-Regi, R. *et al.* Does the human placenta express the canonical cell entry mediators for SARS-CoV-2? *eLife* **9,** (2020).

186. Li, M., Chen, L., Zhang, J., Xiong, C. & Li, X. The SARS-CoV-2 receptor ACE2 expression of maternal-fetal interface and fetal organs by single-cell transcriptome study. *PLoS ONE* **15,** e0230295 (2020).

187. Ashary, N. *et al.* Single-Cell RNA-seq Identifies Cell Subsets in Human Placenta That Highly Expresses Factors Driving Pathogenesis of SARS-CoV-2. *Front Cell Dev Biol* **8,** 783 (2020).

188. Singh, M., Bansal, V. & Feschotte, C. A Single-Cell RNA Expression Map of Human Coronavirus Entry Factors. *Cell Rep* **32,** 108175 (2020).

189. Hikmet, F. *et al.* The protein expression profile of ACE2 in human tissues. *Mol Syst Biol* **16,** e9610 (2020).

190. Patanè, L. *et al.* Vertical transmission of coronavirus disease 2019: severe acute respiratory syndrome coronavirus 2 RNA on the fetal side of the placenta in pregnancies with coronavirus disease 2019-positive mothers and neonates at birth. *The American Journal of Obstetrics & Gynecology MFM* **2,** 100145 (2020).

191. Vivanti, A. J. *et al.* Transplacental transmission of SARS-CoV-2 infection. *Nature Communications* **11,** 3572–7 (2020).

192. Xie, X. *et al.* An Infectious cDNA Clone of SARS-CoV-2. *Cell Host and Microbe* **27,** 841–848.e3 (2020).

193. Graham, C. H. *et al.* Establishment and characterization of first trimester human trophoblast cells with extended lifespan. *Exp Cell Res* **206,** 204–211 (1993).

194. Abou-Kheir, W., Barrak, J., Hadadeh, O. & Daoud, G. HTR-8/SVneo cell line contains a mixed population of cells. *Placenta* **50,** 1–7 (2017).

195. Taglauer, E. *et al.* Consistent localization of SARS-CoV-2 spike glycoprotein and ACE2 over TMPRSS2 predominance in placental villi of 15 COVID-19 positive maternal-fetal dyads. *Placenta* **100,** 69–74 (2020).

196. Facchetti, F. *et al.* SARS-CoV2 vertical transmission with adverse effects on the newborn revealed through integrated immunohistochemical, electron microscopy and molecular analyses of Placenta. *EBioMedicine* **59,** 102951 (2020).

197. Edlow, A. G. *et al.* Assessment of Maternal and Neonatal SARS-CoV-2 Viral Load, Transplacental Antibody Transfer, and Placental Pathology in Pregnancies During the COVID-19 Pandemic. *JAMA Netw Open* **3,** e2030455 (2020).

198. Brien, M.-È. *et al.* Alarmins at the maternal–fetal interface: involvement of inflammation in placental dysfunction and pregnancy complications. *Can J Physiol Pharmacol* **97,** 206–212 (2019).

199. Molvarec, A. *et al.* Circulating heat shock protein 70 (HSPA1A) in normal and pathological pregnancies. *Cell Stress and Chaperones* **15,** 237–247 (2010).

200. Liu, Y. *et al.* HSP70 is associated with endothelial activation in placental vascular diseases. *Mol. Med.* **14,** 561–566 (2008).

201. Vento-Tormo, R. *et al.* Single-cell reconstruction of the early maternal-fetal interface in humans. *Nature* **563,** 347–353 (2018).

202. Pavličev, M. *et al.* Single-cell transcriptomics of the human placenta: inferring the cell communication network of the maternal-fetal interface. *Genome Res* **27,** 349–361 (2017).

203. Suryawanshi, H. *et al.* A single-cell survey of the human first-trimester placenta and decidua. *Sci Adv* **4,** eaau4788 (2018).

204. Goshua, G. *et al.* Endotheliopathy in COVID-19-associated coagulopathy: evidence from a single-centre, cross-sectional study. *Lancet Haematol* **7,** e575–e582 (2020).

205. Acharya, D., Liu, G. & Gack, M. U. Dysregulation of type I interferon responses in COVID-19. *Nat. Rev. Immunol.* **20,** 397–398 (2020).

206. Lee, J. S. & Shin, E.-C. The type I interferon response in COVID-19: implications for treatment. *Nat. Rev. Immunol.* **20,** 585–586 (2020).

207. Rusinova, I. *et al.* Interferome v2.0: an updated database of annotated interferon-regulated genes. *Nucleic Acids Res* **41,** D1040–6 (2013).

208. Efremova, M., Vento-Tormo, M., Teichmann, S. A. & Vento-Tormo, R. CellPhoneDB: inferring cell-cell communication from combined expression of multi-subunit ligand-receptor complexes. *Nat Protoc* **15,** 1484–1506 (2020).

209. Baud, D. *et al.* Second-Trimester Miscarriage in a Pregnant Woman With SARS-CoV-2 Infection. *JAMA* **323,** 2198–2200 (2020).

210. Hecht, J. L. *et al.* SARS-CoV-2 can infect the placenta and is not associated with specific placental histopathology: a series of 19 placentas from COVID-19-positive mothers. *Mod Pathol* **33,** 2092–2103 (2020).

211. Nadeau-Vallée, M. *et al.* Sterile inflammation and pregnancy complications: a review. *Reproduction* **152,** R277–R292 (2016).

212. Weckman, A. M., Ngai, M., Wright, J., McDonald, C. R. & Kain, K. C. The Impact of Infection in Pregnancy on Placental Vascular Development and Adverse Birth Outcomes. *Front Microbiol* **10,** 1924 (2019).

213. Song, E. *et al.* Neuroinvasion of SARS-CoV-2 in human and mouse brain. *The Journal of Experimental Medicine* **218,** (2021).

214. Bloise, E. *et al.* Expression of severe acute respiratory syndrome coronavirus 2 cell entry genes, angiotensin-converting enzyme 2 and transmembrane protease serine 2, in the placenta across gestation and at the maternal-fetal interface in pregnancies complicated by preterm birth or preeclampsia. *American Journal of Obstetrics and Gynecology* **224,** 298.e1–298.e8 (2021).

215. Leung, J. M. *et al.* ACE-2 expression in the small airway epithelia of smokers and COPD patients: implications for COVID-19. *Eur Respir J* **55,** (2020).

216. Shang, J. *et al.* Cell entry mechanisms of SARS-CoV-2. *Proc. Natl. Acad. Sci. U.S.A.* **117,** 11727–11734 (2020).

217. Ou, X. *et al.* Characterization of spike glycoprotein of SARS-CoV-2 on virus entry and its immune cross-reactivity with SARS-CoV. *Nature Communications* **11,** 1620 (2020).

218. Wei, J. *et al.* Genome-wide CRISPR Screens Reveal Host Factors Critical for SARS-CoV-2 Infection. *Cell* **184,** 76–91.e13 (2021).

219. Kliman, H. J., NESTLER, J. E., SERMASI, E., SANGER, J. M. & STRAUSS, J. F., III. Purification, Characterization, and in vitro Differentiation of Cytotrophoblasts from Human Term Placentae*. *Endocrinology* **118,** 1567–1582 (1986).

220. Jurado, K. A. *et al.* Zika virus productively infects primary human placenta-specific macrophages. *JCI Insight* **1,** 267–7 (2016).

221. Tabata, T. *et al.* Zika Virus Targets Different Primary Human Placental Cells, Suggesting Two Routes for Vertical Transmission. *Cell Host and Microbe* **20,** 155–166 (2016).

222. Reyes, L. & Golos, T. G. Hofbauer Cells: Their Role in Healthy and Complicated Pregnancy. *Front. Immunol.* **9,** 535–8 (2018).

223. Simoni, M. K., Jurado, K. A., Abrahams, V. M., Fikrig, E. & Guller, S. Zika virus infection of Hofbauer cells. *Am J Reprod Immunol* **77,** (2017).

224. Kim, J.-M. *et al.* Detection and Isolation of SARS-CoV-2 in Serum, Urine, and Stool Specimens of COVID-19 Patients from the Republic of Korea. *Osong Public Health Res Perspect* **11,** 112–117 (2020).

225. Wang, W. *et al.* Detection of SARS-CoV-2 in Different Types of Clinical Specimens. *JAMA* **323,** 1843–1844 (2020).

226. de Mendonça Vieira, R. *et al.* Human Term Pregnancy Decidual NK Cells Generate Distinct Cytotoxic Responses. *J Immunol* **204,** 3149–3159 (2020).

227. Jabrane-Ferrat, N. Features of Human Decidual NK Cells in Healthy Pregnancy and During Viral Infection. *Front. Immunol.* **10,** 1397 (2019).

228. Hanna, J. *et al.* Decidual NK cells regulate key developmental processes at the human fetal-maternal interface. *Nat Med* **12,** 1065–1074 (2006).

229. Fukui, A. *et al.* Changes of NK cells in preeclampsia. *Am J Reprod Immunol* **67,** 278–286 (2012).

230. Taylor, E. B. & Sasser, J. M. Natural killer cells and T lymphocytes in pregnancy and pre-eclampsia. *Clin. Sci.* **131,** 2911–2917 (2017).

231. Goldman-Wohl, D. & Yagel, S. Symposium: Current knowledge on natural killer cells, pregnancy and pre-eclampsia NK cells and pre-eclampsia. **16,** 227–231 (2008).

232. Cornelius, D. C. & Wallace, K. Decidual natural killer cells: A critical pregnancy mediator altered in preeclampsia. *EBioMedicine* **39,** 31–32 (2019).

233. Papúchová, H., Meissner, T. B., Li, Q., Strominger, J. L. & Tilburgs, T. The Dual Role of HLA-C in Tolerance and Immunity at the Maternal-Fetal Interface. *Front. Immunol.* **10,** 2730 (2019).

234. Pockley, A. G. Heat shock proteins as regulators of the immune response. *Lancet* **362,** 469–476 (2003).

235. Geng, J. *et al.* Functional analysis of HSPA1A and HSPA8 in parturition. *Biochemical and Biophysical Research Communications* **483,** 371–379 (2017).

236. Hromadnikova, I. *et al.* Circulating heat shock protein mRNA profile in gestational hypertension, pre-eclampsia & foetal growth restriction. *Indian J Med Res* **144,** 229–237 (2016).

237. Saghafi, N., Pourali, L., Ghavami Ghanbarabadi, V., Mirzamarjani, F. & Mirteimouri, M. Serum heat shock protein 70 in preeclampsia and normal pregnancy: A systematic review and meta-analysis. *Int J Reprod Biomed* **16,** 1–8 (2018).

238. Molvarec, A. *et al.* Serum heat shock protein 70 levels are decreased in normal human pregnancy. *J. Reprod. Immunol.* **74,** 163–169 (2007).

239. Figueras, F. *et al.* COVID-19 causing HELLP-like syndrome in pregnancy and role of angiogenic factors for differential diagnosis. 1–9 (2020). doi:10.1101/2020.07.10.20133801

240. Futterman, I., Toaff, M., Navi, L. & Clare, C. A. COVID-19 and HELLP: Overlapping Clinical Pictures in Two Gravid Patients. *AJP Rep* **10,** e179–e182 (2020).

241. Makinson, R., Lloyd, K., Grissom, N. & Reyes, T. M. Exposure to in utero inflammation increases locomotor activity, alters cognitive performance and drives vulnerability to cognitive performance deficits after acute immune activation. *Brain Behavior and Immunity* **80,** 56–65 (2019).

242. Yockey, L. J. *et al.* Type I interferons instigate fetal demise after Zika virus infection. *Sci Immunol* **3,** (2018).

243. Zani, A. *et al.* Interferon-induced transmembrane proteins inhibit cell fusion mediated by trophoblast syncytins. *J. Biol. Chem.* **294,** 19844–19851 (2019).

244. Buchrieser, J. *et al.* IFITM proteins inhibit placental syncytiotrophoblast formation and promote fetal demise. *Science* **365,** 176–180 (2019).

245. Allotey, J. *et al.* Clinical manifestations, risk factors, and maternal and perinatal outcomes of coronavirus disease 2019 in pregnancy: living systematic review and meta-analysis. *BMJ* **370,** m3320 (2020).

246. DeBolt, C. A. *et al.* Pregnant women with severe or critical coronavirus disease 2019 have increased composite morbidity compared with nonpregnant matched controls. *American Journal of Obstetrics and Gynecology* **224,** 510.e1–510.e12 (2021).

247. Woodworth, K. R. *et al.* Birth and Infant Outcomes Following Laboratory-Confirmed SARS-CoV-2 Infection in Pregnancy - SET-NET, 16 Jurisdictions, March 29-October 14, 2020. *MMWR Morb Mortal Wkly Rep* **69,** 1635–1640 (2020).

248. Cojocaru, L. *et al.* Increased Risk of Severe COVID-19 Disease in Pregnancy in a Multicenter Propensity Score-Matched Study. *medRxiv* 2021.06.18.21258899–25 (2021). doi:10.1101/2021.06.18.21258899

249. Lai, L. Y. H. *et al.* 'Clinical characteristics, symptoms, management and health outcomes in 8,598 pregnant women diagnosed with COVID-19 compared to 27,510 with seasonal influenza in France, Spain and the US: a network cohort analysis'. *medRxiv* 2020.10.13.20211821–24 (2020). doi:10.1101/2020.10.13.20211821

250. Lokken, E. M. *et al.* Higher severe acute respiratory syndrome coronavirus 2 infection rate in pregnant patients. *American Journal of Obstetrics and Gynecology* **225,** 75.e1–75.e16 (2021).

251. Klein, S. L., Creisher, P. S. & Burd, I. COVID-19 vaccine testing in pregnant females is necessary. *J. Clin. Invest.* **131,** (2021).

252. Shimabukuro, T. T. *et al.* Preliminary Findings of mRNA Covid-19 Vaccine Safety in Pregnant Persons. *N. Engl. J. Med.* **384,** 2273–2282 (2021).

253. Zauche, L. H. *et al.* Receipt of mRNA COVID-19 vaccines preconception and during pregnancy and risk of self-reported spontaneous abortions, CDC v-safe COVID-19 Vaccine Pregnancy Registry 2020-21. *Res Sq* (2021). doi:10.21203/rs.3.rs-798175/v1

254. Kharbanda, E. O. *et al.* Spontaneous Abortion Following COVID-19 Vaccination During Pregnancy. *JAMA* (2021). doi:10.1001/jama.2021.15494

255. Theiler, R. N. *et al.* Pregnancy and birth outcomes after SARS-CoV-2 vaccination in pregnancy. *The American Journal of Obstetrics & Gynecology MFM* 100467 (2021). doi:10.1016/j.ajogmf.2021.100467

256. Polack, F. P. *et al.* Safety and Efficacy of the BNT162b2 mRNA Covid-19 Vaccine. *N. Engl. J. Med.* **383,** 2603–2615 (2020).

257. Baden, L. R. *et al.* Efficacy and Safety of the mRNA-1273 SARS-CoV-2 Vaccine. *N. Engl. J. Med.* **384,** 403–416 (2021).

258. Murphy, J. *et al.* Psychological characteristics associated with COVID-19 vaccine hesitancy and resistance in Ireland and the United Kingdom. *Nature Communications* **12,** 29–15 (2021).

259. Townsel, C. *et al.* COVID-19 vaccine hesitancy among reproductive-aged female tier 1A healthcare workers in a United States Medical Center. *J Perinatol* 1–3 (2021). doi:10.1038/s41372-021-01173-9

260. Goncu Ayhan, S. *et al.* COVID-19 vaccine acceptance in pregnant women. *Int J Gynaecol Obstet* **154,** 291–296 (2021).

261. Sutton, D. *et al.* COVID-19 vaccine acceptance among pregnant, breastfeeding, and nonpregnant reproductive-aged women. *The American Journal of Obstetrics & Gynecology MFM* **3,** 100403 (2021).

262. Adhikari, E. H. & Spong, C. Y. COVID-19 Vaccination in Pregnant and Lactating Women. *JAMA* **325,** 1039–1040 (2021).

263. Male, V. Are COVID-19 vaccines safe in pregnancy? *Nat. Rev. Immunol.* **21,** 200–201 (2021).

264. Holder, B. S., Tower, C. L., Abrahams, V. M. & Aplin, J. D. Syncytin 1 in the human placenta. *Placenta* **33,** 460–466 (2012).

265. Prasad, M. *et al.* No crossreactivity of anti-SARS-CoV-2 spike protein antibodies with Syncytin-1. *Cell Mol Immunol* **18,** 2566–2568 (2021).

266. Mattar, C. N. *et al. Addressing anti-syncytin antibody levels, and fertility and breastfeeding concerns, following BNT162B2 COVID-19 mRNA vaccination*. (medRxiv, 2021). doi:10.1101/2021.05.23.21257686

267. Bentov, Y. *et al.* Ovarian follicular function is not altered by SARS-CoV-2 infection or BNT162b2 mRNA COVID-19 vaccination. *Hum. Reprod.* **36,** 2506–2513 (2021).

268. Morris, R. S. SARS-CoV-2 spike protein seropositivity from vaccination or infection does not cause sterility. *F S Rep* **2,** 253–255 (2021).

269. Orvieto, R. *et al.* Does mRNA SARS-CoV-2 vaccine influence patients' performance during IVF-ET cycle? *Reprod Biol Endocrinol* **19,** 69–4 (2021).

270. Rottenstreich, M. *et al.* Covid-19 vaccination during the third trimester of pregnancy: rate of vaccination and maternal and neonatal outcomes, a multicentre retrospective cohort study. *BJOG* (2021). doi:10.1111/1471-0528.16941

271. Liu, F. *et al.* Newborn Dried Blood Spots for Serologic Surveys of COVID-19. *Pediatr Infect Dis J* **39,** e454–e456 (2020).

272. Beharier, O. *et al.* Efficient maternal to neonatal transfer of antibodies against SARS-CoV-2 and BNT162b2 mRNA COVID-19 vaccine. *J. Clin. Invest.* **131,** (2021).

273. Rottenstreich, A. *et al.* Efficient maternofetal transplacental transfer of anti-SARS-CoV-2 spike antibodies after antenatal SARS-CoV-2 BNT162b2 mRNA vaccination. *Clin Infect Dis* (2021). doi:10.1093/cid/ciab266

274. Mithal, L. B., Otero, S., Shanes, E. D., Goldstein, J. A. & Miller, E. S. Cord blood antibodies following maternal coronavirus disease 2019 vaccination during pregnancy. *American Journal of Obstetrics and Gynecology* **225,** 192–194 (2021).

275. Prabhu, M. *et al.* Antibody Response to Coronavirus Disease 2019 (COVID-19) Messenger RNA Vaccination in Pregnant Women and Transplacental Passage Into Cord Blood. *Obstet Gynecol* **138,** 278–280 (2021).

276. Gray, K. J. *et al.* Coronavirus disease 2019 vaccine response in pregnant and lactating women: a cohort study. *American Journal of Obstetrics and Gynecology* **225,** 303.e1–303.e17 (2021).

277. Perl, S. H. *et al.* SARS-CoV-2-Specific Antibodies in Breast Milk After COVID-19 Vaccination of Breastfeeding Women. *JAMA* **325,** 2013–2014 (2021).

278. Kelly, J. C. *et al.* Anti-severe acute respiratory syndrome coronavirus 2 antibodies induced in breast milk after Pfizer-BioNTech/BNT162b2 vaccination. *American Journal of Obstetrics and Gynecology* **225,** 101–103 (2021).

279. Jakuszko, K. *et al.* Immune Response to Vaccination against COVID-19 in Breastfeeding Health Workers. *Vaccines (Basel)* **9,** (2021).

280. Chua, J. S. C., Rofe, A. M. & Coyle, P. Dietary Zinc Supplementation Ameliorates LPS-Induced Teratogenicity in Mice. *Pediatr Res* **59,** 355–358 (2006).

281. Zhao, L. *et al.* Reactive Oxygen Species Contribute to Lipopolysaccharide-Induced Teratogenesis in Mice. *Toxicological Sciences* **103,** 149–157 (2008).

282. Lee, A. J., Kandiah, N., Karimi, K., Clark, D. A. & Ashkar, A. A. Interleukin-15 is required for maximal lipopolysaccharide-induced abortion. *Journal of Leukocyte Biology* **93,** 905–912 (2013).

283. Murray, K. N. *et al.* Evolution of a maternal immune activation (mIA) model in rats: Early developmental effects. *Brain Behavior and Immunity* **75,** 48–59 (2019).

284. Thaxton, J. E. *et al.* NKG2D blockade inhibits poly(I:C)-triggered fetal loss in wild type but not in IL-10-/- mice. *J Immunol* **190,** 3639–3647 (2013).

285. Lucas, C. *et al.* Impact of circulating SARS-CoV-2 variants on mRNA vaccine-induced immunity in uninfected and previously infected individuals. *medRxiv* 2021.07.14.21260307 (2021).

286. Tokuyama, M. *et al.* Antibodies against human endogenous retrovirus K102 envelope activate neutrophils in systemic lupus erythematosus. *The Journal of Experimental Medicine* **218,** (2021).

287. Adams Waldorf, K. M. & McAdams, R. M. Influence of infection during pregnancy on fetal development. *Reproduction* **146,** R151–62 (2013).

288. Longo, S., Borghesi, A., Tzialla, C. & Stronati, M. IUGR and infections. *Early Hum Dev* **90 Suppl 1,** S42–4 (2014).

289. Atyeo, C. *et al.* Compromised SARS-CoV-2-specific placental antibody transfer. *Cell* **184,** 628–642.e10 (2021).

290. Eberhardt, C. S. *et al.* Maternal Immunization Earlier in Pregnancy Maximizes Antibody Transfer and Expected Infant Seropositivity Against Pertussis. *Clin Infect Dis* **62,** 829–836 (2016).

291. Eberhardt, C. S. *et al.* Pertussis Antibody Transfer to Preterm Neonates After Second- Versus Third-Trimester Maternal Immunization. *Clin Infect Dis* **64,** 1129–1132 (2017).

292. Naidu, M. A., Muljadi, R., Davies-Tuck, M. L., Wallace, E. M. & Giles, M. L. The optimal gestation for pertussis vaccination during pregnancy: a prospective cohort study. *American Journal of Obstetrics and Gynecology* **215,** 237.e1–6 (2016).

293. Healy, C. M. *et al.* Association Between Third-Trimester Tdap Immunization and Neonatal Pertussis Antibody Concentration. *JAMA* **320,** 1464–1470 (2018).

294. Abu-Raya, B. *et al.* The effect of timing of maternal tetanus, diphtheria, and acellular pertussis (Tdap) immunization during pregnancy on newborn pertussis antibody levels - a prospective study. *Vaccine* **32,** 5787–5793 (2014).

295. Hao, Y. *et al.* Integrated analysis of multimodal single-cell data. *Cell* **184,** 3573–3587.e29 (2021).

296. Hafemeister, C. & Satija, R. Normalization and variance stabilization of single-cell RNA-seq data using regularized negative binomial regression. *Genome Biol.* **20,** 296–15 (2019).

297. Yu, Z. *et al.* Beyond t test and ANOVA: applications of mixed-effects models for more rigorous statistical analysis in neuroscience research. *Neuron* **110,** 21–35 (2022).

298. Squair, J. W. *et al.* Confronting false discoveries in single-cell differential expression. *Nature Communications* **12,** 5692 (2021).

299. Zhou, Y. *et al.* Metascape provides a biologist-oriented resource for the analysis of systems-level datasets. *Nature Communications* **10,** 1523–10 (2019).

300. Kliman, H. J. *et al.* Placental protein 13 and decidual zones of necrosis: an immunologic diversion that may be linked to preeclampsia. *Reprod Sci* **19,** 16–30 (2012).

301. Tang, Z. *et al.* Isolation of Hofbauer Cells from Human Term Placentas with High Yield and Purity. *Am J Reprod Immunol* **66,** 336–348 (2011).

302. Vogels, C. B. F. *et al.* Analytical sensitivity and efficiency comparisons of SARS-CoV-2 RT-qPCR primer-probe sets. *Nat Microbiol* **5,** 1299–1305 (2020).

303. Amanat, F. *et al.* A serological assay to detect SARS-CoV-2 seroconversion in humans. *Nat Med* **26,** 1033–1036 (2020).

304. Khong, T. Y. *et al.* Sampling and Definitions of Placental Lesions: Amsterdam Placental Workshop Group Consensus Statement. *Arch Pathol Lab Med* **140,** 698–713 (2016).

305. Kliman, H. J. *et al.* Pathway of Maternal Serotonin to the Human Embryo and Fetus. *Endocrinology* **159,** 1609–1629 (2018).

306. Thike, A. A., Chng, M. J., Fook-Chong, S. & Tan, P. H. Immunohistochemical expression of hormone receptors in invasive breast carcinoma: correlation of results of H-score with pathological parameters. *Pathology* **33,** 21–25 (2001).

307. Xu, Y., Plazyo, O., Romero, R., Hassan, S. S. & Gomez-Lopez, N. Isolation of Leukocytes from the Human Maternal-fetal Interface. *JoVE* e52863 (2015). doi:10.3791/52863

308. Bray, N. L., Pimentel, H., Melsted, P. & Pachter, L. Near-optimal probabilistic RNA-seq quantification. *Nat Biotechnol* **34,** 525–527 (2016).

309. Durinck, S., Spellman, P. T., Birney, E. & Huber, W. Mapping identifiers for the integration of genomic datasets with the R/Bioconductor package biomaRt. *Nat Protoc* **4,** 1184–1191 (2009).

310. Soneson, C., Love, M. I. & Robinson, M. D. Differential analyses for RNA-seq: transcript-level estimates improve gene-level inferences. *F1000Res* **4,** 1521–18 (2015).

311. Stuart, T. *et al.* Comprehensive Integration of Single-Cell Data. *Cell* **177,** 1888–1902.e21 (2019).

312. Lucas, C. *et al.* Longitudinal analyses reveal immunological misfiring in severe COVID-19. *Nature* **584,** 463–469 (2020).

313. Hochberg, M. C. Updating the American College of Rheumatology revised criteria for the classification of systemic lupus erythematosus. *Arthritis Rheum* **40,** 1725–1725 (1997).

314. Tan, E. M. *et al.* The 1982 revised criteria for the classification of systemic lupus erythematosus. *Arthritis Rheum* **25,** 1271–1277 (1982).

315. Lu-Culligan, A & Iwasaki, A. The False Rumors About Vaccines That Are Scaring Women. *The New York Times* (26 Jan 2021).

316. Lu-Culligan, A & Epstein, RH. No, We Don't Know if Vaccines Change Your Period. *The New York Times* (20 Apr 2021).